



DSM Design of Cold-Formed Steel Columns Failing in Distortional Modes at Elevated Temperatures

Alexandre Landesmann¹, Dinar Camotim², Fernanda C.M. Silva¹

Abstract

Recently, the authors employed numerical failure loads and temperatures, obtained by means of ANSYS shell finite element analyses (SFEA), to establish guidelines for the design of cold-formed steel fixed-ended lipped channel and rack-section columns exhibiting distortional failures under fire conditions. The design approach was based on the Direct Strength Method (DSM) and had been previously adopted by other researchers – the currently codified design/strength equations/curves, developed for ambient temperature, were modified to account for the appropriate Young's modulus and yield stress erosion caused by the elevated temperature. Although the modified DSM design curves were shown to predict fairly well the vast majority of available numerical and experimental (only a few) column distortional failure loads under elevated temperatures, it may be argued that the above validation had a limited scope, since it involved exclusively fixed-ended columns with two cross-section shapes and acted by temperatures not exceeding 600°C. This work extends the scope of the previous investigations, by presenting and discussing numerical results concerning columns with two end support conditions (fixed and pinned end supports – the latter associated with free warping), four cross-section shapes (lipped channels, hats, zeds and racks), various cross-section dimensions (six per shape) and subjected to eight uniform temperatures (up to 800°C). Such results consist of column distortional post-buckling equilibrium paths and failure loads, which were determined by means geometrically and materially non-linear ANSYS SFEA. In order to cover a wide distortional slenderness range, several room-temperature yield stresses are considered. The temperature dependence of the steel material properties is simulated using the model prescribed in part 1.2 of Eurocode 3 (EC3-1.2 – CEN 2005) for cold-formed steel. Finally, the numerical failure loads obtained in this work are used to assess the merits of modified DSM distortional strength curves proposed by the authors. It is shown that these curves improve visibly the failure load prediction quality, which provides motivation and encouragement to continue the ongoing search for an efficient (safe and reliable) DSM-based design approach for columns failing in distortional modes under elevated temperatures.

1 Introduction

The combination of high structural efficiency (strength-to-weight ratio), low production costs and remarkable fabrication versatility is responsible for the fact that the usage of cold-formed steel structures in the construction industry has grown steadily during the last few years, particularly in low-rise storage, residential and industrial buildings. On the other hand, the natural/logical search for economical

¹ Civil Engineering Program, COPPE, Federal University of Rio de Janeiro, Brazil. <alandes; fernandacms@coc.ufrj.br>

² CERIS, ICIST, DECivil, Instituto Superior Técnico, Universidade de Lisboa, Portugal. <dcamotim@civil.ist.utl.pt>

solutions leads to the use of quite slender cold-formed steel members, which are invariably prone to various instability phenomena that often govern their strength and safety.

The knowledge about the structural behavior of cold-formed steel members at room temperature has advanced considerably in the last few years and such advances have been incorporated into design specifications at a quite rapid pace. Since it is well known that many cold-formed steel members are prone to distortional failure, the current design specifications include provisions dealing with this collapse mode. In particular, the Direct Strength Method (DSM – *e.g.*, Schafer 2008, Camotim *et al.* 2016), appearing in the current versions of the North-American (AISI 2016), Australian/New Zealand (AS/NZS 2005) and Brazilian (ABNT 2010) specifications for cold-formed steel structures, contains specific provisions (strength curves) for the design of columns and beams against distortional failure. Their application requires only knowing the member yield stress and distortional buckling load/moment. However, such provisions/curves were developed for ambient/room temperature and, therefore, it is not yet known whether they can also be adopted (with more or less relevant modifications) to estimate the ultimate strength of members under elevated temperatures, namely those caused by fire conditions. Indeed, such conditions may alter substantially the steel constitutive law, namely its Young's modulus, yield strength and amount of non-linearity.

The high “section factor”³, associated with the use of high-strength steels and very slender cross-sections, is responsible for making cold-formed steel construction significantly vulnerable to fire conditions. Therefore, the application of the currently available design methods requires the extensive use of costly fireproofing materials, aimed at protecting the steel structures from an excessive heat increase due to fire hazards. This requirement leads quite often to overly conservative (*i.e.*, unduly uneconomical) structural designs. Moreover, it is fair to say that the research activity devoted to cold-formed steel members under fire conditions only started in this century and, in spite of the fairly large number of recent publications, is still relatively scarce. Without claiming to be exhaustive, relevant work has been developed by Outinen *et al.* (2000), Kaitila (2002), Feng *et al.* (2003a-d, 2004), Lee *et al.* (2003), Zhao *et al.* (2005), Feng & Wang (2005a,b), Chen & Young (2006, 2007a,b, 2008), Ranawaka (2006), Lim & Young (2007), Ranawaka & Mahendran (2009, 2010), Landesmann & Camotim (2010a,b, 2011, 2012, 2015), Shahbazian & Wang (2011a,b, 2012, 2013, 2014), Kankanamge & Mahendran (2012), Chen *et al.* (2012, 2013), Abreu & Schafer (2013), Gunalan & Mahendran (2013a,b), Gunalan *et al.* (2013), Ellobody (2013) and Laím *et al.* (2014). Moreover, only a small fraction of the above studies addresses failures associated with the occurrence of distortional buckling, an instability phenomenon often governing the behavior and strength of lipped members with intermediate unrestrained lengths.

Recently, the authors (Landesmann & Camotim 2012, 2015) carried out ANSYS numerical (shell finite element) investigations aimed at assessing the performance of the current Direct Strength Method (DSM) distortional strength curve in predicting the failure loads of fixed-ended cold-formed steel lipped channel and rack-section columns subjected to elevated temperatures, caused by fire conditions. In particular, it was intended (i) to quantify how well the above curve is able to handle the temperature-dependence of the steel material properties and (ii) to assess how sensitive the quality of the failure load prediction is to a change in the (temperature-dependent) steel constitutive model adopted – six models were considered. Concerning the first aspect, it was found that a single distortional strength curve was not able to capture the failure load temperature-dependence – a specific parameter has to be included to

³ The heating rate of a given cross-section varies according to its dimensions, namely the so-called “section factor”, which is given by the H_p/A relationship, where (i) H_p is the steel cross-section perimeter exposed to the fire and (ii) A is the cross-sectional area. A larger H_p/A value corresponds to a higher susceptibility to fire effects (or, alternatively, to a higher need for using fireproofing materials).

reflect this dependence. As far as the second aspect is concerned, it was concluded that the prediction quality is only minutely influenced by the particular temperature-dependent constitutive model adopted.

Although the DSM distortional strength curves proposed in the publications mentioned in the previous paragraph were shown to estimate fairly well the vast majority of available numerical and experimental (only a few) distortional failure loads under elevated temperatures, it may be argued that the above validation procedure had a limited scope, because it involved only fixed-ended columns with two cross-section geometries and temperatures up to 600°C. Therefore, the aim of this work is to extend the scope of the previous study, by considering columns (i) with two end support conditions (fixed-ended and pinned – pinned end cross-sections that can warp freely), four cross-section shapes (lipped channels, hats, zeds and racks) and various cross-section dimensions (six per shape), and (ii) subjected to eight uniform temperatures (20/100-200-300-400-500-600-700-800°C).

The paper begins by presenting the column geometry selection, achieved by means of sequences of “trial-and-error” buckling analyses (Section 2). It aims at identifying column cross-section dimensions and lengths leading, as much as possible, to “pure” distortional buckling and failure modes – *i.e.*, the selected columns exhibit distortional critical buckling loads that are significantly lower than their local and global counterparts. Then, Section 3 briefly describes the shell finite element model employed to perform the geometrically and materially non-linear analyses in the code ANSYS (SAS 2009) for room and elevated temperatures. Section 4 is devoted to room temperature analysis: illustrative numerical results concerning the column distortional post-buckling behavior and ultimate strength are presented and discussed. In particular, the trends of the numerical failure loads obtained are compared with those exhibited by the experimental and numerical values reported in the literature. Moreover, the numerical and experimental failure loads are compared with their estimates provided by the current DSM design curve, enabling a preliminary assessment of how its “prediction quality” is influenced by the column geometry and (mostly) end support conditions.

Finally, Section 5 addresses the influence of the temperature on the column elastic-plastic post-buckling behavior, failure load and corresponding DSM design. In order to cover a wide distortional slenderness range, several room-temperature yield stresses are considered. The model prescribed in EC3-1.2 (CEN 2005) is employed to describe the temperature dependence of the cold-formed steel material properties. Lastly, the numerical failure load data obtained by the authors are used to assess the merits of modified (alternative) DSM distortional strength curves proposed by the authors both in the past (Landesmann & Camotim 2012, 2015) and in this work. It is shown that part of such modifications improve visibly the failure load prediction quality, thus providing encouragement to continue the search for an efficient and reliable DSM-based design approach for columns failing in distortional modes at elevated temperatures.

2 Column Geometry Selection – Buckling Behavior

The first task in this work consisted of carefully selecting the cross-section dimensions and lengths of the lipped channel (C), zed-section (Z), hat-section (H) and rack-section (R) cold-formed steel columns to be analyzed, which exhibit two different end support conditions: “fixed” (F) and “pinned” (P). These designations concern the global (major and minor-axis) and local rotations, as well as the warping displacements, which may be either prevented (F) or free (P) – in both cases, the torsional rotations are prevented. The selection procedure involved sequences of “trial-and-error” buckling analyses, performed by means of either (i) the code GBTUL, based on Generalized Beam Theory (GBT) and developed by Bebiano *et al.* (2008a,b), or (ii) ANSYS shell finite element analyses. This selection procedure aimed at satisfying the following requirements:

- (i) Columns buckling in “pure” distortional modes and, as much as possible, also exhibiting distortional collapses. This goal is achieved by ensuring that the critical buckling stress (i_1) is clearly distortional and (i_2) falls considerably below the lowest local and global bifurcation stresses.
- (ii) Cross-section dimensions associated with “pure” distortional failures for both end support conditions dealt with here (only the lengths are different). Although fulfilling this requirement is by no means essential, it makes the performance of the parametric study obviously easier.
- (iii) Column lengths (iii_1) associated with single half-wave buckling modes and (iii_2) as close as possible to the values of the P-column minimum distortional critical buckling loads.
- (iv) Cross-section dimensions that are commonly used and involve different wall width proportions, namely web-to-flange width ratios. This requirement is intended to enable assessing whether such width proportions have a meaningful influence on the column distortional post-critical strength.

Fortunately, it was possible to fulfill all the above requirements and the end product of the “trial-and-error” selection procedure are the 24 cross-section dimensions (6 per cross-section shape)⁴ given in Table 1 (see also the figure below) – their web-to-flange width ratios (b_1/b_2) equal ≈ 0.69 , 1.00 and ≈ 1.45 . On the other hand, Table 2 provides, for each cross-section dimensions, the corresponding two sets (P and F columns) of (i) lengths associated with the critical distortional buckling (L_D), (ii) corresponding buckling load at room temperature ($P_{cr.D.20}$) and (iii) its ratios with respect to the lowest local ($P_{b1.L.20}$) and global ($P_{b1.e.20}$) buckling loads – all buckling loads were calculated for $E_{20}=205\text{ GPa}$ (steel Young’s modulus at room temperature) and $\nu=0.3$ (Poisson’s ratio, assumed independent of the temperature). It is observed that the first “non-distortional” buckling load always corresponds to local buckling and that the ratio $P_{b1.L.20}/P_{cr.D.20}$ varies between 2.13 and 8.43 (P columns) and 1.55 and 5.64 (F columns). The first global (flexural-torsional or flexural) buckling load is invariably much higher – indeed, the $P_{b1.e.20}/P_{cr.D.20}$ ratio varies from 22.05 to 298.22 (P columns) and from 25.50 to 375.02 (F columns).

Table 1. Cross-section dimensions and area of the selected C + H + Z and R columns

Cross-section	b_1 (mm)	b_2 (mm)	b_1/b_2	b_3 (mm)	b_4 (mm)	t (mm)	Area (cm ²)
C-H-Z 130	124.7	85.7	1.455	7.95		2.65	8.3
C-H-Z 150	144.7	144.7	1.000	7.95	-	2.65	11.9
C-H-Z 180	174.7	251.8	0.694	7.95	-	2.65	18.4
C-H-Z 200a	194.7	134.7	1.445	7.95	-	2.65	12.7
C-H-Z 200b	194.7	194.7	1.000	7.95	-	2.65	15.9
C-H-Z 200c	194.7	280.4	0.694	7.95	-	2.65	20.4
R130	124.7	85.7	1.455	5.3	7.95	2.65	8.5
R150	144.7	144.7	1.000	5.3	7.95	2.65	12.2
R180	174.7	251.8	0.694	5.3	7.95	2.65	18.7
R200a	194.7	134.7	1.445	5.3	7.95	2.65	13.0
R200b	194.7	194.7	1.000	5.3	7.95	2.65	16.2
R200c	194.7	280.4	0.694	5.3	7.95	2.65	20.7

⁴ Note that the C, H and Z columns with the same cross-section dimensions exhibit practically identical distortional and local buckling (bifurcation) loads – obviously, the global ones are clearly different (in value and/or in nature).

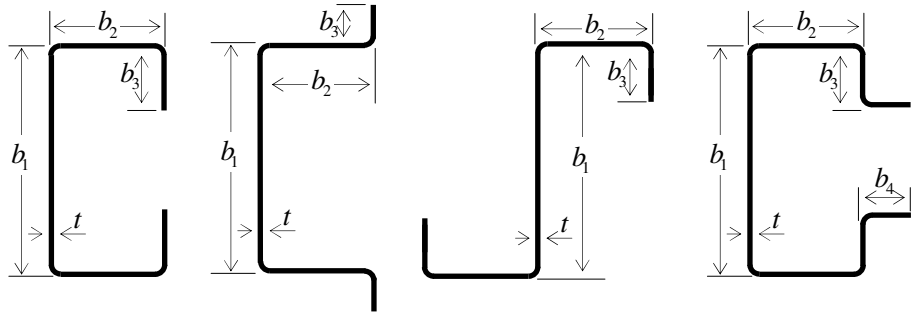


Table 2. Selected column lengths, critical buckling loads and bifurcation-to-critical load ratios

Column	Pinned (P)				Fixed (F)			
	L_D (cm)	$P_{cr.D.20}$ (kN)	$\frac{P_{bl,L.20}}{P_{cr.D.20}}$	$\frac{P_{bl,e.20}}{P_{cr.D.20}}$	L_D (cm)	$P_{cr.D.20}$ (kN)	$\frac{P_{bl,L.20}}{P_{cr.D.20}}$	$\frac{P_{bl,e.20}}{P_{cr.D.20}}$
C130	35	173.6	2.16	24.73	55	242.3	1.58	28.65
C150	50	95.3	3.57	45.60	80	133.9	2.59	50.68
C180	75	49.2	4.32	88.35	100	71.9	3.06	135.97
C200a	50	104.9	2.24	72.67	75	145.9	1.68	92.86
C200b	65	67.7	3.79	90.43	90	96.5	2.72	132.27
C200c	80	43.4	4.42	121.14	120	61.4	3.25	152.22
H130	35	175.8	2.13	22.05	55	245.8	1.55	25.50
H150	50	95.5	3.55	42.93	80	134.2	2.57	47.70
H180	75	49.2	4.31	85.64	110	69.8	3.14	112.28
H200a	50	105.5	2.22	69.01	75	146.8	1.67	88.12
H200b	65	67.8	3.78	87.32	95	95.4	2.74	116.18
H200c	80	43.4	4.42	118.11	120	61.4	3.24	148.39
Z130	35	174.0	2.16	36.41	55	242.6	1.58	42.32
Z150	50	95.5	3.56	91.10	80	134.1	2.58	101.42
Z180	75	49.3	4.31	217.19	100	72.0	3.06	334.73
Z200a	50	105.0	2.24	107.67	75	145.9	1.69	137.82
Z200b	65	67.8	3.78	181.25	90	96.6	2.72	265.52
Z200c	80	43.4	4.41	298.22	120	61.4	3.24	375.02
R130	35	169.8	5.14	27.13	60	239.8	3.71	26.13
R150	50	99.3	5.03	45.61	80	142.2	3.62	49.74
R180	75	54.3	8.28	84.07	100	83.3	5.54	123.22
R200a	55	107.5	4.95	61.33	85	150.9	3.63	73.16
R200b	70	71.4	5.15	76.20	100	102.6	3.70	103.78
R200c	85	46.6	8.43	102.07	110	71.4	5.64	159.10

The curves in Figs. 1(a)-(b) provide the variation of $P_{cr,T}$ (elastic critical buckling loads for different temperatures) with the length L (logarithmic scale) and temperature T for P and F columns with the C-H-Z-R 200b cross-section dimensions. Note that (i) three temperatures are dealt with ($20/100^{\circ}\text{C}$, *i.e.*, room temperature, 400°C and 600°C), (ii) the horizontal scales are different in Figs. 1(a) and 1(b) and (iii) the EC3-1.2 (2005) constitutive model, presented in Section 3.1, is adopted. Also shown are the critical (distortional) buckling mode shapes of P columns with $L_D=65\text{cm}$ (C-H-Z 200b) and $L_D=70\text{cm}$ (R200b) and F columns with $L_D=90\text{cm}$ (C-Z 200b), $L_D=95\text{cm}$ (H200b) and $L_D=100\text{cm}$ (R200b). It is worth pointing out that any given buckling curve is obtained through a “vertical translation” of the top one, with a magnitude depending solely on the Young’s modulus erosion due to the temperature rise⁵. Moreover, the critical distortional load $P_{cr,D,T}$ corresponds to the same length (L_D) for each temperature value.

3 Numerical Model

The column distortional post-buckling analyses were carried out in ANSYS (2009), employing a shell finite element model previously validated by the authors (Landesmann & Camotim 2010ab, 2011) involving column discretizations into fine SHELL181 element meshes – 4-node shear deformable thin-shell elements with six degrees of freedom per node and full integration. Convergence studies showed that $5\text{mm} \times 5\text{mm}$ meshes provide accurate results, while involving a reasonable computational effort. The analyses (i) were performed by means of an incremental-iterative technique combining Newton-Raphson’s method with an arc-length control strategy and (ii) simulate the response of columns subjected to an uniform temperature distribution (*i.e.*, they are deemed engulfed in flames and, thus, share the surrounding air temperature – Landesmann & Camotim 2011) and subsequently axially compressed up to failure – steady state analyses providing failure loads⁶.

As stated earlier, the columns analyzed exhibit two end support conditions (F and P). Concerning the modeling of the “F” or “P” end support conditions, it is worth noting that: (i) in a fixed support, the column end section was attached to a rigid plate, thus precluding the occurrence of local and global displacements and rotations, as well as warping, (ii) in a pinned support, the membrane and bending transverse displacements of all end section nodes were prevented, while keeping the axial (warping) displacements and all the rotations free, and (iii) to enable the load application, the rigid-body axial translation is free at one or both end sections. The axial compression is applied by means of either (i) a set of concentrated forces acting on the nodes (P columns) or (ii) a concentrated force applied on the rigid plate point corresponding to the end section centroid (F columns). The above forces are always increased in small increments, by means of the ANSYS automatic load stepping procedure.

All the columns analyzed contained initial geometrical imperfections with a critical-mode (distortional) shape and small amplitude (10% of the wall thickness t). Following the column distortional post-buckling asymmetry studies carried out by Prola & Camotim (2002a,b) and Silvestre & Camotim (2006), these initial imperfections involve either outward (C+R P columns) or inward (C+H+R F columns and H P columns) flange-stiffener motions⁷ – those shown to lead to the lower post-buckling strengths. Obviously, this distinction does not make sense in the Z columns, since their flange-stiffener motions are always opposite (one outward and the other inward). Each critical buckling mode shape was determined

⁵ Naturally, the Young’s modulus reduction factor k_e , whose variation with the temperature T is illustrated in Fig. 2(a), makes it possible to quantify the decrease in the column critical buckling load $P_{cr,T}$ associated with a given length.

⁶ Note that the authors (*e.g.*, Landesmann & Camotim 2011) have shown that the failure loads yielded by the steady state analyses match the more realistic failure temperatures obtained through the “corresponding” transient analyses (axially compressed columns heated up to failure), which means that the column (distortional) failure under fire conditions can be fully investigated by resorting only to failure loads.

⁷ One exception: the C180 F column, which exhibits lower post-buckling strengths for outward flange-stiffener motions.

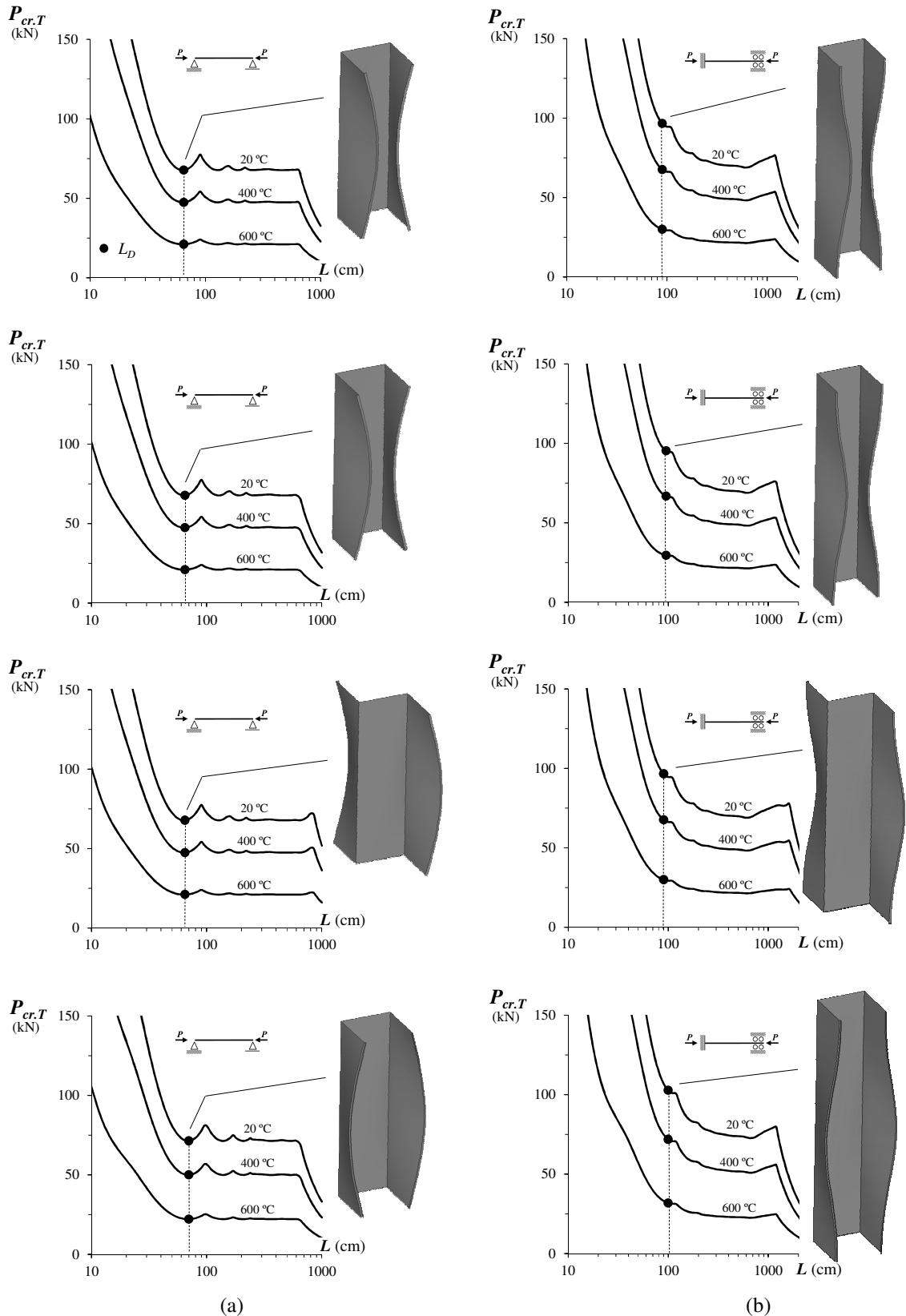


Figure 1. Variation of $P_{cr,T}$ with L and T for P and F C-H-Z-R 200b columns (EC3-1.2 model)

by means of a preliminary ANSYS buckling analysis, performed with exactly the same shell finite element mesh employed to carry out the subsequent non-linear (post-buckling) analysis – this procedure makes it very easy to “transform” the buckling analysis output into a non-linear analysis input. It is still worth noting that no strain-hardening, residual stresses and/or corner strength effects were considered in this work, since their combined influence on the column strength has been shown to be negligible by several authors (*e.g.*, Ellobody & Young 2005).

3.1 Steel Material Behavior

The multi-linear stress-strain curve available in ANSYS is adopted to model the steel material behavior corresponding to several yield stresses⁸. The cold-formed steel constitutive law at elevated temperatures adopted in this work is defined by the analytical expressions prescribed in Part 1.2 of Eurocode 3 (EC3-1.2 – CEN 2005). Fig. 2(a) makes it possible to compare the temperature dependence of the reduction factors applicable to the cold-formed steel Young’s modulus ($k_e = E_T/E_{20}$) nominal yield stress ($k_y = \sigma_{y,T}/\sigma_{y,20}$) and proportionality limit stress ($k_p = \sigma_{p,T}/\sigma_{p,20}$), which are tabulated in EC3-1.2⁹. As for Fig. 2(b), it illustrates the qualitative differences between the stress-strain curves prescribed by EC3-1.2 for $T=20/100^\circ\text{C}$ (room temperature), $T=400^\circ\text{C}$, and $T=600^\circ\text{C}$ – $\sigma_T/\sigma_{y,20}$ vs. ε , where the applied stress at a given temperature (σ_T) is normalized with respect to the room temperature yield stress $\sigma_{y,20}$. Note that the stress-strain curve non-linearity increases largely with the temperature (for $T=20/100^\circ\text{C}$, the constitutive law is bi-linear – elastic-perfectly plastic material). The stress-strain curves prescribed by EC3-1.2 are divided into three regions, associated with distinct strain ranges¹⁰. Note that the stress-strain curve proportionality limit strain ($\varepsilon_{p,T} = \sigma_{p,T}/E_T$) and non-linear shape are considerably influenced by the temperature.

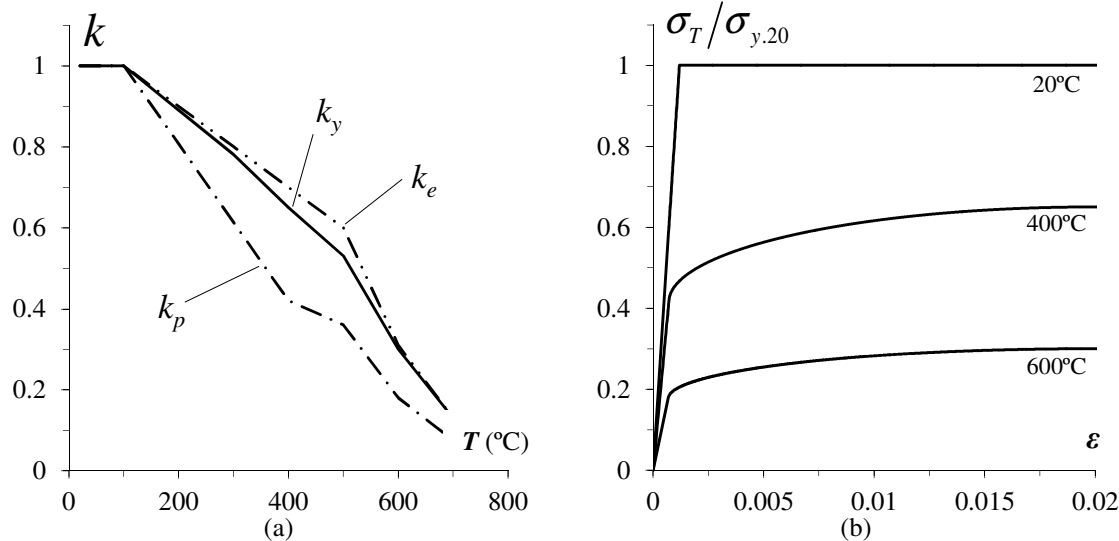


Figure 2. (a) Variation of the reduction factors k_e , k_y , k_p with the temperature for $T \leq 800^\circ\text{C}$ and (b) cold-formed steel stress-strain curves $\sigma_T/\sigma_{y,20}$ vs. ε ($\varepsilon \leq 2\%$) for $T=20/100-400-600^\circ\text{C}$ – as prescribed by the EC3-1.2 model

⁸ Note that a considerably large fraction of the (nominal) yield stresses considered in this work are unrealistically high, leading to $\sigma_{y,20}$ values largely exceeding the current DSM limit for pre-qualified columns ($\sigma_{y,20} < 655 \text{ MPa}$ [95 ksi] – Table B4.1-1 of AISI 2016). The reason for selecting such high yield stresses was to enable the analysis slender and very slender columns, *i.e.*, to make it possible to cover a wide column slenderness range.

⁹ For $T=20/100-200-300-400-500-600-700-800^\circ\text{C}$, EC3-1.2 prescribes $k_p=1-0.807-0.613-0.42-0.36-0.18-0.075-0.05$, $k_y=1-0.89-0.78-0.65-0.53-0.3-0.13-0.07$ and $k_e=1-0.9-0.8-0.7-0.6-0.31-0.13-0.09$.

¹⁰ Although the EC3-1.2 model further extends the stress-strain relationship, to include strain-hardening, for temperatures below 400°C (such strain-hardening is negligible for temperatures higher than 400°C), this effect is not considered in this work.

For elevated temperatures, the first part of the well-defined yield plateau exhibited by the $T=20/100\text{ }^{\circ}\text{C}$ curve is replaced by a strain-hardening region that becomes more pronounced as the temperature rises. The stress-strain curve (i) is linear elastic, with slope E_T ($E_{20}=205\text{ GPa}$), up to the proportional limit stress $\sigma_{p,T}$, then (ii) becomes elliptic in the transition between the elastic and plastic ranges, up to the effective yield stress $\sigma_{y,T}$ (corresponding to $\varepsilon_{y,T}=0.02$), which accounts for (kinematic) strain-hardening and (iii) ends with a perfectly flat yield plateau up to the limit strain $\varepsilon_{u,T}=0.15$ – in all cases, Prandtl-Reuss's plasticity model (von Mises yield criterion and associated flow rule) is adopted. Finally, since the distortional post-buckling analyses carried out involve large inelastic strains, the nominal (engineering) static stress-strain curve is substituted by a relation between the true stress and the logarithmic plastic strain, which reads

$$\sigma_T = \begin{cases} \varepsilon \cdot E_T & \text{for } \varepsilon \leq \varepsilon_{p,T} \\ \sigma_{p,T} - c + (b/a) \left[a^2 - (\varepsilon_{y,T} - \varepsilon)^2 \right]^{0.5} & \text{for } \varepsilon_{p,T} < \varepsilon < \varepsilon_{y,T} \\ \sigma_{y,T} & \text{for } \varepsilon_{y,T} \leq \varepsilon \leq \varepsilon_{u,T} \end{cases}, \quad (1)$$

$$a^2 = (\varepsilon_{y,T} - \varepsilon_{p,T}) (\varepsilon_{y,T} - \varepsilon_{p,T} + c/E_T), \quad b^2 = c (\varepsilon_{y,T} - \varepsilon_{p,T}) E_T + c^2,$$

$$c = \frac{(\sigma_{y,T} - \sigma_{p,T})^2}{(\varepsilon_{y,T} - \varepsilon_{p,T}) E_T - 2(\sigma_{y,T} - \sigma_{p,T})}$$

4 Distortional Response at Room Temperature

This section presents and discusses numerical results concerning the influence of the cross-section dimensions and end support conditions (F or P) on the column distortional post-buckling behavior and strength. Elastic and elastic-plastic results are addressed separately.

4.1 Elastic Post-Buckling Behavior and Strength

Figures 3(a)-(b) show the elastic post-buckling equilibrium paths $P/P_{cr,D,20}$ vs. $|\delta|/t$ ($|\delta|$ is the maximum absolute vertical displacement occurring along the flange-stiffener longitudinal edges and t is the wall thickness) obtained for the P and F C-H-Z-R columns whose geometries are defined in Tables 1 and 2. These figures also include illustrative examples of the shell finite element meshes adopted to analyze the initially imperfect for C-H-Z-R 200b columns (initial geometrical imperfection amplified 5 times). The observation of these eight distortional post-buckling equilibrium path sets prompts the following remarks:

- (i) First of all, the expected higher stiffness and strength exhibited by the F columns is readily confirmed by comparing Figs. 3(a) and 3(b). There is also a clear difference between the shapes of the P and F column equilibrium paths: while the former exhibit a pronounced convexity, associated with a progressive stiffness degradation that leads to elastic limit points (more visible in the Z columns), the latter display a concavity, stemming from the stiffness increase provided by the end support warping fixity and precluding the occurrence of elastic limit points (at least for not too high $|\delta|$ values). Note that, for both the P and F columns, the C-H-Z-R equilibrium paths virtually coincide up to $|\delta|/t \approx 3$ and $|\delta|/t \approx 1.5$, respectively.
- (ii) Regarding the influence of the cross-section dimensions on the column post-critical stiffness and strength, there is a visible trend in all the F columns: they increase as the web-to-flange width ratio (b_1/b_2) decreases. Indeed, recalling that the C-H-Z-R columns share the same web, flange and lip dimensions (the R columns just have additional stiffeners), the stiffness and strength increase as

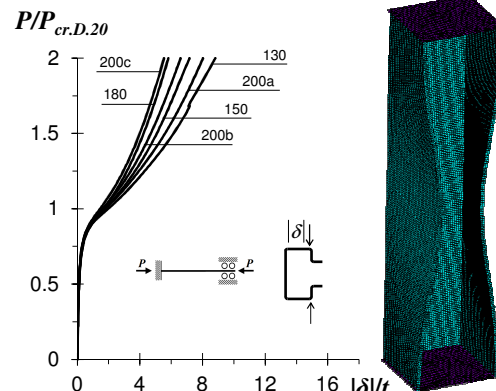
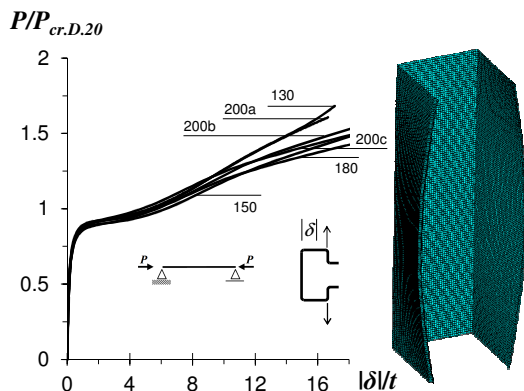
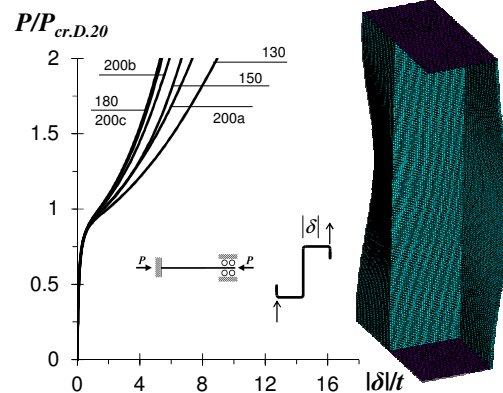
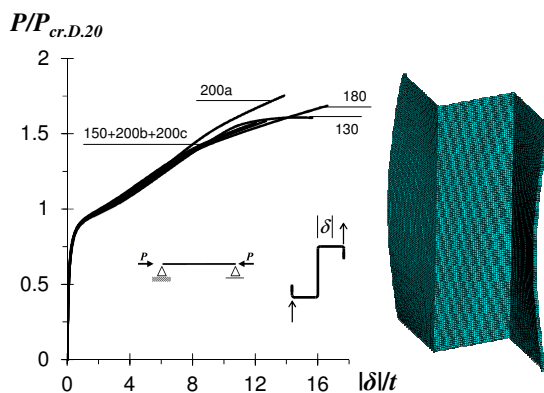
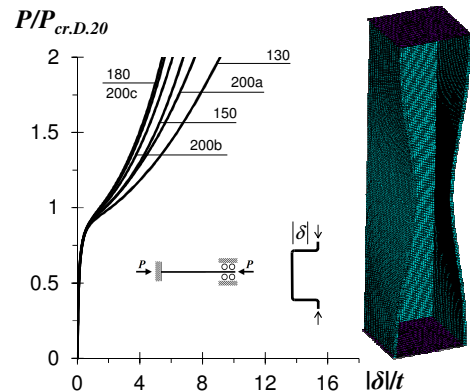
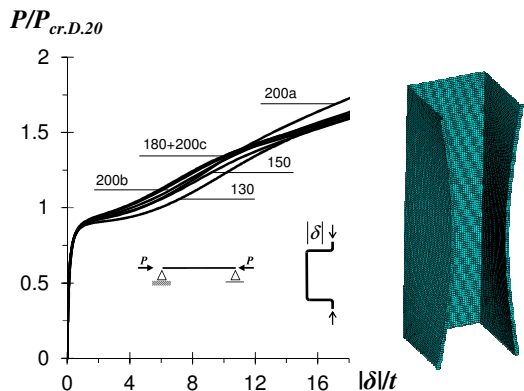
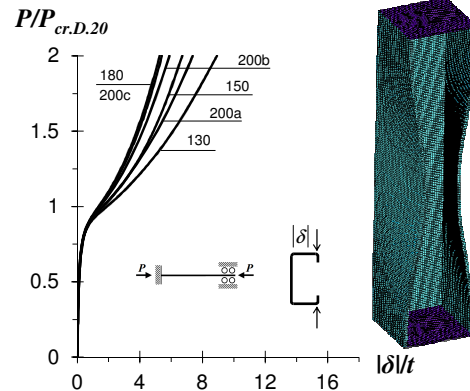
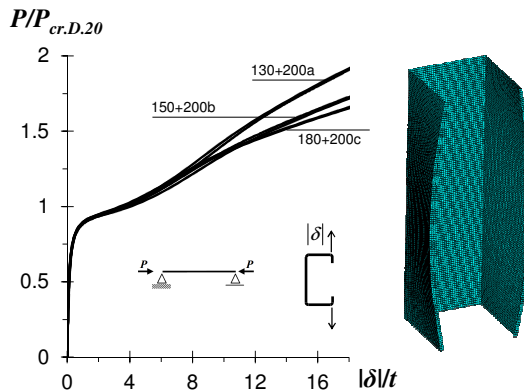


Figure 3. Elastic equilibrium paths $P/P_{cr,D,20}$ vs. $|\delta|/t$ concerning the (a) P and (b) F columns

one travels from columns 130+200a ($b_1/b_2 > 1$) to columns 150+200b ($b_1/b_2 \approx 1$) and columns 180+200c ($b_1/b_2 < 1$). On the other hand, the above assertion is not applicable to the P columns, for which no clear trend exists. Nevertheless, note that, for the lipped channel P columns, an opposite trend is observed: the post-critical stiffness and strength increase slightly with b_1/b_2 – moreover, the columns with similar b_1/b_2 ratios share the same elastic equilibrium path.

- (iii) In spite of its limited scope (only 24 columns analyzed), this study makes it possible to conclude that the column elastic distortional post-buckling stiffness and strength are influenced by both the end support conditions and the web-to-flange width ratio (b_1/b_2). This influence may have non-negligible implications on the column elastic-plastic ultimate strength and, therefore, also on its prediction by design methods. This issue deserves further investigation in the future¹¹.

4.2 Elastic-Plastic Post-Buckling Behavior and Strength

The ANSYS shell finite element model is next employed to investigate the elastic-plastic post-buckling and strength behavior of P and F columns buckling and failing in distortional modes at room temperature, and (ii) to gather failure load data intended to assess the adequacy of the currently codified DSM design curve in predicting them. The numerical results presented and discussed concern a total of 336 columns, combining (i) the 24 columns geometries defined in Tables 1 and 2, (ii) the two end support conditions dealt with (P and F) and (iii) seven room temperature yield stresses, selected to enable covering wide distortional slenderness ranges for all column sets: $\lambda_{D,20}$ varies between 0.40 and 3.60 for both P and F columns – recall that $\lambda_{D,20} = (P_{y,20}/P_{cr,D,20})^{0.5}$, where $P_{y,20} = A \cdot \sigma_{y,20}$ and A is the cross-section area (given in Table 1). Tables A1 to A4, included in Annex A, provide, for each column analyzed, the (i) distortional slenderness $\lambda_{D,20}$, (ii) squash load $P_{y,20}$ and (iii) numerical failure load $P_{u,20}$.

Figures 4(a)-(b) display a sample of the P and F column non-linear equilibrium paths $P/P_{cr,D,20}$ vs. $|\delta|/t$, determined to obtain the failure loads $P_{u,20}$ (identified by white circles) – note that vertical scales differ for the P and F columns. These equilibrium paths concern C-H-Z-R 200b columns with distortional slenderness $\lambda_{D,20}=0.5-1.0-1.5-2.0-2.5-3.0-3.5-4.0$ – the elastic paths, already shown in Figs. 3(a)-(b), are displayed again for comparison purposes. Figs. 4(a)-(b) also depict the deformed configurations and von Mises stress (σ_{VM}) contours, at the peak load, of the P and F C-H-Z-R 200b columns with $\lambda_{D,20}=1.5$ – the distortional nature of the column collapse is clearly visible. The observation of the results shown in the above figures and the data provided in Tables A1 to A4 leads to the following conclusions:

- (i) The P column elastic-plastic post-buckling and strength behaviors are different from their F column counterparts, both qualitatively and quantitatively – note that the F column values only exceed their P column counterparts for very high $\lambda_{D,20}$ values (*i.e.*, very high yield stresses $\sigma_{y,20}$).
- (ii) As expected, the failure load ratio $P_{u,20}/P_{cr,D,20}$ increases with $\lambda_{D,20}$ for all columns, regardless of their cross-section shape (C, H, Z or R) and end support conditions (P or F).
- (iii) Both the P and F columns exhibit similar single half-wave distortional buckling and collapse modes. The latter is associated with the full yielding of the mid-height web-flange corner region, leading to the formation of an “X-shaped distortional plastic hinge”, which means that plasticity also spreads throughout the mid-height flange and lip regions.

Figures 5(a)-(b) plot the P and F column failure load ratios $P_{u,20}/P_{cr,D,20}$ against $\lambda_{D,20}$. In order to assess the influence of the web-to-lip width ratio b_1/b_2 , the $P_{u,20}/P_{cr,D,20}$ values are represented by (i) black symbols,

¹¹ The effect of the cross-section geometry and/or end support conditions in the column distortional post-buckling behavior deserves further study. To the authors' best knowledge, the only available work on this topic is due Landesmann *et al.* (2013).

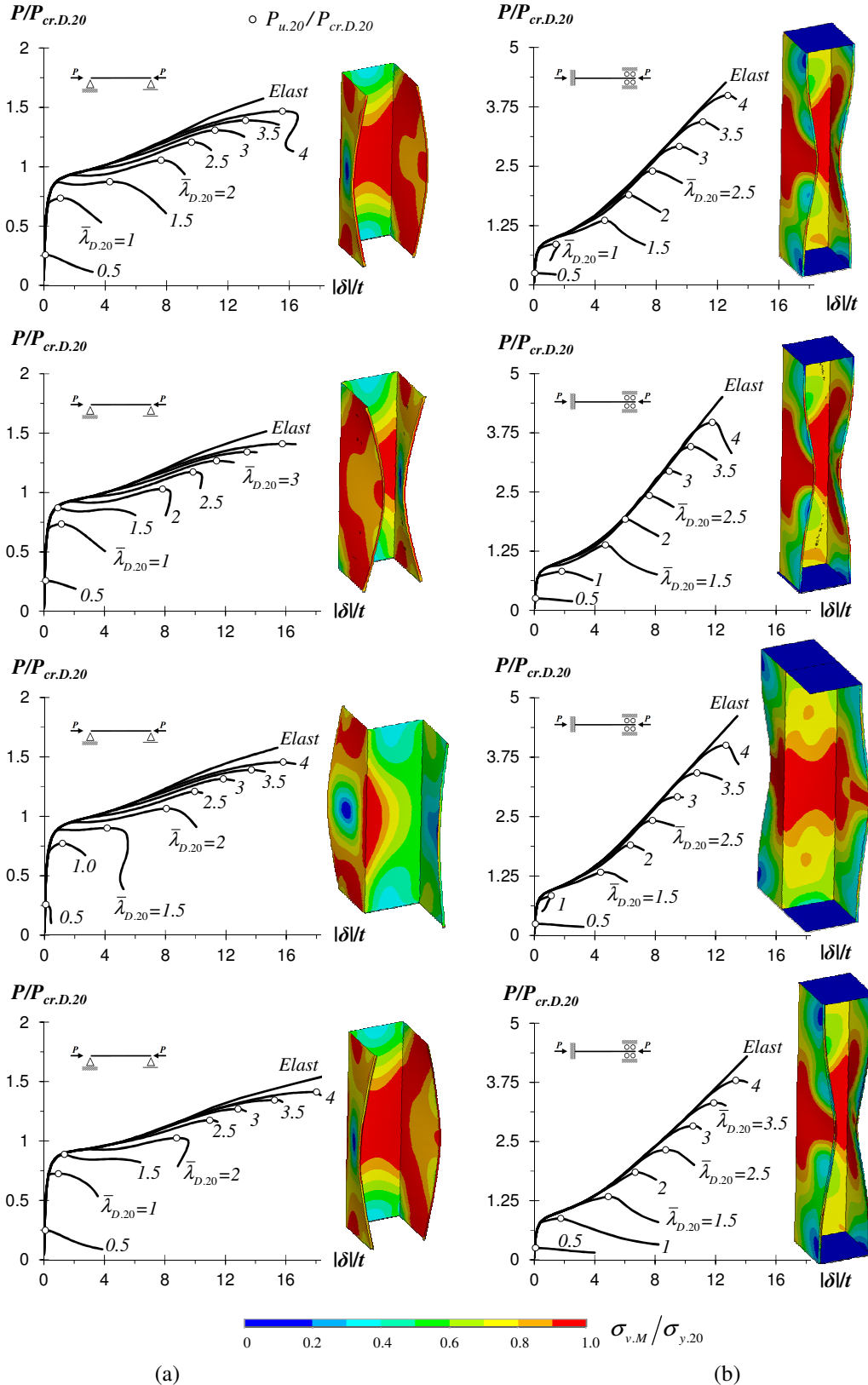


Figure 4. Room temperature elastic-plastic distortional equilibrium paths ($P/P_{cr,D,20}$ vs. $|\delta|/t$) and failure modes (for $\bar{\lambda}_{D,20}=1.5$) concerning (a) P and (b) F C-H-Z-R 200b columns with $\bar{\lambda}_{D,20}=0.5-1.0-1.5-2.0-2.5-3.0-3.5-4.0$

for $b_1/b_2 < 1$ (circles, diamonds, squares and triangles for C-H-Z-R columns, respectively), (ii) gray symbols, for $b_1/b_2 \approx 1$, and (iii) white symbols ones, for $b_1/b_2 > 1$. The observation of the results shown in these figures, as well as the failure load data given in Tables A1-A4, leads to the following conclusions:

- (i) Naturally, the failure load ratios $P_{u,20}/P_{cr,D,20}$ of all columns analyzed (C-H-Z-R) increase with the distortional slenderness $\bar{\lambda}_{D,20}$, regardless of the cross section shape and end support conditions. Moreover, there is no visible influence of the cross-section shape on the $P_{u,20}/P_{cr,D,20}$ value.
- (ii) All columns failing below the critical axial load level (*i.e.*, $P_{u,20}/P_{cr,D,20} < 1$) exhibit a rather small elastic-plastic strength reserve and very little ductility prior to failure. Moreover, there are no visible qualitative differences between the values concerning the P and F columns. This assertion does not remain valid when $P_{u,20}/P_{cr,D,20} > 1$: while the P columns collapse almost immediately after the onset of yielding, the F columns exhibit a considerable elastic-plastic strength reserve, which is a direct consequence of the elastic post-buckling differences addressed earlier.
- (iii) The F-column plot $P_{u,20}/P_{cr,D,20}$ vs. $\bar{\lambda}_{D,20}$ is practically linear. For $\bar{\lambda}_{D,20} \leq 2$, all the $P_{u,20}/P_{cr,D,20}$ values align along the same line. This is no longer true for $\bar{\lambda}_{D,20} > 2$, as the $P_{u,20}/P_{cr,D,20}$ values exhibit a small amount of scatter. Indeed, it seems possible to establish a correlation between the slope of the $P_{u,20}/P_{cr,D,20}$ vs. $\bar{\lambda}_{D,20}$ plot and the value of the width ratio b_1/b_2 : the slope decreases when b_1/b_2 grows – in particular, note that the values concerning the columns with $b_1/b_2 > 1$ are visibly below the remaining ones. On the other hand, it is also clear that there is no influence of the b_1/b_2 ratio on the $P_{u,20}/P_{cr,D,20}$ vs. $\bar{\lambda}_{D,20}$ plot for the P columns – this plot exhibits a well defined bi-linear shape, with the change (drop) in slope occurring for $\bar{\lambda}_{D,20} \approx 1$.

Figures 6(a)-(b) plot the failure load ratios $P_{u,20}/P_{y,20}$ against the $\bar{\lambda}_{D,20}$ for (i) the 336 P and F columns failure loads obtained in this work and also (ii) the fairly large set of experimental values reported by Schafer (2000, 2008) and concerning F columns. The observation of these plots shows that:

- (i) Although both $P_{u,20}/P_{y,20}$ vs. $\bar{\lambda}_{D,20}$ “clouds” clearly align along “Winter-type” strength/design curves, a sizeable $P_{u,20}/P_{y,20}$ “vertical dispersion” occurs in the F columns – such dispersion does not exist in the P column $P_{u,20}/P_{y,20}$ values (all obtained in this work).
- (ii) Like the $P_{u,20}/P_{cr,D,20}$ ratio, the $P_{u,20}/P_{y,20}$ is also clearly influenced by b_1/b_2 , as far as the F columns are concerned – see the vertical dispersion of the failure loads obtained in this work in Fig. 6(b)

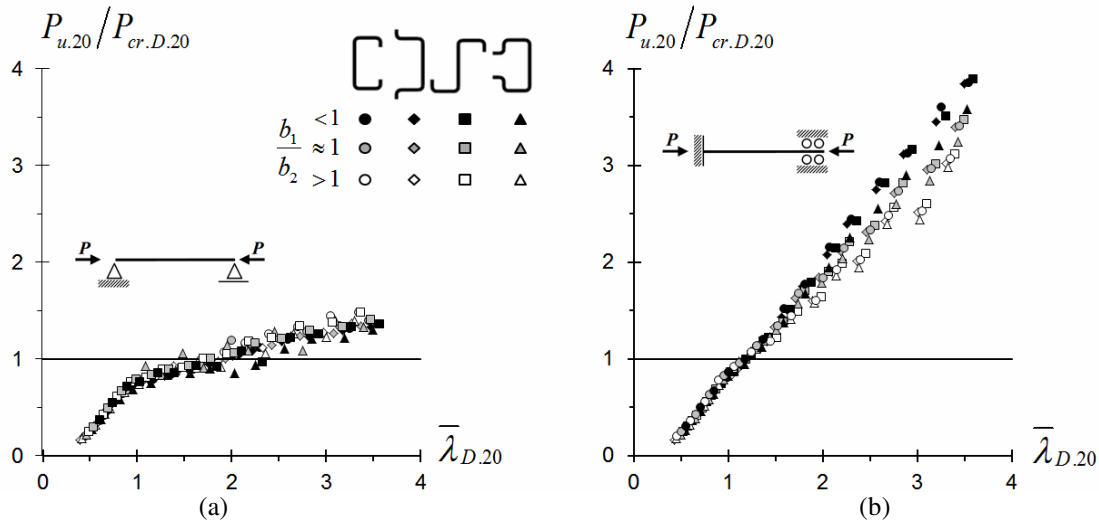


Figure 5. Plots $P_{u,20}/P_{cr,D,20}$ vs. $\bar{\lambda}_{D,20}$ concerning the (a) P and (b) F column failure loads obtained in this work

and note that $P_{u,20}/P_{cr,D,20}$ increases as b_1/b_2 decreases. On the other hand, the above influence is again undetected in the P columns.

- (iii) The experimental F column failure loads reported by Schafer (2000, 2008), which involve mostly columns with $b_1/b_2 > 1$, also align along a “Winter-type” curve and “mingle” reasonably well with those obtained in this work (with similar b_1/b_2 ratios), even if they are a bit below and exhibit a significant vertical dispersion.

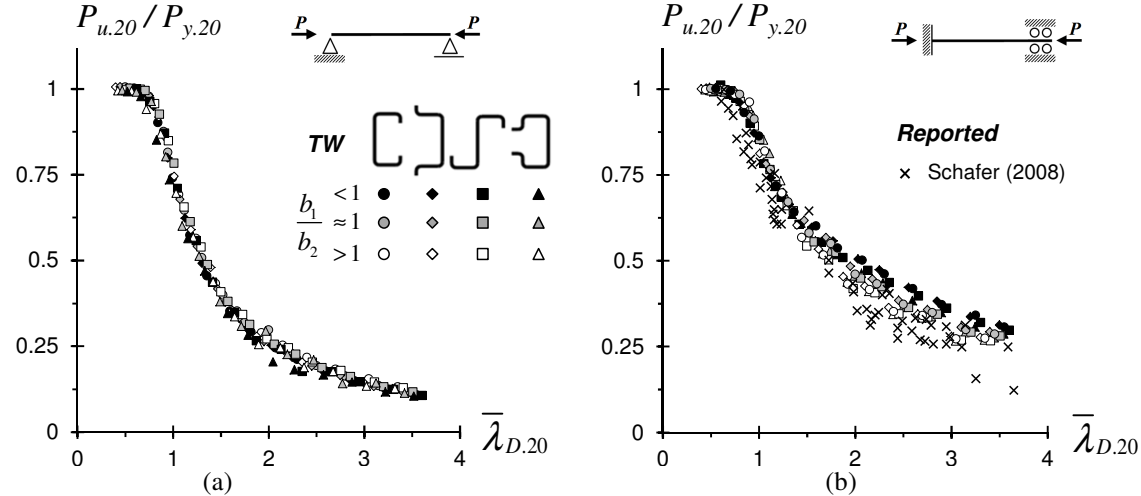


Figure 6. Plots $P_{u,20}/P_{y,20}$ vs. $\bar{\lambda}_{D,20}$ concerning the (a) P and (b) F column failure loads obtained in this work (P and F columns) and reported by Schafer (2008) (F columns only)

4.3 DSM Design

This section addresses the quality of prediction of the C-H-Z-R column experimental and numerical failure load data considered in this work by the currently codified (in the context of room temperature) DSM distortional design curve (AISI 2016). The nominal failure load of cold-formed steel columns failing in distortional modes ($P_{n,D,20}$) is given by

$$P_{n,D,20} = \begin{cases} P_{y,20} & \text{for } \bar{\lambda}_{D,20} \leq 0.561 \\ P_{y,20} \left[1 - 0.25 \left(P_{cr,D,20}/P_{y,20} \right)^{0.6} \right] \left(P_{cr,D,20}/P_{y,20} \right)^{0.6} & \text{for } \bar{\lambda}_{D,20} > 0.561 \end{cases}, \quad (2)$$

where (i) $P_{cr,D,20}$ and $P_{y,20}$ are the column distortional critical buckling and squash loads, respectively, and (ii) $\bar{\lambda}_{D,20} = (P_{y,20}/P_{cr,D,20})^{0.5}$ is the column distortional slenderness.

Figures 7(a)-(b) compare the above design curve with the numerical and distortional column failure load ratios displayed in Fig. 6(a)-(b). As for Figs. 8(a)-(b), they plot the ratios $P_{u,20}/P_{n,D,20}$ against $\bar{\lambda}_{D,20}$, thus providing pictorial representations of the accuracy and safety of the currently codified DSM distortional strength curve prediction quality. The observation of these figures leads to the following comments:

- (i) Naturally, the DSM design curve provides accurate and mostly safe predictions of the F column experimental distortional failure loads reported by Schafer (2000, 2008), since they were part of those used in its development and calibration – this assertion can be confirmed by looking at the corresponding $P_{u,20}/P_{n,D,20}$ values in Fig. 8(b) (their average, standard deviation, maximum and minimum values are 1.03-0.13-1.32-0.61, respectively).
- (ii) Concerning the F column numerical failure loads obtained in this work, it is observed that their DSM estimates are virtually all safe and become progressively less accurate as $\bar{\lambda}_{D,20}$ increases –

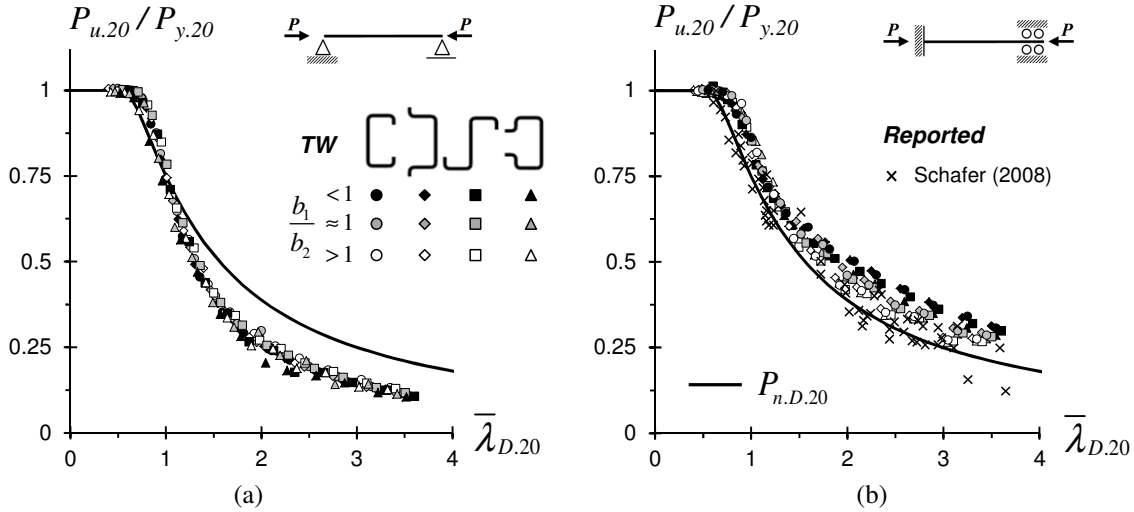


Figure 7. Comparison of the (a) P and (b) F column failure load ratios $P_{u.20}/P_{y.20}$ with their predictions provided by the current DSM distortional design curve

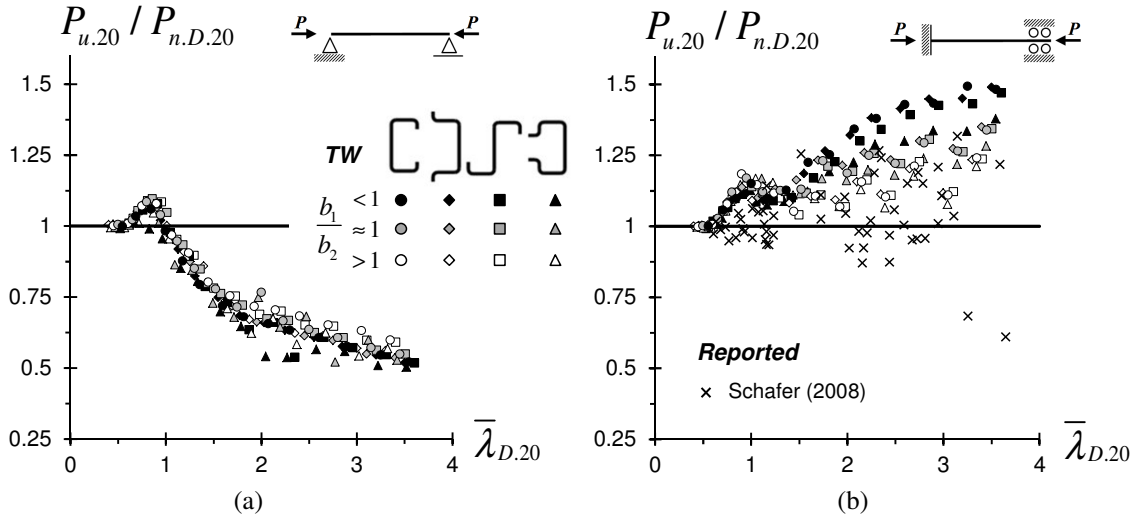


Figure 8. Plots $P_{u.20}/P_{n.D.20}$ vs. $\bar{\lambda}_{D.20}$ for the (a) P and (b) F column experimental and numerical failure loads

– the $P_{u.20}/P_{n.D.20}$ statistical indicators read 1.17-0.12-1.49-0.99. A closer look at the $P_{u.20}/P_{n.D.20}$ values reveals that, in fact, such values (ii₁) are only reasonably accurate for columns with $\bar{\lambda}_{D.20} \leq 1.5$ and (ii₂) tend to be excessively conservative for columns with $\bar{\lambda}_{D.20} > 1.5$ (the underestimation grows with $\bar{\lambda}_{D.20}$ and is particularly severe for the most slender columns with $b_1/b_2 < 1$). These facts are reflected in the $P_{u.20}/P_{n.D.20}$ averages and standard deviations: 1.08-0.05 ($\bar{\lambda}_{D.20} \leq 1.5$) and 1.24-0.11 ($\bar{\lambda}_{D.20} > 1.5$). If only columns with $b_1/b_2 \geq 1$ are considered, those indicators improve to 1.07-0.08 and 1.19-0.08, respectively. Finally, it is worth mentioning that there is no visible influence of the cross-section shape (C-H-Z-R) on the quality of the failure load predictions.

- (iii) Concerning the P numerical failure loads, it is observed that, for non-sticky columns ($\bar{\lambda}_{D.20} \geq 1.15$), they are grossly overestimated by the DSM design curve – the $P_{u.20}/P_{n.D.20}$ average, standard deviation, maximum and minimum values are 0.79-0.19-1.09-0.50, respectively. Accurate (safe or unsafe) predictions only occur for sticky columns ($\bar{\lambda}_{D.20} < 1.15$). Similar findings were reported by Landesmann & Camotim (2013), who concluded that the significant differences between the F

and P column distortional post-critical strengths are not adequately reflected by their (distortional) critical buckling stresses. Moreover, based the failure load data gathered, these authors (preliminarily) proposed an alternative DSM design curve for P columns, defined by the expressions

$$P_{n.D.20}^P = \begin{cases} P_{y.20} & \text{for } \bar{\lambda}_{D.20} \leq 0.561 \\ P_{y.20} \left[1 - 0.25 \left(P_{cr.D.20}/P_{y.20} \right)^{0.6} \right] \left(P_{cr.D.20}/P_{y.20} \right)^{0.6} & \text{for } 0.561 < \bar{\lambda}_{D.20} \leq 1.133 \\ P_{y.20} \left[0.65 + 0.2 \left(P_{cr.D.20}/P_{y.20} \right)^{0.75} \right] \left(P_{cr.D.20}/P_{y.20} \right)^{0.75} & \text{for } \bar{\lambda}_{D.20} > 1.133 \end{cases}, \quad (3)$$

and only differing from the current design curve for $\bar{\lambda}_{D.20} > 1.133$. Fig. 9(a) makes it possible to compare the two design curves (black and blue solid line) between themselves and with the P column numerical failure loads obtained in this work – the $P_{u.20}/P_{n.D.20}^P$ values are also given in Tables A1-A4 (Annex A) and plotted against $\bar{\lambda}_{D.20}$ in Fig. 9(b). One readily observes that the prediction quality of the proposed curve is substantially higher, as attested by the $P_{u.20}/P_{n.D.20}^P$ average, standard deviation, maximum and minimum values: 1.02-0.07-1.20-0.83.

- (iv) In view of the above results, it is decided to adopt in this work the currently codified and proposed DSM design/strength curves to predict the F and P column failure loads at room temperature. In order to make this option more clear in the remainder of the paper, estimates provided by the first strength curve are termed $P_{n.D.20}^F$ (the “F” stands for “fixed-ended columns”) – on the other hand, in the designation of the estimates provided by second strength curve the “P” stands for both “pin-ended columns” and “proposed design curve”.

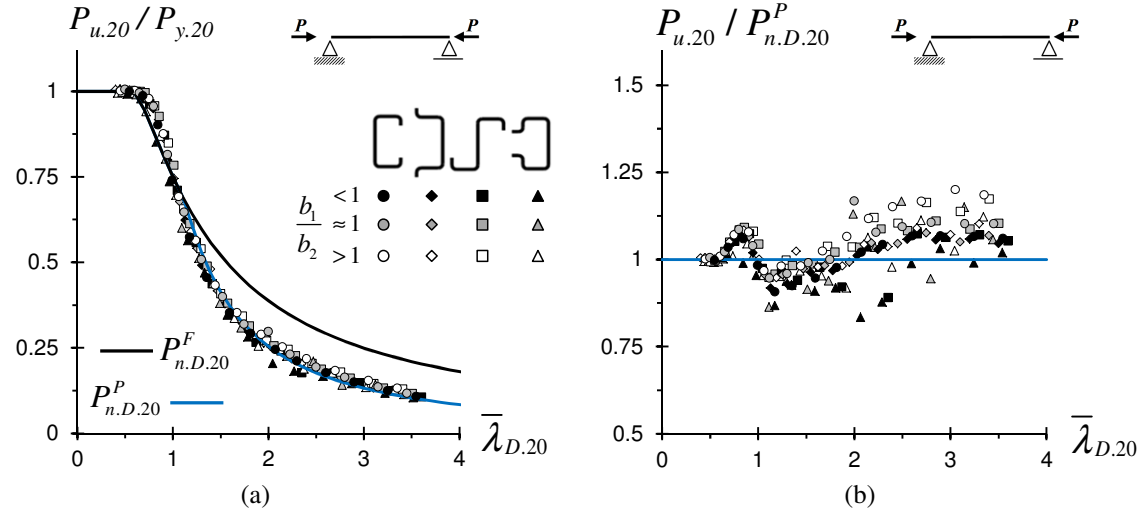


Figure 9. (a) Comparison of the current and proposed DSM distortional design curves with the P column failure load ratios $P_{u.20}/P_{y.20}$ and (b) $P_{u.20}/P_{n.D.20}^P$ values, concerning the P columns, plotted against $\bar{\lambda}_{D.20}$

5 Distortional Response under Elevated Temperature

5.1 Elastic-Plastic Post-Buckling Behavior

The influence of the (elevated) temperature on the distortional elastic-plastic post-buckling behavior and failure load of cold-formed steel P and F C-H-Z-R columns are examined in this section. The temperature dependence of the steel constitutive law follows the model prescribed in EC3-1.2 (2005). Figures 10(a)-(b) show the non-linear equilibrium paths ($P/P_{cr.D.20}$ vs. $|\delta l|/t$) of C-H-Z-R 200b columns

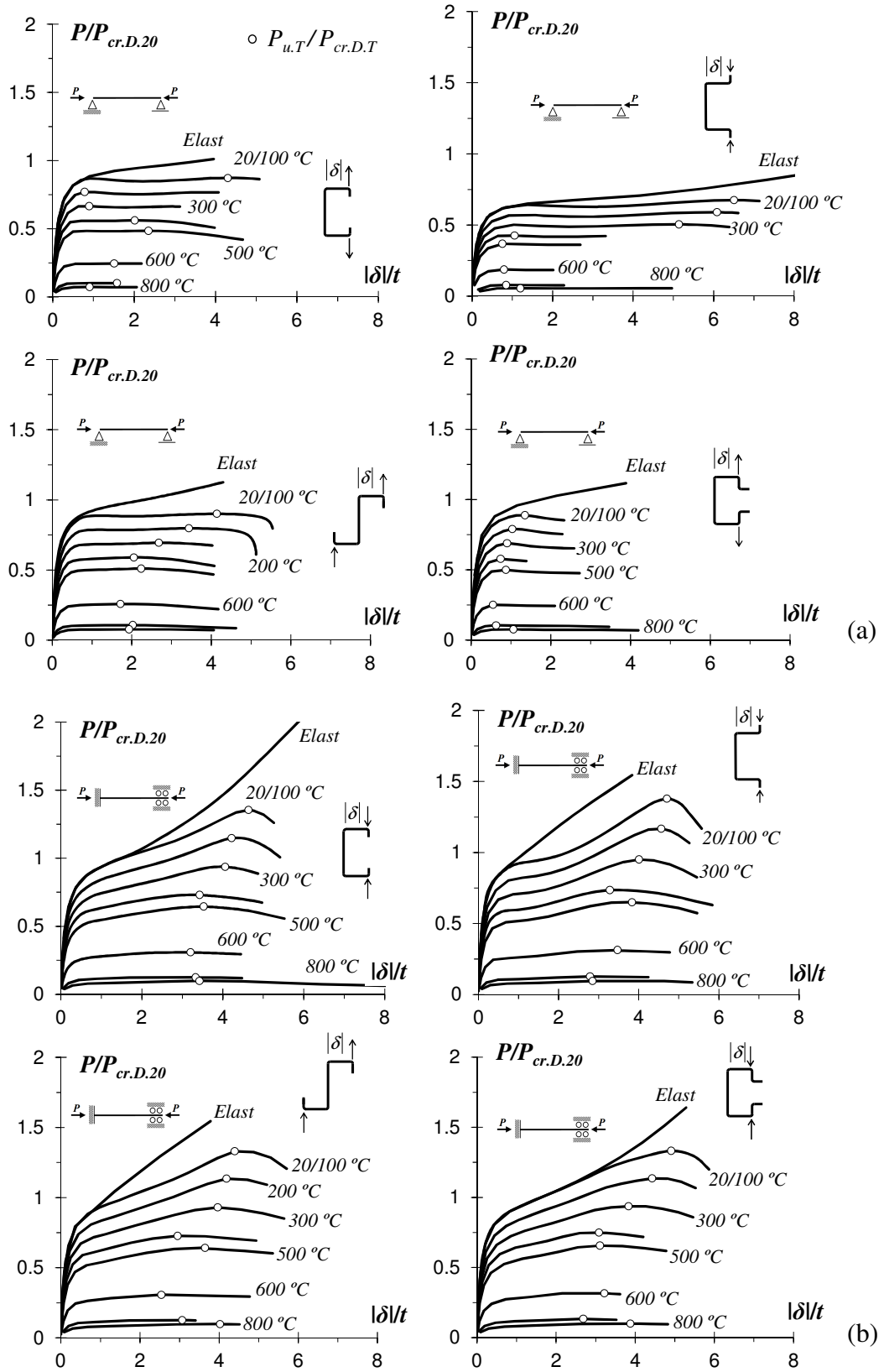


Figure 10. F C-H-Z-R 200b (a) P and (b) F columns distortional post-buckling equilibrium paths for $\bar{\lambda}_{D.20} = 1.5$ and temperatures $T=20/100-200-300-400-500-600-700-800^{\circ}\text{C}$

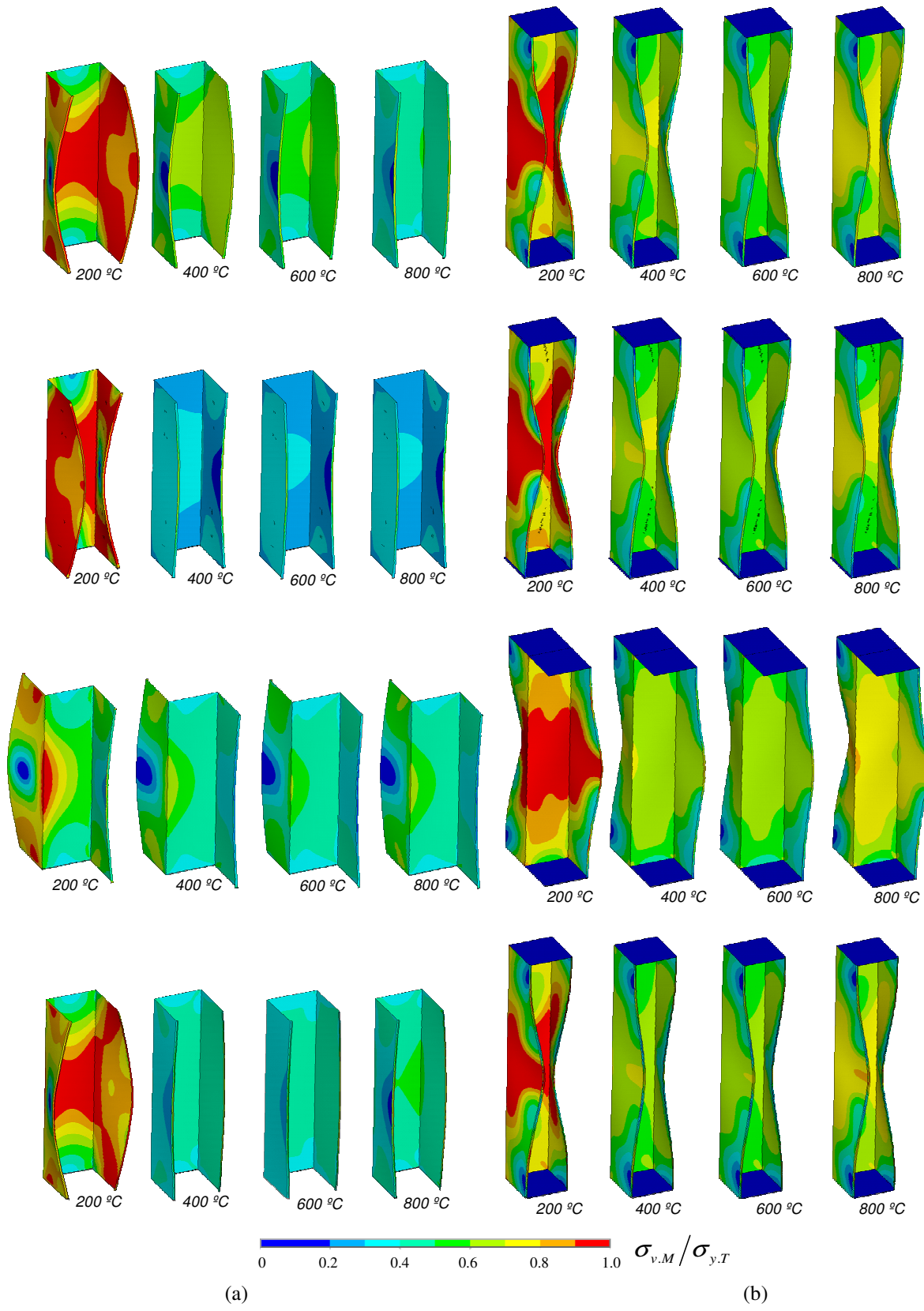


Figure 11. C-H-Z-R 200b (a) P and (b) F columns deformed configurations and von Mises stress contours at collapse, for $\lambda_{D,20}=1.5$ and temperatures $T=200-400-600-800\text{ }^{\circ}\text{C}$

with $\lambda_{D,20}=1.5$ under temperatures $T=20/100-200-300-400-500-600-700-800\text{ }^{\circ}\text{C}$ – the white circles identify the failure loads $P_{u,T}$ and the room temperature curves (elastic and elastic-plastic) are displayed again for comparative purposes. As for Figs. 11(a)-(b), they display the deformed configurations and von Mises stress contours at collapse ($P=P_{u,T}$) for those columns under temperatures $T=200-400-600-800\text{ }^{\circ}\text{C}$. The observation of these results prompts the following remarks:

- (i) Naturally, the various column equilibrium paths “move down” as the temperature rises, which implies that the failure load decreases.
- (ii) Since the thermal action effects are negligible (uniform temperature and free-to-deform columns), the distortional failure modes do not depend on the temperature and, therefore, are virtually identical for all the 64 columns analyzed – see Figs. 11(a)-(b). However, such similarity does not extend to the corresponding von Mises stress contours, which are qualitatively amongst themselves and with respect to the room temperature ones. Indeed, the spread of plasticity in the flange, associated with the formation of the “distortional plastic hinge”, becomes gradually less pronounced as T rises. This stems directly from the temperature dependence of the stress-strain curve shape – recall that $k_p=0.81-0.42-0.18-0.05$ for $T=200-400-600-800\text{ }^{\circ}\text{C}$. Quantitatively speaking, the stresses obviously decrease as the temperature rises and continuously erodes the steel material behavior.
- (iii) The $T \geq 600\text{ }^{\circ}\text{C}$ curves are clearly apart from (and below) their $T \leq 500\text{ }^{\circ}\text{C}$ counterparts (see Figs. 10(a)-(b)). This reflects the heavy degradation of the steel material behavior between $500\text{ }^{\circ}\text{C}$ and $600\text{ }^{\circ}\text{C}$, namely felt via the proportionality limit strain and smoothness of the (elliptic) transition between the elastic and plastic ranges (see Figs. 2(a)-(b)). For $T \geq 600\text{ }^{\circ}\text{C}$, the stress-strain curve regains a well-defined yield plateau.
- (iv) No clear trend was observed concerning the influence of the temperature, geometry and/or steel grade on the amount of elastic-plastic strength reserve and ductility prior to failure.

5.2 Failure Load Data

This section presents the output of a parametric study carried out to gather failure load data that will be used to develop and assess the merits of DSM design approaches intended to handle column distortional failures under elevated temperatures. A total of 2688 columns are analyzed, corresponding to all possible combinations of (i) the 24 geometries defined in Tables 1 and 2, (ii) the P and F end support conditions, (iii) 8 uniform temperatures ($T=20/100-200-300-400-500-600-700-800\text{ }^{\circ}\text{C}$)¹² and (iv) 7 room temperature yield stresses, which enable covering wide distortional slenderness ranges: $\lambda_{D,T}$ varies from 0.35 to 3.6. The numerical failure loads obtained in this parametric study are provided in four sets of tables included in Annex B: Tables B1 to B4 – each table set concerns columns exhibiting one cross-section shape and comprises seven tables, each one associated with a given (elevated) temperature. The tables provide the values of the distortional slenderness $\lambda_{D,T}$, squash load $P_{y,T}$ and failure load $P_{u,T}$. Figures 12 and 13, concerning P and F columns, respectively, plot the failure load ratios $P_{u,T}/P_{y,T}$ against $\lambda_{D,T}$ for each temperature value. The joint observation of these plots makes it possible to draw the following conclusions:

- (i) Regardless of the temperature, the $P_{u,T}/P_{y,T}$ vs. $\lambda_{D,T}$ “clouds” follows the trend of “Winter-type” strength curves and exhibit a small amount of “vertical dispersion” along the whole slenderness range considered (more visible in F columns – for additional clarity, see Fig. 17), which reflects the influence of the cross-section shape and geometry on the column distortional post-critical strength. Qualitatively speaking, the temperature rise does not alter the traits detected/unveiled in Figs. 6(a)-(b),

¹² The room temperature failure loads obtained in this work, already presented in Section 4.2, are displayed again for comparative purposes.

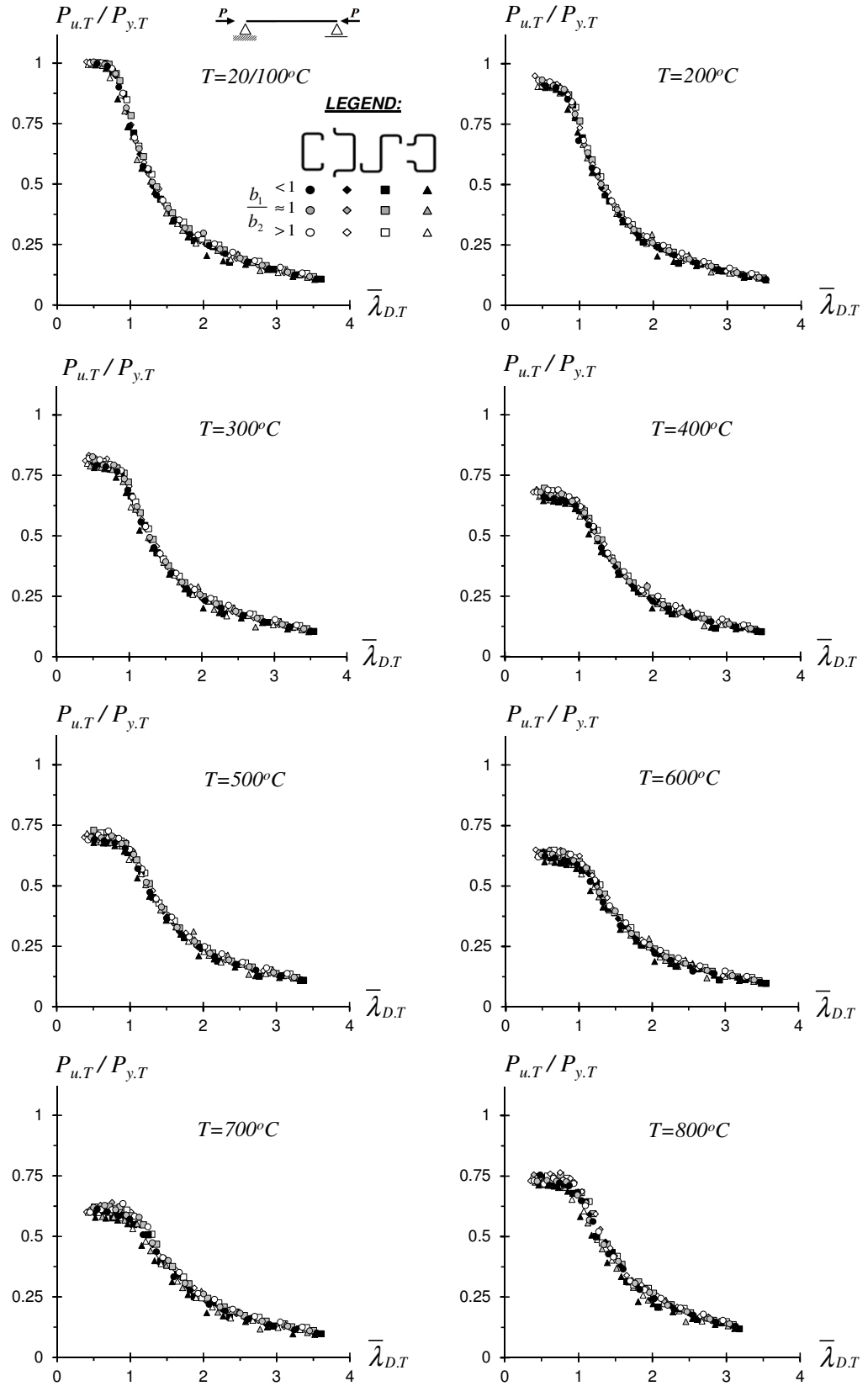


Figure 12. Plots $P_{u,T}/P_{y,T}$ vs. $\bar{\lambda}_{D,T}$ for the P columns under $T=20/100-200-300-400-500-600-700-800^{\circ}C$

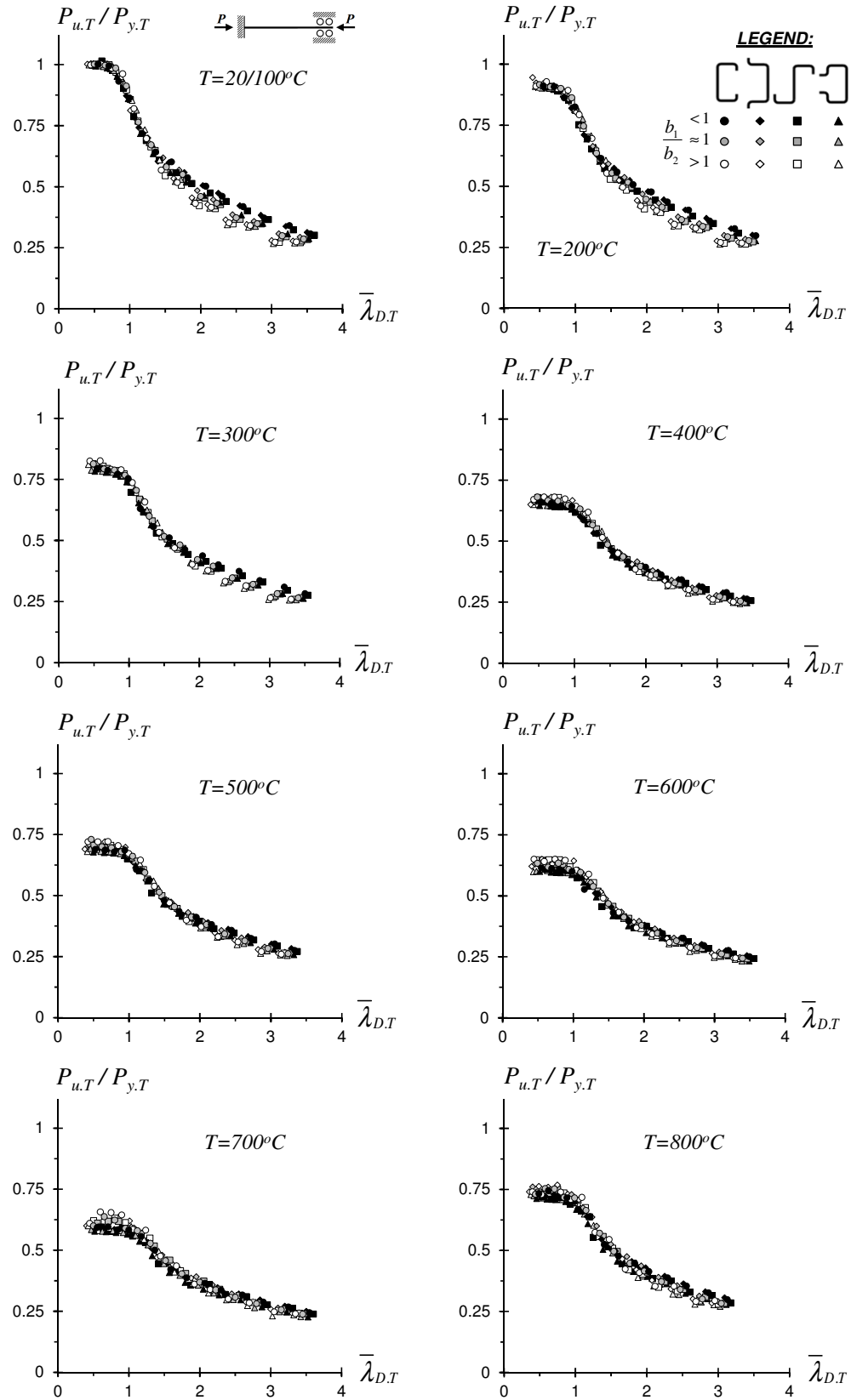


Figure 13. Plots $P_{u,T}/P_{y,T}$ vs. $\bar{\lambda}_{D,T}$ for the F columns under $T=20/100-200-300-400-500-600-700-800^\circ C$

- for room temperature. Indeed, (i₁) the $P_{u,T}/P_{y,T}$ values are considerably lower for the P columns and, in the F columns, (i₂) there is a visible influence of the width ratio b_1/b_2 on $P_{u,T}/P_{y,T}$ in the moderate-to-high slenderness range: for a given $\bar{\lambda}_{D,T}$ value, $P_{u,T}/P_{y,T}$ increases as b_1/b_2 decreases.
- (ii) As expected, all $P_{u,T}/P_{y,T}$ values concerning P and F columns at elevated temperatures ($T > 100^\circ\text{C}$) are below those concerning these columns at room/moderate temperatures ($T \leq 100^\circ\text{C}$). Moreover, the “size” (maximum $\bar{\lambda}_{D,T}$ value) of the $P_{u,T}/P_{y,T}$ vs. $\bar{\lambda}_{D,T}$ plot well defined plateaus varies with the temperature and end support conditions. The above plateaus are followed by descending curve branches that, unexpectedly, are not ordered in the “logical” temperature sequence – indeed, the curves are ordered in the sequence $T=20/100-200-300-800-500-400-600-700^\circ\text{C}$. This order stems directly from the model prescribed in EC3-1.2 to describe the temperature-dependence of the cold-formed steel constitutive law. In particular, the reduction factor ratio k_p/k_y does not decrease monotonically with the temperature – $k_p/k_y=1-0.907-0.786-0.646-0.679-0.6-0.577-\underline{0.714}$ for $T=20/100-200-300-400-500-600-700-800^\circ\text{C}$ (the “out of order” values are underlined).
- (iii) The above results provide promising indications about the possibility of developing an efficient (safe and reliable) DSM approach to estimate the distortional failure loads of P and F columns subjected to elevated temperatures. Nevertheless, such results also show very clearly that the distortional failure load predictions for columns at room and elevated temperatures must be handled separately in the low-to-moderate slenderness range (at least when adopting the EC3-1.2 temperature-dependence model) – the DSM design of P and F columns failing in distortional modes at elevated temperatures is addressed next.

5.3 DSM Design

As just mentioned, this section addresses the DSM-based prediction of the failure loads of columns exhibiting distortional collapses at elevated temperatures, using the failure load data gathered (see Section 5.2). The first step is to assess the adequacy of the available strength curves, developed in the context of columns at room temperature, namely (i) the currently codified DSM distortional design curve, for F columns, and (ii) the strength curve proposed by Landesmann & Camotim (2013), for P columns – they are defined by the expressions given in Eqs. (2) and (3), respectively. Of course, these strength curves must be modified to reflect the temperature effects according to the constitutive model prescribed in EC3-1.2, by incorporating the temperature-dependence of the critical distortional buckling and squash loads. The above approach was already explored by other researchers, namely Ranawaka & Mahendran (2009) and Landesmann & Camotim (2010a,b, 2011, 2012), but only in the context of F columns.

The influence of the temperature on $P_{cr,D}$ and P_y (*i.e.*, $P_{cr,D,20}$ and $P_{y,20}$) is felt through the Young’s modulus and yield stress values¹³, which are reduced as the temperature rises. Therefore, the modification of Eqs. (2) and (3) consists of replacing $P_{cr,D,20}$ and $P_{y,20}$ (or $\sigma_{y,20}$) by $P_{cr,D,T}$ and $P_{y,T}$ (or $\sigma_{y,T}$), which implies that $\bar{\lambda}_{D,20}$ also varies with T ($\bar{\lambda}_{D,T}$). Then, the nominal load-carrying capacity of cold-formed steel P and F columns failing in distortional modes is given, respectively, by the DSM strength curves

$$P_{n,D,T}^P = \begin{cases} P_{y,T} & \text{for } \bar{\lambda}_{D,T} \leq 0.561 \\ P_{y,T} \left[1 - 0.25 \left(P_{cr,D,T} / P_{y,T} \right)^{0.6} \right] \left(P_{cr,D,T} / P_{y,T} \right)^{0.6} & \text{for } 0.561 < \bar{\lambda}_{D,T} \leq 1.133 \\ P_{y,T} \left[0.65 + 0.2 \left(P_{cr,D,T} / P_{y,T} \right)^{0.75} \right] \left(P_{cr,D,T} / P_{y,T} \right)^{0.75} & \text{for } \bar{\lambda}_{D,T} > 1.133 \end{cases}, \quad (4)$$

¹³ Recall that, at elevated temperatures, the so-called “yield stress” ($\sigma_{y,T}$) effectively corresponds to the stress at strain $\varepsilon_{y,T}=0.02$.

$$P_{n.D.T}^F = \begin{cases} P_{y.T} & \text{for } \bar{\lambda}_{D.T} \leq 0.561 \\ P_{y.T} \left[1 - 0.25 \left(P_{cr.D.T} / P_{y.T} \right)^{0.6} \right] \left(P_{cr.D.T} / P_{y.T} \right)^{0.6} & \text{for } \bar{\lambda}_{D.T} > 0.561 \end{cases}, \quad (5)$$

where (i) $P_{cr.D.T}$ and $P_{y.T}$ are the column distortional critical buckling and yield loads, and (ii) the column distortional slenderness is given by $\bar{\lambda}_{D.T} = (P_{y.T} / P_{cr.D.T})^{0.5}$.

The plots shown in Figs. 14 (P columns) and 15 (F columns) make it possible to compare the (i) $P_{u.T} / P_{y.T}$ values with (ii) the available DSM distortional strength curves, including temperature effects (solid blue and black lines, respectively for P and F columns), for temperatures $T=20/100-200-300-400-500-600-700-800^\circ C$ – moreover, Tables B1 to B4, included in Annex B, supply the failure load ratios $P_{u.T} / P_{n.D.T}^P$ and $P_{u.T} / P_{n.D.T}^F$. As for Figs. 16 and 17, they provide $P_{u.T} / P_{n.D.T}^P$ and $P_{u.T} / P_{n.D.T}^F$ vs. $\bar{\lambda}_{D.T}$ plots that enable a quick quantitative assessment of the quality (accuracy and safety) of the DSM strength curve predictions – the $P_{u.T} / P_{n.D.T}^P$ and $P_{u.T} / P_{n.D.T}^F$ averages, standard deviations and maximum/minimum values are also given. The observation of the results presented in the above figures concerning columns at elevated temperatures prompts the following remarks (note that the results concerning columns at room temperature were already discussed in Section 4.3):

- (i) The predictions provided by the available DSM strength curves for the failure loads of columns subjected to elevated temperatures are reasonably accurate and mostly safe only in a relatively high slenderness range ($\bar{\lambda}_{D.T} > 2.0$), regardless of the temperature (*i.e.*, for $T \geq 200^\circ C$). On the other hand, the failure loads of columns with lower slenderness ($\bar{\lambda}_{D.T} \leq 2.0$) at elevated temperatures are clearly overestimated by the available DSM design curves. The $P_{u.T} / P_{n.D.T}^P$ or $P_{u.T} / P_{n.D.T}^F$ values confirm the above assertions: their averages and standard deviations vary from (i₁) 0.97 to 1.05 and 0.07 to 0.08 (P columns) or 1.02 to 1.23 and 0.07 to 0.15 (F columns), for $\bar{\lambda}_{D.T} > 2.0$, and (i₂) 0.79 to 0.95 and 0.04-0.14 (P columns) or 0.78 to 1.04 and 0.07 to 0.12 (F columns), for $\bar{\lambda}_{D.T} \leq 2.0$.
- (ii) The vast majority of distortional failure loads of columns with low-to-moderate slenderness values, at elevated temperatures, are overestimated by the available DSM design curves. This overestimation, which is more pronounced for $T > 300^\circ C$, does not seem to be significantly influenced by the column cross-section shape. Conversely, the amount of overestimation is clearly influenced by the b_1/b_2 width ratio in the F-columns (such influence is not visible in the P columns).
- (iii) In view of the findings presented in the above items, it is clear that the available DSM strength curves are unable to predict adequately distortional failure loads, at elevated temperatures, of columns with low-to-moderate slenderness values – indeed, most of such failure loads are heavily overestimated. Therefore, it is necessary to modify/lower the above DSM strength curves in the low-to-moderate slenderness range, in order to improve the quality of the failure load prediction.

5.3.1 Modified/lowered DSM distortional strength curves

On the basis of the numerical failure load data gathered in this work (see Section 5.2), a first attempt is now made to find modified/lowered DSM design curves able to provide adequate (safe, accurate and reliable) predictions for the failure loads of P and F columns collapsing in distortional modes at elevated temperatures ($T > 100^\circ C$). The main idea behind this attempt is the incorporation of the reduction factor ratio k_p/k_y (shown earlier to play a key role in the steel constitutive law temperature-dependence prescribed by the EC3-1.2 model – see Section 5.2) into the expressions defining the DSM-based strength curves. On the basis of the above idea and the P and F column failure loads obtained in this work, “trial-and-error” curve fitting procedures were carried out and their outputs are the modified/lowered DSM strength curves defined by the expressions (their failure load predictions are identified by an asterisk)

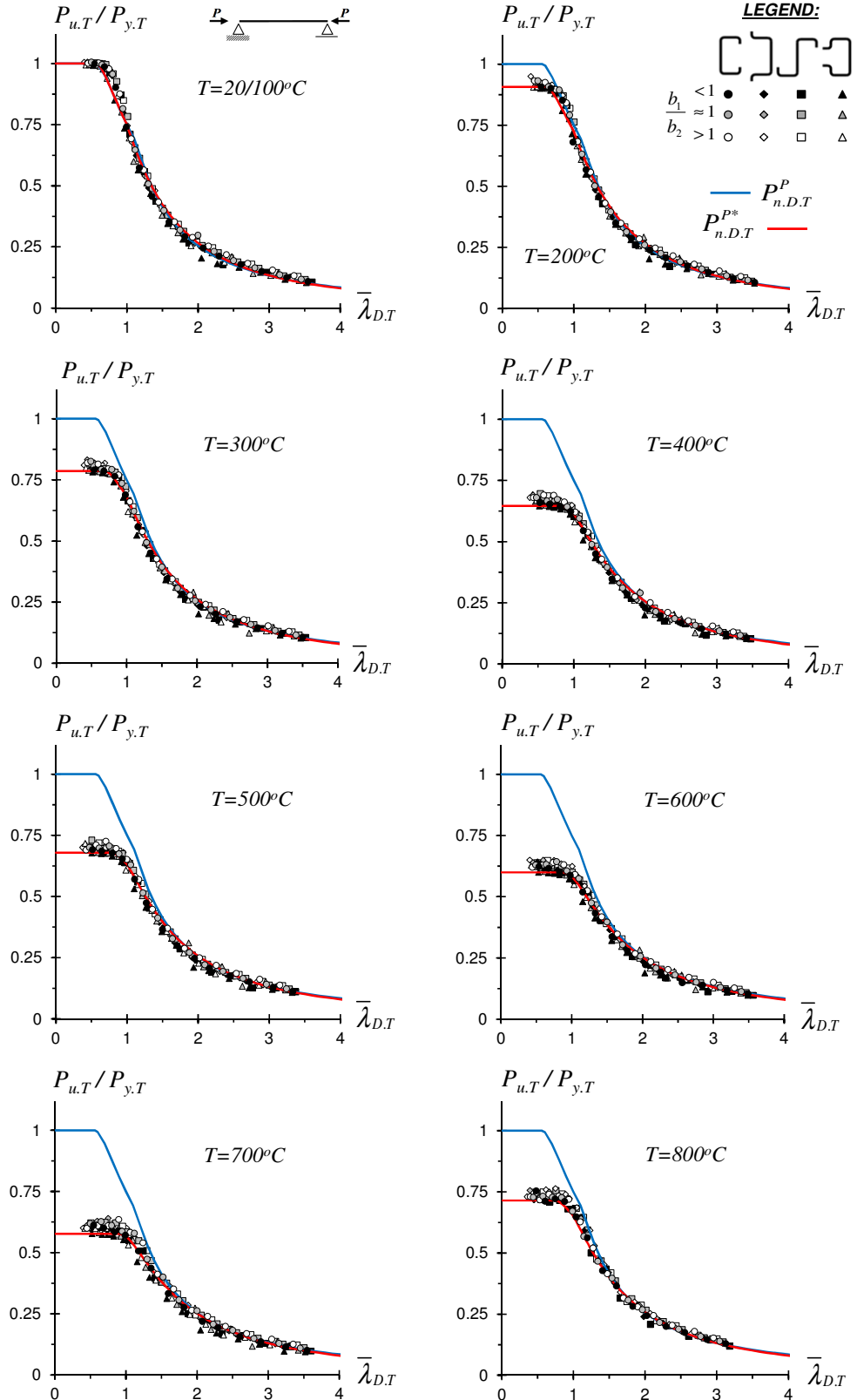


Figure 14. Comparison of the P-column failure load ratios with the available and modified DSM distortional design curves
 $(T=20/100-200-300-400-500-600-700-800^\circ C)$

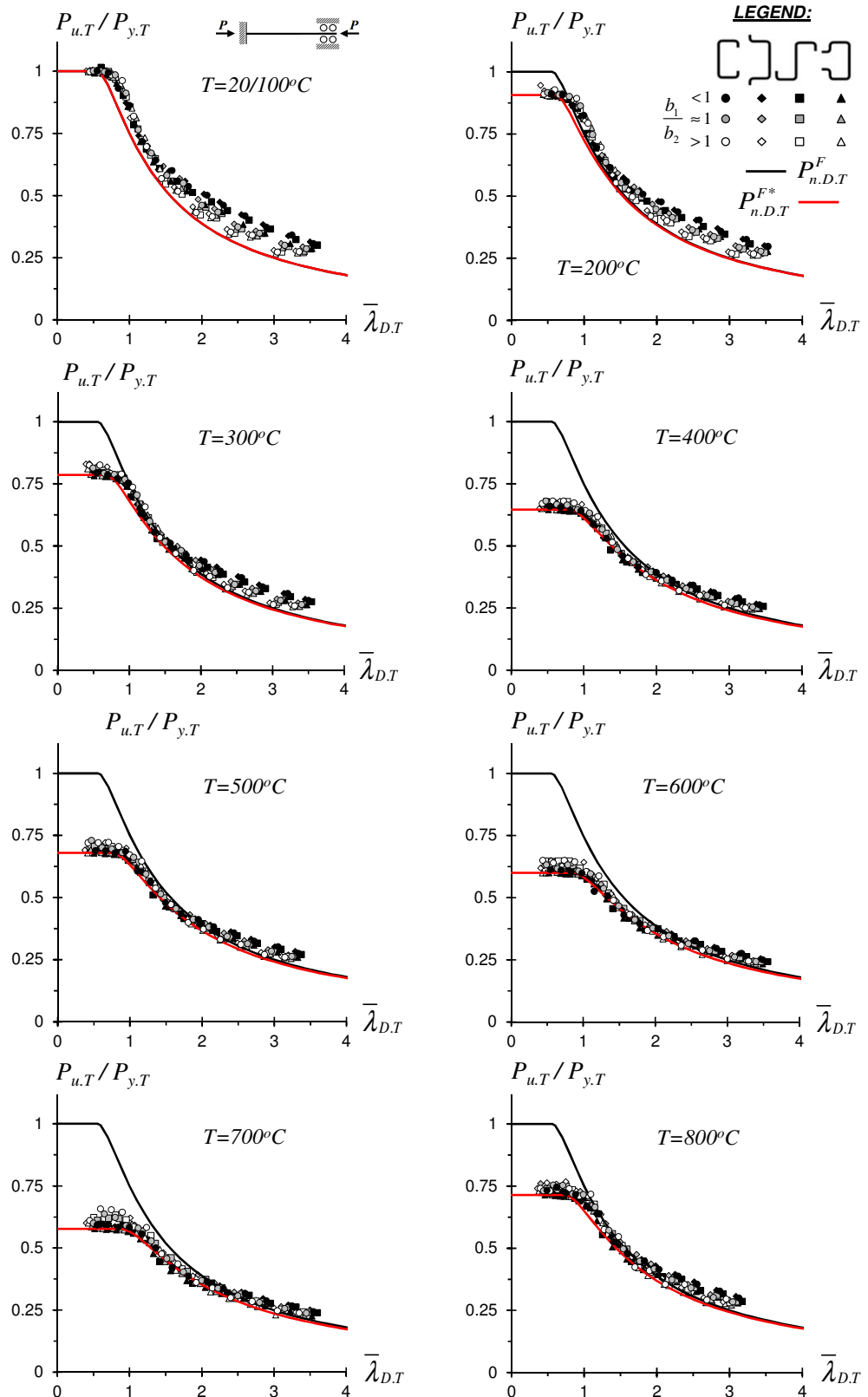


Figure 15. Comparison of the F-column failure loads with the available and modified DSM distortional design curves ($T=20/100-200-300-400-500-600-700-800^\circ C$)

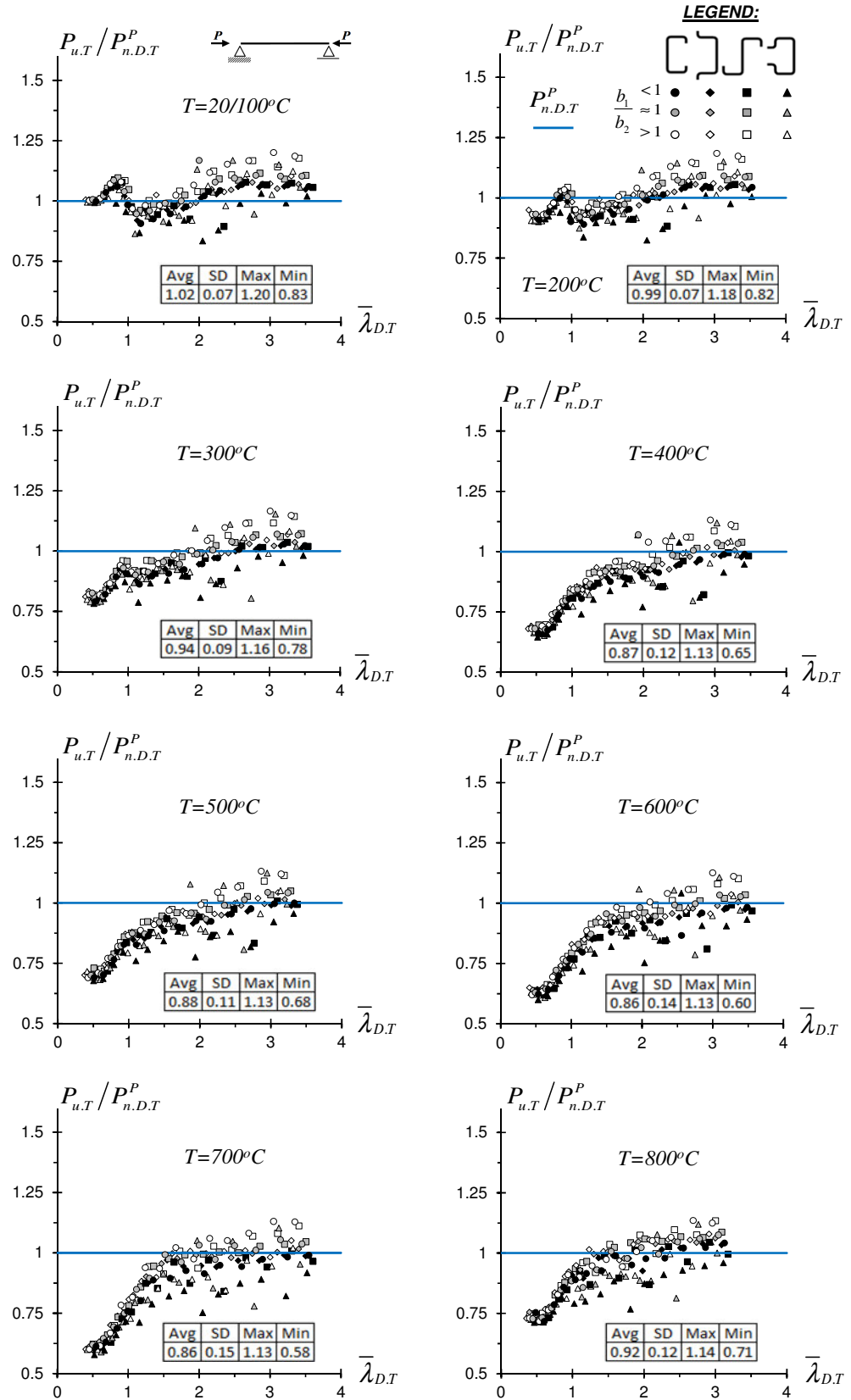


Figure 16. $P_{u,T} / P_{n,D,T}^P$ vs. $\bar{\lambda}_{D,T}$ plots of the P columns ($T=20/100-200-300-400-500-600-700-800^\circ C$)

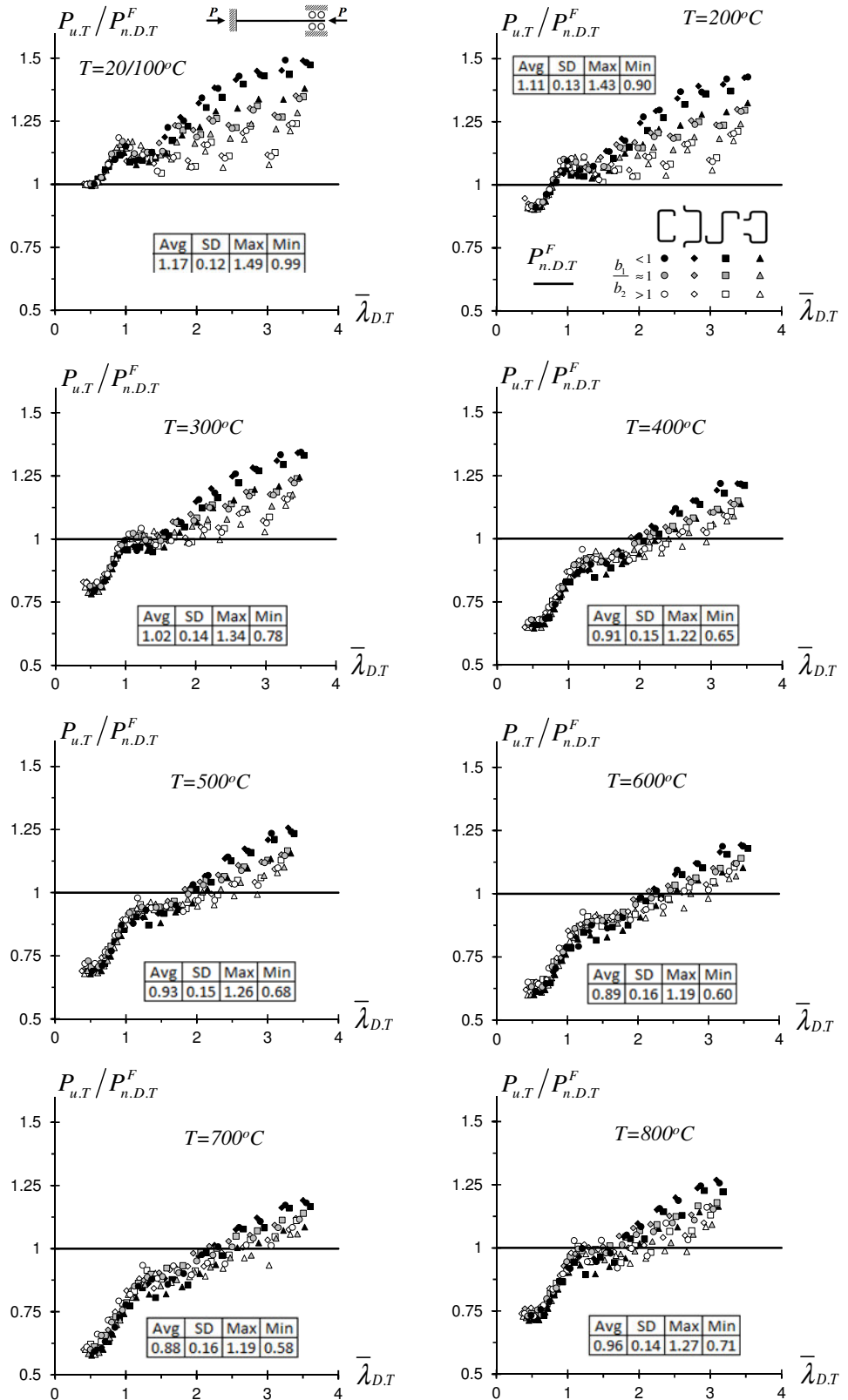


Figure 17. $P_{u,T} / P_{n,D,T}^F$ vs. $\bar{\lambda}_{D,T}$ plots of the F columns ($T=20/100-200-300-400-500-600-700-800\text{ }^\circ C$)

$$P_{n.D.T}^{P*} = \begin{cases} P_{y,20} \cdot k_p & \text{for } \bar{\lambda}_{D.T} \leq \eta \\ P_{y,T} \left[1 - \frac{0.25}{(k_p/k_y)} \left(P_{cr.D.T}/P_{y,T} \right)^{0.6} \right] \left(P_{cr.D.T}/P_{y,T} \right)^{0.6} & \text{for } \eta < \bar{\lambda}_{D.T} \leq 1 \\ P_{y,T} \left[1 - \frac{0.25}{(k_p/k_y)} \left(P_{cr.D.T}/P_{y,T} \right)^{0.9} \right] \left(P_{cr.D.T}/P_{y,T} \right)^{0.9} & \text{for } \bar{\lambda}_{D.T} > 1 \end{cases}, \quad (6)$$

with $\eta = 0.9284(k_p/k_y)^2 - 2.2244(k_p/k_y) + 1.8570$

$$P_{n.D.T}^{F*} = \begin{cases} P_{y,20} \cdot k_p & \text{for } \bar{\lambda}_{D.T} \leq \frac{0.561}{(k_p/k_y)} \\ P_{y,T} \left[1 - \frac{0.25}{(k_p/k_y)} \left(P_{cr.D.T}/P_{y,T} \right)^{0.6} \right] \left(P_{cr.D.T}/P_{y,T} \right)^{0.6} & \text{for } \bar{\lambda}_{D.T} > \frac{0.561}{(k_p/k_y)} \end{cases}. \quad (7)$$

These design equations differ from the available ones (Eqs. (4) and (5)) in the fact that (i) the squash load $P_{y,T}$ is replaced by $P_{y,20}k_p$ ($k_p=\sigma_{p,T}/\sigma_{p,20}$ defines the proportionality limit stress $\sigma_{p,T}$), (ii) the distortional slenderness transition value 0.561 is replaced by either $\eta=0.9284(k_p/k_y)^2 - 2.2244(k_p/k_y) + 1.8570$ (P columns) or $0.561/(k_p/k_y)$ (F columns)¹⁴, (iii) the coefficient 0.25 is replaced by $0.25/(k_p/k_y)$ and (iv) the P-column expressions valid for intermediate and slender column now differ only in the exponents (0.6 vs. 0.9), thus leading to a distortional slenderness transition value equal to 1.0 (instead of 1.133).

The DSM-based distortional design curves provided by Eqs. (6) and (7) (P and F columns) are displayed in Figs. 18(a)-(b), respectively. From the observation of these design curves it is readily concluded that:

- (i) The design curves concerning columns at room temperature either remain unchanged (F columns) or exhibit minute changes (P columns).

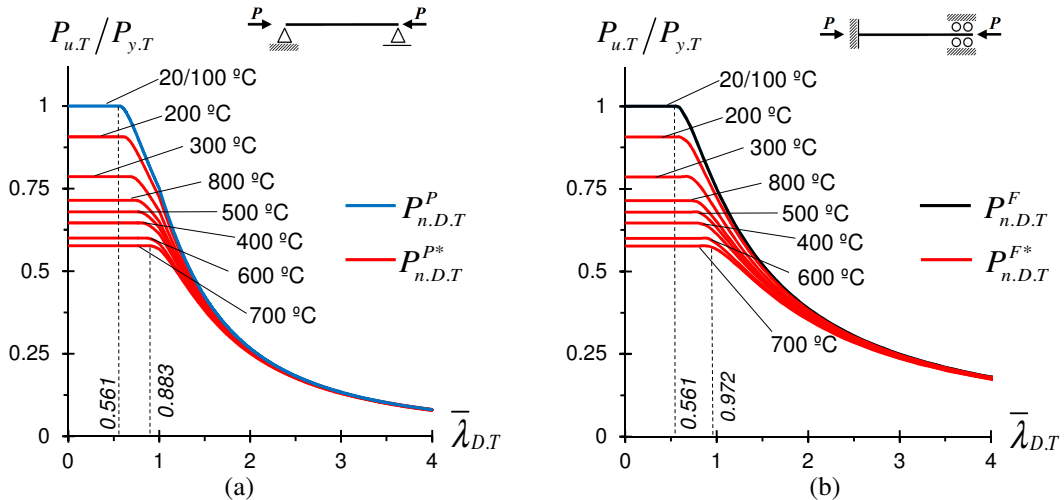


Figure 18. Comparison between the available and modified/lowered DSM distortional design curves for (a) P and (b) F columns at temperatures $T=20/100-200-300-400-500-600-700-800$ °C

¹⁴ Recall that EC3-1.2 prescribes $k_p=1-0.807-0.613-0.42-0.36-0.18-0.075-0.05$ and $k_y=1-0.89-0.78-0.65-0.53-0.3-0.13-0.07$ for $T=20/100-200-300-400-500-600-700-800$ °C, which leads to $\eta=0.561-0.603-0.682-0.807-0.774-0.857-0.883-0.742$.

- (ii) Although the design curves for P and F columns at elevated temperatures are modified, these modifications are felt only for slenderness values below around 2.0. Therefore, the failure load predictions concerning slender ($\lambda_{D,T} \geq 2.0$) P and F columns remain practically unaltered.
- (iii) Since the modification of the available design curves consists essentially of incorporating k_p/k_y into the column squash load and distortional slenderness transition values, it is just logical to expect that the temperature-dependence of this ratio will be directly reflected in the design curve variation with the temperature. Indeed, this is the case: as clearly illustrated in Figs. 18(a)-(b), for both the P and F columns, the modified design curves are ordered like the k_p/k_y values, *i.e.*, in the sequence $T=20/100-200-300-800-500-400-600-700\text{ }^{\circ}\text{C}$.

In order to assess the quality of the failure load predictions provided by the modified/lowered DSM-based design curves, Figs. 19 and 20 plot the $P_{u,T} / P_{n,D,T}^{P^*}$ or $P_{u,T} / P_{n,D,T}^{F^*}$ values against $\lambda_{D,T}$ and include also the associated statistical indicators (averages, standard deviations and maximum/minimum values). The corresponding $P_{u,T} / P_{n,D,T}^{P^*}$ and $P_{u,T} / P_{n,D,T}^{F^*}$ are given in Tables A1 to A4 (P columns at room temperature) and B1 to B4 (P and F columns at elevated temperatures), presented in Annexes A and B, respectively. The observation and analysis of the results (failure load predictions) presented in these figures and tables prompt the following remarks:

- (i) The $P_{u,T} / P_{n,D,T}^P$ and $P_{u,T} / P_{n,D,T}^{P^*}$ values for room temperature are very close to each other, as attested by the similarity between their statistical indicators (1.02-0.07-1.20-0.83 vs. 1.01-0.07-1.20-0.80).
- (ii) Despite the inherent simplicity of the modifications, the failure load estimates yielded by the modified/lowered proposed DSM distortional strength curves, for P and F columns at elevated temperatures, outperform those provided by their available counterparts.
- (iii) Concerning the P columns, the $P_{u,T} / P_{n,D,T}^{P^*}$ statistical indicators are very similar (and fairly good) for all the temperatures considered. Indeed, the average varies between 1.01 and 0.99, the standard deviation varies between 0.06 and 0.07, the maximum value varies between 1.14 and 1.20, and the minimum value varies between 0.79 and 0.76. Nevertheless, it should be noted that the numbers of unsafe predictions are still reasonably high, most of them concerning columns of intermediate slenderness, particularly rack-section ones – a similar finding was previously reported by the authors (Landesmann & Camotim 2013), following an investigation carried out in the context of R columns at room temperature. Further studies are required in order to develop and propose a DSM-based design curve that ensures a better quality of the P-column failure load prediction – obviously, the new features to be included in such design curve must focus on the intermediate slenderness range, in general, and on R columns, in particular.
- (iv) Concerning the F columns, the $P_{u,T} / P_{n,D,T}^{F^*}$ statistical indicators are again fairly similar and good for all the temperatures considered. Indeed, the variations of the average, standard deviation and maximum/minimum value are now from 1.06 to 1.14, 0.06 to 0.11, 1.24 to 1.44 and 1.00 to 0.94, respectively. Unlike for the P columns, the numbers of unsafe predictions are now very small (again for columns of intermediate slenderness) and the overestimations never exceed 6%.
- (v) The success of the above modifications, in the sense that they improve visibly the quality of the failure load prediction, provides encouragement to proceed with this approach in the search for an efficient (safe and reliable) DSM-based design methodology for columns failing in distortional modes at elevated temperatures. The next step consists of collecting all the numerical and experimental failure load data currently available in the literature, and assessing the merits of the proposed DSM-based design curves in predicting them. Such assessment will make it possible to obtain either additional evidence concerning the adequacy of such curves or guidelines for their improvement. It is

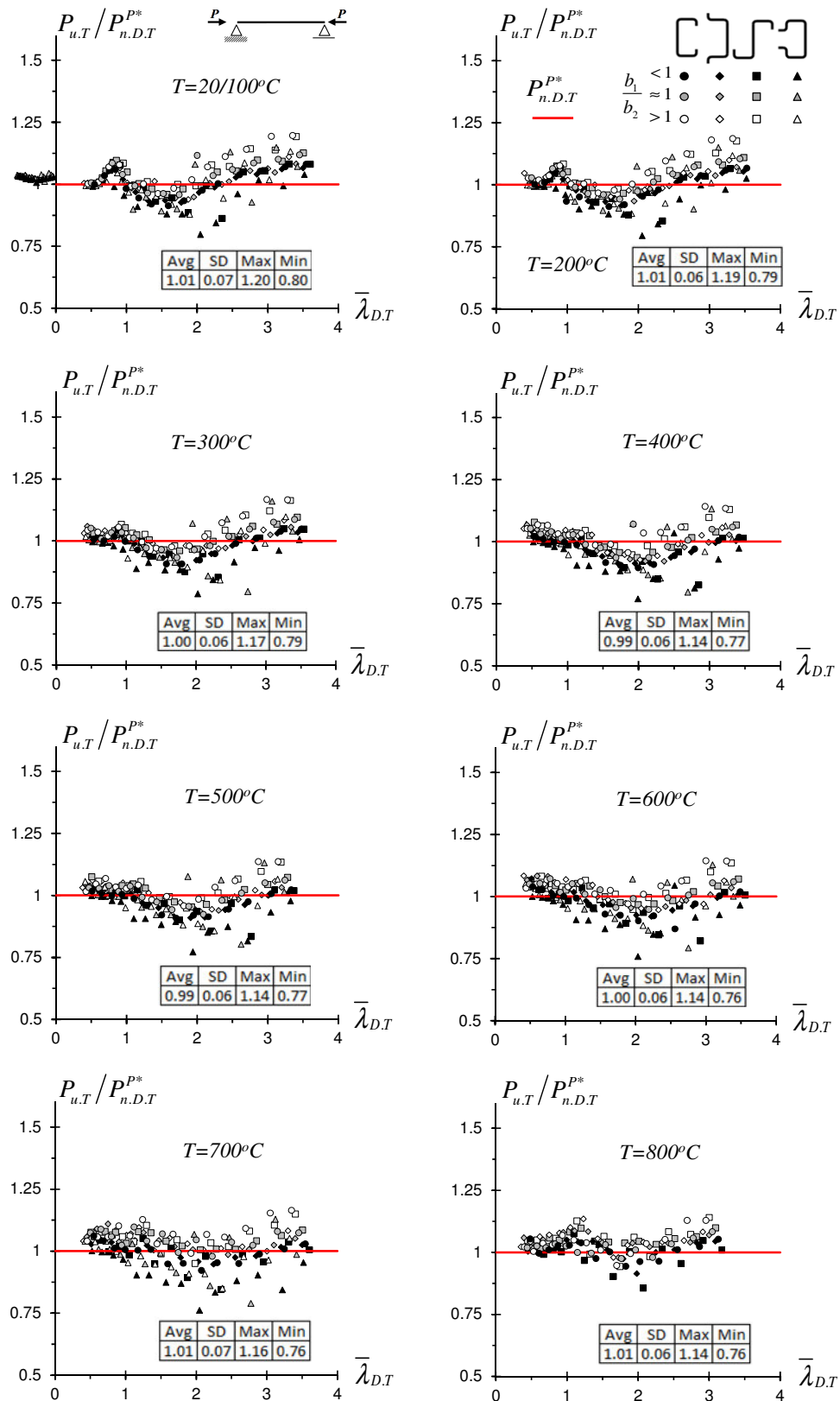


Figure 19. $P_{u,T} / P_{n,D,T}^{P*}$ ratios plotted against the distortional slenderness $\bar{\lambda}_{D,T}$ concerning P columns at temperatures $T=20/100-200-300-400-500-600-700-800^\circ C$.

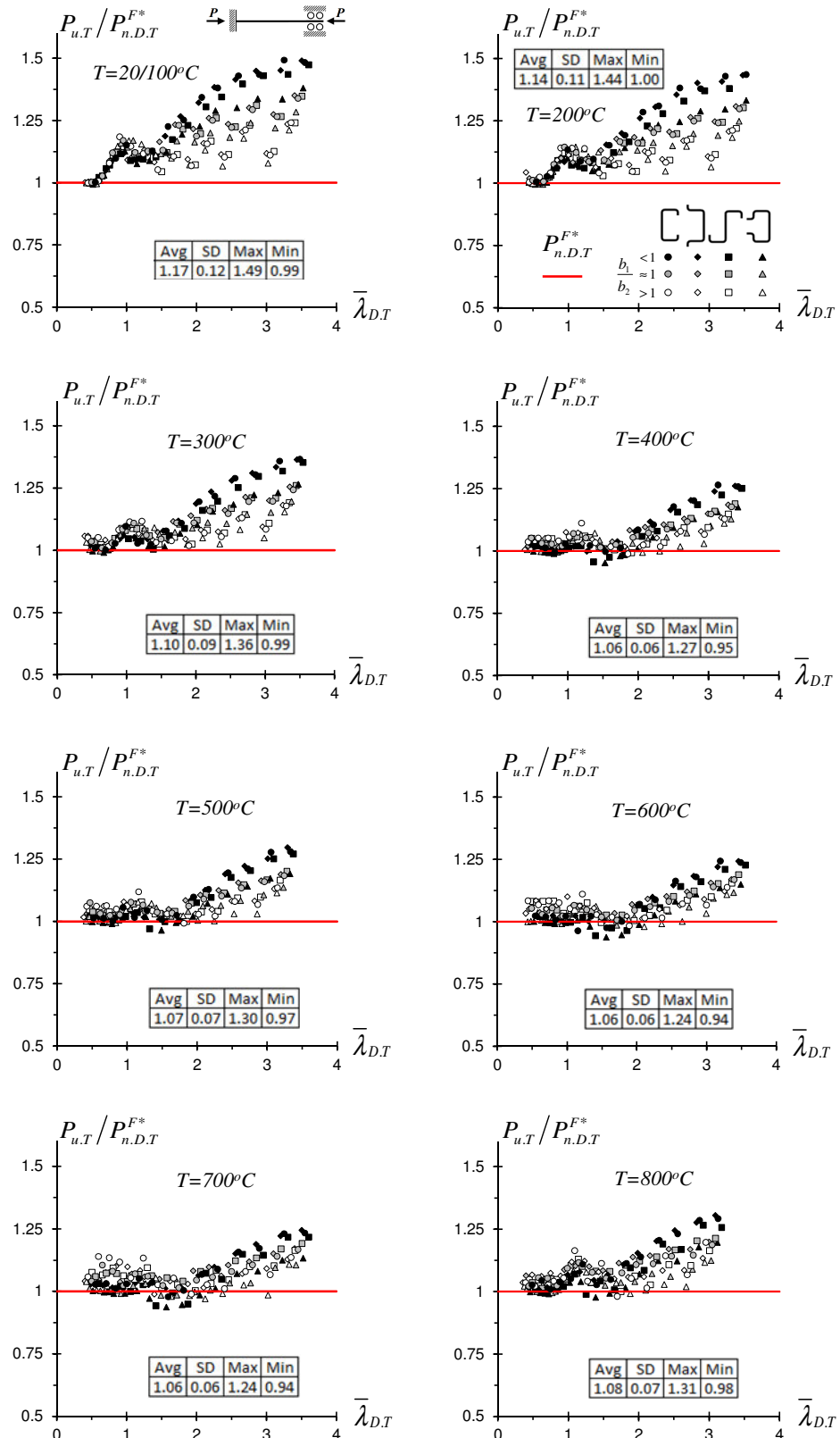


Figure 20. $P_{u,T} / P_{n,D,T}^{F*}$ ratios plotted against the distortional slenderness $\bar{\lambda}_{D,T}$ concerning F columns at temperatures $T=20/100-200-300-400-500-600-700-800^{\circ}C$

worth noting that, given the well known scarcity of column experimental distortional failure loads at elevated temperatures, the authors are also planning for the near future the performance of a test campaign involving lipped channel columns (at both room and elevated temperatures).

6 Concluding Remarks

This paper reported the most recent numerical (ANSYS SFEA) results of an ongoing investigation, initiated by the authors a few years ago, on the post-buckling behavior, ultimate strength and DSM design of cold-formed steel columns failing in distortional modes at elevated temperatures. These results concern 2688 columns that exhibit (i) four cross-section shapes (lipped channels, hats, zeds and racks), with various dimensions (six per shape) and lengths selected to ensure pure distortional buckling and failure modes, (ii) two support conditions (end cross-section fixed and pinned – P and F columns), differing mostly in the warping restraint (null or full), (iv) temperature-dependent material properties as prescribed by the EC3-1.2 model, (iv) seven room-temperature yield stresses, chosen to cover wide distortional slenderness ranges ($0.35 \leq \lambda_{D,T} \leq 3.6$), and (v) seven uniform temperatures (up to 800°C).

Several sets of elastic and elastic-plastic distortional post-buckling results, both at room and elevated temperatures, were presented and discussed, with the aim of acquiring in-depth knowledge about the joint influence of the (i) end support conditions, (ii) cross-section shape and dimensions and (iii) temperature level on the distortional structural response and load-carrying capacity of cold-formed steel columns. Then, a fairly extensive (2688 columns) parametric study was carried out to gather a significant data bank of column distortional failure loads, at both room and elevated temperatures. These failure loads were subsequently used to propose a first contribution towards the development of an efficient DSM-based design approach for columns failing in distortional modes at elevated temperatures.

Out of the various findings reported in this work, the following ones deserve to be specially mentioned:

- (i) Regardless of the temperature, the $P_{u,T}/P_{y,T}$ vs. $\lambda_{D,T}$ “clouds” follow the trend of “Winter-type” strength curves and exhibit a small amount of “vertical dispersion” (more visible in the F columns). Moreover, the $P_{u,T}/P_{y,T}$ values are much smaller in the P columns than in their F counterparts, due to the considerably lower post-critical strength of the former – this justifies the need for two different DSM distortional design curves. Finally, there is a visible influence of the width ratio b_1/b_2 on the F-column $P_{u,T}/P_{y,T}$ values, particularly in the moderate-to-high slenderness range (this stems again from post-critical strength differences) – such influence is not felt in the P columns.
- (ii) As expected, all the $P_{u,T}/P_{y,T}$ values concerning P and F columns at elevated temperatures ($T > 100^{\circ}\text{C}$) are below those concerning these columns at room/moderate temperatures ($T \leq 100^{\circ}\text{C}$). Moreover, the “size” (maximum $\lambda_{D,T}$ value) of the well defined plateaus appearing in the $P_{u,T}/P_{y,T}$ vs. $\lambda_{D,T}$ plots varies with the temperature and end support conditions. Those plateaus are followed by descending curve branches that are ordered in the sequence $T = 20/100-200-300-800-500-400-600-700^{\circ}\text{C}$, which is the same of the temperature-dependent reduction factor ratio k_p/k_y associated with the model prescribed in EC3-1.2 to quantify the variation of the steel constitutive law with the temperature.
- (iii) Following an approach already explored by other researchers (for F columns only), the available DSM design curves, developed in the context of P and F columns failing in distortional modes at room temperature, were employed to predict failure loads at elevated temperatures – predictions based on critical distortional buckling and squash loads calculated with the (temperature-dependent) reduced Young’s modulus and yield stress values prescribed in EC3-1.2. It was found that such failure load predictions are reasonably accurate and mostly safe only for columns with fairly high slenderness values ($\lambda_{D,T} > 2.0$). Outside of this slenderness range ($\lambda_{D,T} \leq 2.0$), the column failure

loads were shown to be clearly overestimated by the available DSM design curves, thus meaning that some modification was required.

- (iv) A modification of the available DSM distortional design curves, which involved the incorporation of the reduction factor ratio k_p/k_y (reduction factors prescribed in EC3-1.2), was proposed. It led to a set of temperature-dependent “lowered” strength curves that differ from the available ones only for slenderness values below around 2.0. In spite of the inherent simplicity of the above modification, the ensuing DSM distortional design curves were shown to improve visibly the quality of the failure load prediction, thus providing encouragement to proceed with this approach in the pursuit of an efficient DSM-based design methodology for columns failing in distortional modes at elevated temperatures.

The next step of this ongoing investigation consists of assessing the merits of the proposed DSM-based design curves in predicting numerical and experimental failure load data collected from the literature. The output of such assessment will provide either additional evidence on the adequacy of the proposed curves or guidelines to improve them. Moreover, the authors are also planning for the near future the performance of (i) a test campaign involving lipped channel columns (at room and elevated temperatures) and (ii) parametric studies aimed at gathering failure load data concerning columns with a wider variety of cross-section shapes and dimensions (e.g., cross-sections with intermediate stiffeners). Finally, in the long run, it is intended to extend this investigation to cover also columns subjected to non-uniform elevated temperature distributions.

References

- ABNT (Brazilian Standards Association) (2010). *Brazilian Standard on Design of Cold-Formed Steel Structures* (ABNT NBR 14762:2010), Rio de Janeiro. (Portuguese)
- Abreu JCB, Schafer BW (2013). Stability of cold-formed steel compression members under thermal gradients, *USB Proceedings of SSRC Annual Stability Conference* (St. Louis, 17-19/4).
- AISI (American Iron and Steel Institute) (2016). *North American Specification (NAS) for the Design of Cold-Formed Steel Structural Members* (AISI-S100-16), Washington DC.
- AS/NZS (Standards of Australia – SA – and Standards of New Zealand – SNZ) (2005). *Cold-Formed Steel Structures* (AS/NZS 4600 – 2nd ed.), Sydney-Wellington.
- Bebiano R, Pina P, Silvestre N, Camotim D (2008a). *GBTUL 1.0β – Code for Buckling and Vibration Analysis of Thin-Walled Members*, DECivil/IST, Technical University of Lisbon. (available at <http://www.civil.ist.utl.pt/gbt>)
- Bebiano R, Silvestre N, Camotim D (2008b). GBTUL – a code for the buckling analysis of cold-formed steel members, *Proceedings of 19th International Specialty Conference on Recent Research and Developments in Cold-Formed Steel Design and Construction* (St. Louis, 14-15/10), R LaBoube, WW Yu (eds.), 61-79.
- Camotim D, Dinis PB, Martind AD (2016). Direct Strength Method (DSM) – a general approach for the design of cold-formed steel structures, *Recent Trends in Cold-Formed Steel Construction*, C. Yu (ed.), Woodhead Publishing (Series in Civil and Structural Engineering), Amsterdam, 69-105.
- Chen J, Young B (2006). Corner properties of cold-formed steel sections at elevated temperatures, *Thin-Walled Structures*, **44**(2), 216-223.
- Chen J, Young B (2007a). Experimental investigation of cold-formed steel material at elevated temperatures. *Thin-Walled Structures*, **45**(1), 96-110.
- Chen J, Young B (2007b). Cold-formed steel lipped channel columns at elevated temperatures, *Engineering Structures*, **29**(10), 2445-2456.
- Chen J, Young B (2008). Design of high strength steel columns at elevated temperatures, *Journal of Constructional Steel Research*, **64**(6), 689-703.
- Chen W, Ye J, Bai Y, Zhao XL (2012). Full-scale fire experiments on load-bearing cold-formed steel walls lined with different panels, *Journal of Constructional Steel Research*, **79**(December), 242-254.

- Chen W, Ye J, Bai Y, Zhao XL (2013). Improved fire resistant performance of load bearing cold-formed steel interior and exterior wall systems, *Thin-Walled Structures*, **73**(December), 145-157.
- Comité Européen de Normalisation (CEN) (2005). *Eurocode 3: Design of Steel Structures – Part 2: General Rules – Structural Fire Design*, Brussels.
- Ellobody E (2013). A consistent nonlinear approach for analysing steel, cold-formed steel, stainless steel and composite columns at ambient and fire conditions, *Thin-Walled Structures*, **68**(July), 1-17.
- Ellobody E, Young B (2005). Behaviour of cold-formed steel plain angle columns, *Journal of Structural Engineering* (ASCE), **131**(3), 457-466.
- Feng M, Wang YC (2005a). An analysis of the structural behaviour of axially loaded full-scale cold-formed thin-walled steel structural panels tested under fire conditions, *Thin-Walled Structures*, **43**(2), 291-332.
- Feng M, Wang YC (2005b). An experimental study of loaded full-scale cold-formed thin-walled steel structural panels under fire conditions, *Fire Safety Journal*, **40**(1), 43-63.
- Feng M, Wang YC, Davies JM (2003a). Structural behaviour of cold-formed thin-walled short steel channel columns at elevated temperatures – Part 1: experiments, *Thin-Walled Structures*, **41**(6), 543-570.
- Feng M, Wang YC, Davies JM (2003b). Structural behaviour of cold-formed thin-walled short steel channel columns at elevated temperatures – Part 2: design calculations and numerical analysis, *Thin-Walled Structures*, **41**(6), 571-594.
- Feng M, Wang YC, Davies JM (2003c). Thermal performance of cold-formed thin-walled steel panel systems in fire, *Fire Safety Journal*, **38**(4), 365-394.
- Feng M, Wang YC, Davies JM (2003d). Axial strength of cold-formed thin-walled steel channels under non-uniform temperatures in fire, *Fire Safety Journal*, **38**(8), 679-707.
- Feng M, Wang YC, Davies JM (2004). A numerical imperfection sensitivity study of cold-formed thin-walled tubular steel columns at uniform elevated temperatures, *Thin-Walled Structures*, **42**(4), 533-555.
- Gunalan S, Kolarkar P, Mahendran M (2013). Experimental study of load bearing cold-formed steel wall systems under fire conditions, *Thin-Walled Structures*, **65**(April), 72-92.
- Gunalan S, Mahendran M (2013a). Finite element modelling of load bearing cold-formed steel wall systems under fire conditions, *Engineering Structures*, **56**(November), 1007-1027.
- Gunalan S, Mahendran M (2013b). Development of improved fire design rules for cold-formed steel wall systems, *Journal of Constructional Steel Research*, **88**(September), 339-362.
- Kaitila O (2002). Imperfection sensitivity analysis of lipped channel columns at high temperatures, *Journal of Constructional Steel Research*, **58**(3), 333-51.
- Kankanamge ND, Mahendran M (2012). Behaviour and design of cold-formed steel beams subject to lateral-torsional buckling at elevated temperatures, *Thin-Walled Structures*, **61**(December), 213-228.
- Laím L, Rodrigues JPC, Silva LS (2014). Experimental analysis on cold-formed steel beams subjected to fire, *Thin-Walled Structures*, **74**(January), 104-117.
- Landesmann A, Camotim D (2010a). Distortional failure and design of cold-formed steel lipped channel columns under fire conditions, *Proceedings of SSRC Annual Stability Conference* (Orlando, 12-15/5), 505-532.
- Landesmann A, Camotim D (2010b). Distortional failure and design of cold-formed steel rack-section columns under fire conditions, *Proceedings of Fourth International Conference on Steel & Composite Structures* (ICSCS'2011 – Sydney, 21-23/7), B. Uy *et al.* (eds.), 287-289. (full paper in CD-ROM Proceedings)
- Landesmann A, Camotim D (2011). On the distortional buckling, post-buckling and strength of cold-formed steel lipped channel columns under fire conditions, *Journal of Structural Fire Engineering*, **2**(1), 1-19.
- Landesmann A, Camotim D (2012). Application of direct strength method design to distortional buckling resistance of thin-walled steel columns exposed to fire, *Proceedings of Eleventh International Conference on Computational Structures Technology* (CST 2012 – Dubrovnik, 4-7/9), B.H.V. Topping. (ed.), Civil-Comp Press (Stirling), paper 30. (full paper in USB Key Drive Proceedings).
- Landesmann A, Camotim D (2013). On the Direct Strength Method (DSM) design of cold-formed steel columns against distortional failure, *Thin-Walled Structures*, **2**(67), 168-187.
- Landesmann A, Camotim D (2015). DSM to predict distortional failures in cold-formed steel columns exposed to fire: effect of the constitutive law temperature-dependence, *Computers & Structures*, **147**(15 January), 47-67.

- Landesmann A, Camotim D, Basaglia C (2013). Distortional post-buckling behavior and strength of cold-formed steel columns: how does the cross-section affect it?", *USB Key Drive Proceedings of 2013 SSRC Annual Stability Conference* (St. Louis, 16-20/4).
- Lee JH, Mahendran M, Makelainen P (2003). Prediction of mechanical properties of light gauge steels at elevated temperatures, *Journal of Constructional Steel Research*, **59**(12), 1517-1532.
- Lim JBP, Young B (2007). Effects of elevated temperatures on bolted moment-connections between cold-formed steel members, *Engineering Structures*, **29**(10), 2419-2427.
- Outinen J, Kaitila O, Makelainen P (2000). A study for the development of the design of steel structures in fire conditions, *Proceedings of First International Workshop on Structures in Fire* (SiF 2000 – Copenhagen, 19-20/6), JM Franssen (ed.), 267-281.
- Prola LC, Camotim D. (2002a). On the distortional post-buckling behavior of cold-formed lipped channel steel columns, *Proceedings of SSRC 2002 Annual Stability Conference* (Seattle, 24-27/4), 571-590.
- Prola LC, Camotim D. (2002b). On the distortional post-buckling behaviour of rack-section cold-formed steel columns, *Proceedings of Sixth International Conference on Computational Structures Technology* (CST 2002 – Prague, 4-6/9), B. Topping, Z. Bittnar (eds.), Civil-Comp Press (Stirling), 233-234. (full paper in CD-ROM Proceedings).
- Ranawaka T (2006). *Distortional Buckling Behaviour of Cold-Formed Steel Compression Members at Elevated Temperatures*, Ph.D. Thesis, Queensland University of Technology, Australia.
- Ranawaka T, Mahendran M (2009). Distortional buckling tests of cold-formed steel compression members at elevated temperatures, *Journal of Constructional Steel Research*, **65**(2), 249-259.
- Ranawaka T, Mahendran M (2010). Numerical modelling of light gauge cold-formed steel compression members subjected to distortional buckling at elevated temperatures, *Thin-Walled Structures*, **48**(3-4), 334-344.
- SAS (Swanson Analysis Systems Inc.) (2009). *ANSYS Reference Manual* (version 12).
- Schafer BW (2000). *Distortional Buckling of Cold-Formed Steel Columns*, American Iron and Steel Institute (AISI) Report, Washington DC.
- Schafer BW (2008). Review: the Direct Strength Method of cold-formed steel member design, *Journal of Constructional Steel Research*, **64**(7-8), 766-788.
- Shahbazian A, Wang YC (2011a). Calculating the global buckling resistance of thin-walled steel members with uniform and non-uniform elevated temperatures under axial compression, *Thin-Walled Structures*, **49**(11), 1415-1428.
- Shahbazian A, Wang YC (2011b). Application of the Direct Strength Method to local buckling resistance of thin-walled steel members with non-uniform elevated temperatures under axial compression, *Thin-Walled Structures*, **49**(12), 1573-1583.
- Shahbazian A, Wang YC (2012). Direct Strength Method for calculating distortional buckling capacity of cold-formed thin-walled steel columns with uniform and non-uniform elevated temperatures, *Thin-Walled Structures*, **53**(April), 188-199.
- Shahbazian A, Wang YC (2013). A simplified approach for calculating temperatures in axially loaded cold-formed thin-walled steel studs in wall panel assemblies exposed to fire from one side, *Thin-Walled Structures*, **64**(March), 60-72.
- Shahbazian A, Wang YC (2014). A fire resistance design method for thin-walled steel studs in wall panel constructions exposed to parametric fires, *Thin-Walled Structures*, **77**(April), 67-76.
- Silvestre N, Camotim D (2006). Local-plate and distortional post-buckling behavior of cold-formed steel lipped channel columns with intermediate stiffeners. *Journal of Structural Engineering* (ASCE), **132**(4), 529-540.
- Zhao B, Kruppa J, Renaud C, O'Connor M, Mecozzi E et al. (2005), *Calculation Rules of Lightweight Steel Sections in Fire Situations*, EUR-21426 (Technical Steel Research Series) – Steel Products and Applications for Building, Construction and Industry, European Commission Technical Steel Research, Luxembourg.

ANNEX A – DATA CONCERNING COLUMNS AT ROOM TEMPERATURE

Tables A1 to A4 provide information concerning the column numerical failure loads and their DSM-based estimates. Each table deals with one column cross-section shape (C, H, Z, R) and the two end support conditions considered (P and F). It includes the values of the (i) distortional slenderness $\lambda_{D,20}$, (ii) squash load $P_{y,20}$, (iii) numerical failure load $P_{u,20}$, and (iv) numerical-to-predicted failure load ratios $P_{u,20} / P_{n,D,20}$, $P_{u,20} / P_{n,D,20}^P$ and $P_{u,20} / P_{n,D,20}^{P*}$ (P columns), and $P_{u,20} / P_{n,D,20}$ (F columns).

Table A1: Numerical failure loads and their DSM estimates concerning the pinned and fixed lipped channel columns

Column	Pinned (P)					Fixed (F)				
	$\bar{\lambda}_{D,20}$	$P_{v,20}$ (kN)	$P_{u,20}$ (kN)	$\frac{P_{u,20}}{P_{n,D,20}}$	$\frac{P_{u,20}}{P_{n,D,20}^P}$	$\frac{P_{u,20}}{P_{n,D,20}^{P^*}}$	$\bar{\lambda}_{D,20}$	$P_{v,20}$ (kN)	$P_{u,20}$ (kN)	$\frac{P_{u,20}}{P_{n,D,20}}$
C130	0.45	35.55	35.59	1.00	1.00	1.00	0.45	48.78	48.69	1.00
	0.75	97.56	95.41	1.07	1.07	1.07	0.75	136.42	134.33	1.08
	1.06	195.12	134.99	0.97	0.97	0.99	1.06	272.02	222.91	1.15
	1.44	362.14	156.70	0.80	0.98	0.96	1.45	506.00	287.18	1.05
	1.93	643.25	185.96	0.72	1.07	1.02	1.92	897.90	387.40	1.07
	2.40	999.60	217.86	0.68	1.15	1.11	2.40	1395.64	491.29	1.10
	3.05	1614.74	250.10	0.63	1.20	1.19	3.05	2253.86	613.45	1.11
C150	0.50	23.85	23.98	1.01	1.01	1.01	0.60	52.15	52.19	1.01
	0.80	60.82	58.15	1.09	1.09	1.09	0.90	118.30	113.82	1.18
	1.12	119.25	77.10	0.95	0.95	0.99	1.24	223.87	155.95	1.12
	1.52	220.61	88.05	0.78	0.99	0.96	1.67	407.04	210.34	1.11
	2.00	381.60	113.46	0.77	1.17	1.12	2.15	674.16	279.98	1.16
	2.50	596.25	115.49	0.63	1.09	1.06	2.70	1063.39	361.69	1.21
	3.15	945.65	127.88	0.57	1.10	1.10	3.35	1637.06	448.27	1.24
C180	0.55	14.72	14.69	1.00	1.00	1.00	0.50	33.39	33.44	1.00
	0.84	34.95	31.50	1.06	1.06	1.06	0.80	85.86	84.57	1.12
	1.18	68.07	39.02	0.88	0.91	0.94	1.12	168.14	128.58	1.12
	1.59	125.09	44.04	0.72	0.95	0.91	1.52	308.86	179.46	1.13
	2.07	211.56	51.82	0.66	1.02	0.98	2.00	535.43	246.55	1.19
	2.60	332.97	59.09	0.61	1.07	1.04	2.50	837.14	312.19	1.22
	3.25	518.78	64.64	0.55	1.07	1.07	3.15	1328.45	397.43	1.27
C200a	0.60	38.16	38.22	1.01	1.01	1.01	0.65	41.34	41.24	1.03
	0.90	85.22	74.64	1.08	1.08	1.08	0.95	87.45	79.74	1.17
	1.24	161.54	91.09	0.91	0.98	1.00	1.30	163.77	109.87	1.13
	1.67	292.56	103.06	0.75	1.02	0.98	1.75	294.15	161.72	1.23
	2.15	484.63	122.55	0.70	1.12	1.07	2.23	478.59	207.02	1.25
	2.70	764.47	139.81	0.65	1.17	1.14	2.80	756.84	263.87	1.29
	3.35	1177.87	155.38	0.60	1.19	1.20	3.45	1149.57	328.40	1.34
C200b	0.65	28.62	28.48	1.02	1.02	1.02	0.55	22.08	22.10	1.00
	0.94	60.42	49.20	1.04	1.04	1.04	0.85	51.51	47.96	1.10
	1.30	114.48	58.09	0.85	0.96	0.96	1.18	99.34	71.28	1.10
	1.75	206.70	65.89	0.71	1.00	0.96	1.59	182.12	109.48	1.23
	2.23	335.49	77.32	0.67	1.08	1.03	2.07	309.06	154.95	1.34
	2.80	531.06	86.78	0.61	1.11	1.09	2.60	485.66	203.04	1.43
	3.45	806.13	94.42	0.55	1.10	1.12	3.25	759.77	258.77	1.49
C200c	0.69	20.44	20.17	1.03	1.03	1.03	0.71	30.66	30.51	1.06
	0.99	42.93	31.78	0.98	0.98	0.98	1.00	61.33	52.93	1.15
	1.36	79.72	36.28	0.79	0.92	0.92	1.37	114.48	73.50	1.13
	1.82	143.09	41.76	0.68	0.98	0.93	1.82	202.38	108.66	1.25
	2.30	228.95	48.50	0.63	1.04	1.00	2.30	325.03	149.79	1.38
	2.90	363.87	54.44	0.58	1.07	1.05	2.90	515.14	191.70	1.43
	3.55	545.80	58.87	0.52	1.06	1.08	3.55	772.71	236.87	1.48

Table A2: Numerical failure loads and their DSM estimates concerning the pinned and fixed hat-section columns

Column	Pinned (P)					Fixed (F)			
	$\bar{\lambda}_{D,20}$	$P_{y,20}$ (kN)	$P_{u,20}$ (kN)	$\frac{P_{u,20}}{P_{n,D,20}}$	$\frac{P_{u,20}}{P_{n,D,20}^P}$	$\bar{\lambda}_{D,20}$	$P_{y,20}$ (kN)	$P_{u,20}$ (kN)	$\frac{P_{u,20}}{P_{n,D,20}}$
H130	0.40	28.11	28.23	1.00	1.00	0.40	39.69	39.72	1.00
	0.70	85.99	85.47	1.05	1.05	0.70	120.71	119.70	1.05
	1.01	179.42	133.58	1.00	1.00	1.01	250.52	203.46	1.09
	1.40	342.30	164.01	0.86	1.02	1.40	478.72	288.97	1.08
	1.87	617.62	171.98	0.67	0.98	1.87	864.01	392.06	1.09
	2.35	970.66	197.12	0.62	1.04	2.35	1357.61	493.39	1.11
	3.00	1582.50	224.60	0.57	1.07	3.00	2212.52	616.93	1.12
H150	0.45	19.08	19.18	1.01	1.01	0.45	27.43	27.51	1.00
	0.75	53.66	52.57	1.07	1.07	0.75	75.13	74.63	1.09
	1.07	109.71	74.28	0.96	0.96	1.07	153.83	120.18	1.10
	1.47	206.30	85.90	0.78	0.97	1.47	289.78	178.90	1.16
	1.95	363.71	95.73	0.66	0.99	1.95	510.39	246.95	1.21
	2.45	573.59	109.75	0.61	1.05	2.45	806.13	310.32	1.23
	3.10	918.23	121.28	0.55	1.05	3.10	1290.29	395.58	1.27
H180	0.51	12.88	12.90	1.00	1.00	0.49	16.56	16.63	1.00
	0.80	31.27	29.64	1.07	1.07	0.80	44.15	42.52	1.09
	1.13	62.55	38.96	0.92	0.92	1.13	88.30	65.47	1.09
	1.55	117.74	44.45	0.75	0.96	1.55	167.41	100.08	1.19
	2.03	202.36	50.94	0.66	1.01	2.03	286.98	144.89	1.32
	2.55	320.10	58.12	0.61	1.06	2.55	454.39	191.75	1.41
	3.20	504.06	63.83	0.55	1.06	3.20	713.78	240.65	1.45
H200a	0.55	31.80	31.85	1.00	1.00	0.55	44.52	44.74	1.00
	0.85	76.32	69.98	1.08	1.08	0.85	105.58	100.35	1.12
	1.19	148.82	87.66	0.91	0.95	1.19	207.34	148.81	1.11
	1.62	277.30	98.19	0.74	0.98	1.62	385.42	205.45	1.11
	2.10	465.55	114.16	0.67	1.04	2.10	647.45	275.98	1.16
	2.65	741.58	130.41	0.61	1.09	2.65	1031.59	355.41	1.20
	3.30	1148.62	144.41	0.56	1.10	3.30	1598.90	443.07	1.23
H200b	0.59	23.85	23.87	1.00	1.00	0.61	34.98	34.99	1.01
	0.91	55.65	47.92	1.06	1.06	0.90	77.91	71.80	1.14
	1.25	106.53	57.49	0.87	0.96	1.25	149.46	104.49	1.13
	1.69	193.98	64.18	0.72	0.98	1.69	273.48	155.38	1.23
	2.18	321.18	74.63	0.66	1.05	2.18	451.56	201.69	1.26
	2.75	511.98	83.95	0.60	1.08	2.75	721.86	258.03	1.30
	3.40	783.87	91.05	0.54	1.07	3.40	1101.87	322.91	1.35
H200c	0.65	18.40	18.26	1.02	1.02	0.66	26.57	26.44	1.03
	0.95	38.84	30.99	1.02	1.02	0.95	55.19	48.13	1.12
	1.30	73.59	36.11	0.82	0.93	1.32	106.30	70.53	1.12
	1.78	136.96	41.10	0.68	0.97	1.77	192.16	107.16	1.27
	2.25	218.73	47.43	0.63	1.03	2.25	310.72	146.97	1.38
	2.85	351.60	53.50	0.57	1.06	2.85	498.79	190.93	1.45
	3.50	531.49	57.81	0.52	1.05	3.50	752.27	235.29	1.49

Table A3: Numerical failure loads and their DSM estimates concerning the pinned and fixed zed-section columns

Column	Pinned (P)						Fixed (F)			
	$\bar{\lambda}_{D,20}$	$P_{v,20}$ (kN)	$P_{u,20}$ (kN)	$\frac{P_{u,20}}{P_{n,D,20}}$	$\frac{P_{u,20}}{P_{n,D,20}^P}$	$\frac{P_{u,20}}{P_{n,D,20}^{P^*}}$	$\bar{\lambda}_{D,20}$	$P_{y,20}$ (kN)	$P_{u,20}$ (kN)	$\frac{P_{u,20}}{P_{n,D,20}}$
Z130	0.50	43.82	43.61	1.00	1.00	1.00	0.50	60.36	60.12	1.00
	0.80	111.62	106.65	1.09	1.09	1.09	0.80	155.44	150.19	1.10
	1.11	214.14	140.08	0.95	0.95	0.99	1.11	299.30	229.52	1.12
	1.49	388.60	158.02	0.78	0.98	0.95	1.49	542.38	295.21	1.04
	1.97	678.80	183.21	0.69	1.04	0.99	1.97	946.69	398.28	1.07
	2.45	1045.08	211.60	0.65	1.11	1.07	2.45	1457.65	505.40	1.11
	3.10	1672.62	239.80	0.60	1.14	1.14	3.10	2333.23	631.33	1.12
Z150	0.55	28.62	28.63	1.00	1.00	1.00	0.55	40.55	40.57	1.00
	0.85	69.17	63.96	1.09	1.09	1.09	0.85	96.59	91.77	1.12
	1.17	131.18	80.15	0.93	0.96	1.00	1.17	183.65	132.88	1.10
	1.57	234.92	88.95	0.76	0.99	0.96	1.57	330.32	183.93	1.12
	2.05	401.87	101.83	0.67	1.04	0.99	2.05	564.05	254.74	1.20
	2.55	621.29	115.65	0.62	1.08	1.05	2.55	871.72	318.56	1.22
	3.20	977.85	127.41	0.56	1.09	1.09	3.20	1373.76	403.56	1.26
Z180	0.61	18.40	18.36	1.01	1.01	1.01	0.60	25.75	26.12	1.02
	0.91	40.47	35.20	1.08	1.08	1.08	0.90	58.87	53.12	1.11
	1.24	75.42	41.96	0.89	0.96	0.98	1.23	108.54	74.58	1.09
	1.64	132.45	46.03	0.73	0.98	0.94	1.65	195.00	108.36	1.17
	2.13	222.60	53.25	0.66	1.04	0.99	2.13	325.61	154.16	1.30
	2.65	345.85	60.04	0.61	1.08	1.05	2.65	505.90	202.09	1.40
	3.30	537.17	65.59	0.54	1.07	1.08	3.30	783.68	252.11	1.43
Z200a	0.65	44.52	44.40	1.02	1.02	1.02	0.65	61.06	61.04	1.02
	0.95	94.13	79.75	1.08	1.08	1.08	0.95	131.02	117.23	1.14
	1.29	174.26	93.77	0.89	1.00	1.01	1.29	242.95	160.88	1.10
	1.72	310.37	105.71	0.75	1.04	1.00	1.72	431.21	217.50	1.11
	2.20	508.80	124.30	0.70	1.12	1.08	2.20	705.96	288.46	1.17
	2.75	793.73	140.76	0.64	1.17	1.14	2.75	1102.82	372.85	1.23
	3.40	1213.49	155.15	0.59	1.18	1.19	3.40	1686.67	453.44	1.24
Z200b	0.70	33.39	33.16	1.05	1.05	1.05	0.70	47.70	47.56	1.06
	1.00	68.37	53.43	1.05	1.05	1.05	1.00	96.99	82.91	1.14
	1.35	124.02	60.31	0.85	0.98	0.98	1.35	176.49	114.14	1.12
	1.79	217.83	68.06	0.72	1.02	0.98	1.80	311.64	164.02	1.21
	2.28	351.39	78.93	0.66	1.09	1.05	2.27	499.26	212.62	1.26
	2.85	550.14	88.04	0.61	1.11	1.10	2.85	783.87	271.31	1.31
	3.50	829.98	95.34	0.55	1.10	1.12	3.50	1182.96	334.32	1.35
Z200c	0.75	24.53	23.60	1.05	1.05	1.05	0.75	34.75	33.89	1.07
	1.04	47.02	33.31	0.98	0.98	0.99	1.05	67.46	52.95	1.09
	1.41	85.86	37.36	0.79	0.94	0.93	1.41	122.65	74.55	1.10
	1.87	151.27	39.90	0.63	0.92	0.88	1.87	214.64	109.82	1.23
	2.35	239.17	41.91	0.54	0.89	0.86	2.35	339.34	148.78	1.34
	2.95	378.18	54.77	0.57	1.06	1.05	2.95	533.54	194.00	1.43
	3.60	562.16	59.03	0.52	1.05	1.08	3.60	795.20	238.33	1.47

Table A4: Numerical failure loads and their DSM estimates concerning the pinned and fixed rack-section columns

Column	Pinned (P)						Fixed (F)			
	$\bar{\lambda}_{D,20}$	$P_{y,20}$ (kN)	$P_{u,20}$ (kN)	$\frac{P_{u,20}}{P_{n,D,20}}$	$\frac{P_{u,20}}{P_{n,D,20}^P}$	$\frac{P_{u,20}}{P_{n,D,20}^{P^*}}$	$\bar{\lambda}_{D,20}$	$P_{y,20}$ (kN)	$P_{u,20}$ (kN)	$\frac{P_{u,20}}{P_{n,D,20}}$
R130	0.43	30.78	30.61	0.99	0.99	0.99	0.43	43.60	43.55	1.00
	0.72	88.91	83.62	1.01	1.01	1.01	0.72	125.67	123.48	1.06
	1.04	182.09	126.73	0.95	0.95	0.97	1.03	256.47	218.79	1.17
	1.42	342.81	150.46	0.80	0.97	0.95	1.42	483.87	295.01	1.11
	1.90	612.96	156.33	0.62	0.92	0.88	1.90	866.00	379.77	1.07
	2.37	957.48	180.55	0.58	0.98	0.94	2.37	1352.44	465.63	1.07
	3.03	1554.19	208.52	0.54	1.03	1.02	3.03	2194.50	585.20	1.08
R150	0.47	21.97	21.89	1.00	1.00	1.00	0.47	31.74	31.65	1.00
	0.78	59.81	57.64	1.08	1.08	1.08	0.78	85.44	83.46	1.09
	1.10	119.62	71.77	0.86	0.86	0.90	1.10	170.88	138.95	1.17
	1.50	222.15	84.42	0.73	0.92	0.89	1.49	317.35	185.08	1.12
	1.97	386.93	113.96	0.75	1.13	1.08	1.98	555.37	253.62	1.16
	2.47	607.85	127.95	0.68	1.17	1.13	2.48	871.50	317.86	1.18
	3.13	970.37	138.63	0.60	1.15	1.15	3.12	1389.03	404.17	1.22
R180	0.52	14.94	14.82	0.99	0.99	0.99	0.52	22.41	22.27	0.99
	0.83	37.35	31.80	0.99	0.99	0.99	0.82	56.03	53.35	1.10
	1.16	72.84	41.09	0.85	0.87	0.91	1.15	110.20	79.06	1.08
	1.57	134.48	46.54	0.70	0.91	0.88	1.57	205.45	114.80	1.12
	2.05	227.86	46.54	0.54	0.83	0.80	2.05	349.26	162.10	1.23
	2.58	360.47	60.18	0.57	0.99	0.96	2.58	552.85	212.45	1.30
	3.22	564.05	66.09	0.51	0.99	0.99	3.23	866.62	266.53	1.34
R200a	0.57	35.10	34.90	0.99	0.99	0.99	0.57	49.40	49.16	1.00
	0.87	81.91	71.19	1.05	1.05	1.05	0.88	115.71	109.99	1.15
	1.21	158.61	90.12	0.89	0.95	0.98	1.21	222.32	163.16	1.15
	1.65	291.22	97.96	0.71	0.95	0.92	1.64	408.23	213.07	1.10
	2.12	484.93	119.05	0.67	1.06	1.02	2.13	681.25	280.25	1.13
	2.68	769.65	136.16	0.62	1.11	1.09	2.67	1079.07	360.43	1.18
	3.32	1188.28	150.41	0.57	1.12	1.13	3.33	1668.02	449.70	1.21
R200b	0.62	27.51	27.24	1.00	1.00	1.00	0.63	40.45	40.13	1.01
	0.93	61.49	49.34	1.01	1.01	1.01	0.92	87.38	80.76	1.16
	1.28	116.50	59.64	0.84	0.94	0.95	1.27	166.66	113.60	1.12
	1.72	210.35	64.91	0.68	0.94	0.90	1.72	304.20	161.02	1.17
	2.20	344.65	77.94	0.64	1.04	0.99	2.20	496.75	208.92	1.20
	2.78	550.15	77.94	0.52	0.95	0.93	2.77	789.63	266.73	1.24
	3.42	836.55	95.15	0.53	1.06	1.07	3.42	1203.86	332.69	1.28
R200c	0.67	20.72	20.27	1.01	1.01	1.01	0.68	33.16	32.69	1.03
	0.97	43.52	32.02	0.96	0.96	0.96	0.98	68.39	58.79	1.13
	1.33	82.89	38.90	0.81	0.93	0.93	1.33	126.41	80.35	1.09
	1.79	149.21	42.04	0.65	0.92	0.88	1.80	230.03	119.25	1.19
	2.27	240.39	43.71	0.54	0.88	0.84	2.27	368.87	160.91	1.29
	2.88	385.45	56.31	0.56	1.03	1.02	2.88	590.61	206.65	1.34
	3.52	578.17	60.68	0.50	1.02	1.04	3.53	886.94	254.93	1.38

ANNEX B – DATA CONCERNING COLUMNS UNDER ELEVATED TEMPERATURES

The sets of Tables B1 to B4 provide information concerning the column numerical failure loads and their DSM-based estimates at (elevated) temperatures $T=200$ to $T=800^{\circ}\text{C}$ – there are seven tables in each set, one per (elevated) temperature. Each table deals with one column cross-section shape (C, H, Z, R), on temperature value and the two end support conditions considered (P and F). It includes the values of the (i) distortional slenderness $\lambda_{D,T}$, (ii) squash load $P_{y,T}$, (iii) numerical failure load $P_{u,T}$, and (iv) numerical-to-predicted failure load ratios $P_{u,T} / P_{n,D,T}^F$, $P_{u,T} / P_{n,D,T}^P$, $P_{u,T} / P_{n,D,T}^{P^*}$ (P columns), and $P_{u,T} / P_{n,D,T}^F$ and $P_{u,T} / P_{n,D,T}^{F^*}$ (F columns).

Table B1-200: Numerical failure loads and their DSM estimates for the pinned and fixed lipped channel columns at 200°C

Column	Pinned (P)						Fixed (F)					
	$\bar{\lambda}_{D.T}$	$P_{y,T}$ (kN)	$P_{u,T}$ (kN)	$\frac{P_{u,T}}{P_{n,D.T}^F}$	$\frac{P_{u,T}}{P_{n,D.T}^P}$	$\frac{P_{u,T}}{P_{n,D.T}^{P*}}$	$\bar{\lambda}_{D.T}$	$P_{y,T}$ (kN)	$P_{u,T}$ (kN)	$\frac{P_{u,T}}{P_{n,D.T}^F}$	$\frac{P_{u,T}}{P_{n,D.T}^{P*}}$	
C130	0.45	31.64	29.47	0.93	0.93	1.03	0.45	43.42	39.51	0.91	1.00	
	0.75	86.83	77.88	0.98	0.98	1.04	0.75	121.42	109.16	0.98	1.04	
	1.05	173.66	118.56	0.95	0.95	1.00	1.05	242.10	191.96	1.10	1.14	
	1.44	322.30	139.04	0.79	0.97	0.97	1.44	450.34	249.08	1.02	1.04	
	1.91	572.49	163.06	0.70	1.04	1.00	1.91	799.14	334.92	1.03	1.05	
	2.39	889.65	191.97	0.67	1.13	1.10	2.39	1242.12	427.60	1.07	1.08	
	3.03	1437.12	221.61	0.63	1.18	1.18	3.03	2005.93	540.28	1.09	1.10	
C150	0.50	21.23	19.78	0.93	0.93	1.03	0.50	29.72	27.24	0.92	1.01	
	0.79	54.13	48.36	1.01	1.01	1.06	0.80	76.42	68.82	1.02	1.07	
	1.11	106.13	67.02	0.92	0.92	0.99	1.11	149.65	111.74	1.09	1.12	
	1.51	196.35	77.73	0.77	0.97	0.96	1.51	274.88	152.34	1.07	1.09	
	1.99	339.62	88.20	0.67	1.01	0.97	1.99	476.53	213.10	1.15	1.16	
	2.49	530.66	101.75	0.62	1.07	1.04	2.49	745.05	270.72	1.18	1.19	
	3.13	841.63	113.62	0.57	1.09	1.09	3.13	1182.32	346.79	1.23	1.24	
C180	0.54	13.10	11.89	0.91	0.91	1.00	0.55	19.65	17.92	0.91	1.01	
	0.84	31.11	26.52	1.00	1.00	1.05	0.84	45.84	39.53	1.01	1.06	
	1.17	60.58	34.42	0.86	0.89	0.95	1.17	88.41	61.49	1.06	1.09	
	1.59	111.33	38.95	0.71	0.93	0.91	1.58	162.09	90.47	1.13	1.15	
	2.06	188.29	45.15	0.64	0.99	0.95	2.06	275.06	131.10	1.27	1.28	
	2.59	296.35	51.86	0.60	1.04	1.02	2.58	432.24	174.20	1.37	1.38	
	3.23	461.71	57.24	0.54	1.05	1.06	3.23	676.19	220.43	1.42	1.43	
C200a	0.60	33.96	31.39	0.93	0.93	1.02	0.59	46.42	43.08	0.93	1.02	
	0.90	75.85	63.87	1.03	1.03	1.08	0.90	105.28	93.95	1.09	1.14	
	1.23	143.77	80.17	0.89	0.96	1.00	1.23	199.25	138.72	1.11	1.14	
	1.66	260.38	90.92	0.74	1.01	0.98	1.66	362.27	179.70	1.06	1.07	
	2.14	431.32	107.06	0.69	1.09	1.05	2.14	600.00	240.38	1.11	1.12	
	2.68	680.38	123.37	0.64	1.15	1.12	2.68	946.42	310.29	1.16	1.17	
	3.33	1048.31	137.93	0.59	1.17	1.19	3.33	1456.99	389.32	1.20	1.21	
C200b	0.65	25.47	23.13	0.93	0.93	1.01	0.65	36.79	33.36	0.93	1.01	
	0.94	53.77	42.53	1.00	1.00	1.04	0.95	77.83	67.11	1.10	1.14	
	1.29	101.89	51.13	0.84	0.94	0.96	1.30	145.76	92.61	1.06	1.09	
	1.74	183.96	57.61	0.70	0.97	0.94	1.74	261.79	135.08	1.15	1.17	
	2.21	298.59	67.49	0.65	1.05	1.01	2.21	425.95	176.41	1.19	1.20	
	2.79	472.64	76.65	0.60	1.09	1.07	2.78	673.59	226.24	1.24	1.25	
	3.43	717.46	83.53	0.54	1.09	1.10	3.43	1023.12	283.47	1.29	1.30	
C200c	0.68	18.19	16.38	0.94	0.94	1.01	0.70	27.29	24.76	0.96	1.03	
	0.99	38.21	26.03	0.90	0.90	0.93	0.99	54.58	45.01	1.09	1.13	
	1.35	70.95	32.37	0.79	0.92	0.93	1.36	101.88	62.60	1.07	1.10	
	1.81	127.35	36.59	0.67	0.95	0.92	1.81	180.12	91.32	1.17	1.19	
	2.28	203.77	42.33	0.62	1.01	0.98	2.29	289.28	125.97	1.30	1.31	
	2.88	323.84	48.00	0.57	1.05	1.04	2.88	458.48	163.77	1.37	1.38	
	3.53	485.77	52.07	0.51	1.04	1.07	3.53	687.71	204.23	1.43	1.44	

Table B2-200: Numerical failure loads and their DSM estimates for the pinned and fixed hat-section columns at 200°C

Column	Pinned (P)						Fixed (F)					
	$\bar{\lambda}_{D,T}$	$P_{y,T}$ (kN)	$P_{u,T}$ (kN)	$\frac{P_{u,T}}{P_{n,D,T}^F}$	$\frac{P_{u,T}}{P_{n,D,T}^P}$	$\frac{P_{u,T}}{P_{n,D,T}^{Ps}}$	$\bar{\lambda}_{D,T}$	$P_{y,T}$ (kN)	$P_{u,T}$ (kN)	$\frac{P_{u,T}}{P_{n,D,T}^F}$	$\frac{P_{u,T}}{P_{n,D,T}^{Fs}}$	
H130	0.40	25.02	23.75	0.95	0.95	1.05	0.40	35.32	33.42	0.95	1.04	
	0.70	76.53	70.02	0.96	0.96	1.03	0.70	107.43	98.00	0.96	1.03	
	1.00	159.68	117.31	0.98	0.98	1.02	1.00	222.96	179.22	1.08	1.11	
	1.39	304.64	143.18	0.84	0.99	1.00	1.39	426.06	249.07	1.04	1.06	
	1.86	549.68	159.41	0.69	1.01	0.98	1.86	768.97	339.92	1.06	1.07	
	2.34	863.89	174.04	0.61	1.02	0.99	2.34	1208.27	430.42	1.08	1.10	
	2.98	1408.42	199.52	0.56	1.06	1.05	2.98	1969.14	543.85	1.10	1.11	
	0.44	16.98	15.80	0.93	0.93	1.03	0.45	24.41	22.56	0.92	1.02	
H150	0.75	47.76	43.04	0.98	0.98	1.04	0.74	66.86	60.38	0.98	1.04	
	1.07	97.64	64.88	0.93	0.93	0.99	1.06	136.91	102.35	1.05	1.08	
	1.46	183.61	76.61	0.78	0.97	0.96	1.46	257.90	152.73	1.11	1.13	
	1.94	323.70	84.03	0.65	0.97	0.93	1.94	454.25	212.68	1.17	1.18	
	2.44	510.50	96.62	0.60	1.02	1.00	2.44	717.46	268.93	1.19	1.21	
	3.08	817.22	107.67	0.54	1.04	1.04	3.08	1148.35	344.32	1.24	1.25	
	0.51	11.46	10.46	0.91	0.91	1.01	0.48	14.74	13.50	0.92	1.01	
	0.79	27.83	24.57	1.00	1.00	1.05	0.79	39.29	35.01	1.01	1.06	
H180	1.12	55.67	34.37	0.91	0.91	0.98	1.12	78.59	55.89	1.04	1.07	
	1.54	104.79	39.28	0.74	0.95	0.93	1.54	148.99	85.59	1.13	1.15	
	2.02	180.10	45.02	0.65	0.99	0.96	2.02	255.41	122.29	1.25	1.26	
	2.54	284.89	51.10	0.60	1.04	1.01	2.54	404.41	163.07	1.34	1.36	
	3.18	448.61	56.47	0.54	1.04	1.05	3.18	635.26	207.67	1.40	1.41	
	0.55	28.30	26.10	0.92	0.92	1.02	0.55	39.62	36.51	0.92	1.02	
	0.85	67.92	59.22	1.03	1.03	1.08	0.84	93.96	83.34	1.04	1.09	
	1.18	132.45	77.34	0.90	0.93	0.99	1.18	184.53	127.89	1.06	1.09	
H200a	1.61	246.79	87.88	0.74	0.97	0.95	1.61	343.02	179.72	1.08	1.10	
	2.09	414.34	99.93	0.65	1.02	0.98	2.09	576.23	238.01	1.11	1.13	
	2.64	660.00	115.01	0.60	1.07	1.05	2.64	918.12	306.99	1.16	1.17	
	3.28	1022.27	128.11	0.55	1.09	1.10	3.28	1423.02	385.67	1.20	1.21	
	0.59	21.23	19.37	0.92	0.92	1.01	0.60	31.13	28.38	0.92	1.01	
	0.90	49.53	40.96	1.02	1.02	1.06	0.90	69.34	59.51	1.05	1.10	
	1.25	94.81	50.50	0.86	0.93	0.97	1.24	133.02	88.37	1.07	1.10	
	1.68	172.64	56.88	0.71	0.97	0.94	1.68	243.40	130.76	1.16	1.18	
H200b	2.16	285.85	65.23	0.64	1.02	0.98	2.16	401.89	172.98	1.21	1.22	
	2.73	455.66	73.99	0.59	1.06	1.04	2.74	642.46	222.84	1.25	1.26	
	3.38	697.64	80.82	0.53	1.06	1.07	3.38	980.66	278.30	1.30	1.31	
	0.65	16.37	14.80	0.93	0.93	1.00	0.65	23.65	21.46	0.93	1.01	
	0.94	34.57	26.75	0.98	0.98	1.02	0.94	49.12	40.29	1.04	1.09	
	1.30	65.50	31.81	0.81	0.91	0.94	1.31	94.61	59.20	1.06	1.08	
	1.77	121.90	36.19	0.67	0.95	0.92	1.76	171.02	89.63	1.18	1.20	
	2.23	194.67	41.44	0.62	1.00	0.97	2.24	276.54	123.06	1.29	1.31	
H200c	2.83	312.93	47.16	0.57	1.04	1.02	2.83	443.92	164.25	1.39	1.40	
	3.48	473.03	51.27	0.51	1.03	1.05	3.48	669.52	201.52	1.42	1.43	

Table B3-200: Numerical failure loads and their DSM estimates for the pinned and fixed zed-section columns at 200°C

Column	Pinned (P)						Fixed (F)					
	$\bar{\lambda}_{D.T}$	$P_{y,T}$ (kN)	$P_{u,T}$ (kN)	$\frac{P_{u,T}}{P_{n,D.T}^F}$	$\frac{P_{u,T}}{P_{n,D.T}^P}$	$\frac{P_{u,T}}{P_{n,D.T}^{P*}}$	$\bar{\lambda}_{D.T}$	$P_{y,T}$ (kN)	$P_{u,T}$ (kN)	$\frac{P_{u,T}}{P_{n,D.T}^F}$	$\frac{P_{u,T}}{P_{n,D.T}^{P*}}$	
Z130	0.50	39.00	35.48	0.91	0.91	1.00	0.50	53.72	48.75	0.91	1.00	
	0.80	99.34	87.60	1.00	1.00	1.05	0.80	138.34	123.39	1.01	1.06	
	1.10	190.59	123.97	0.94	0.94	1.01	1.10	266.38	197.05	1.07	1.10	
	1.49	345.85	140.29	0.77	0.97	0.96	1.49	482.72	256.32	1.01	1.03	
	1.96	604.13	161.32	0.68	1.02	0.98	1.96	842.55	344.97	1.04	1.05	
	2.44	930.12	187.20	0.64	1.09	1.06	2.44	1297.31	441.21	1.08	1.09	
	3.08	1488.63	213.55	0.59	1.13	1.13	3.08	2076.57	557.54	1.11	1.12	
Z150	0.54	25.47	23.39	0.92	0.92	1.01	0.55	36.09	32.95	0.91	1.01	
	0.85	61.56	53.73	1.03	1.03	1.08	0.84	85.97	76.20	1.04	1.09	
	1.17	116.75	70.38	0.91	0.94	1.00	1.16	163.44	114.78	1.06	1.09	
	1.56	209.08	79.08	0.76	0.98	0.96	1.56	293.99	157.34	1.07	1.09	
	2.04	357.67	89.05	0.66	1.01	0.97	2.04	502.01	219.03	1.15	1.16	
	2.54	552.95	102.07	0.61	1.07	1.04	2.54	775.83	277.40	1.19	1.20	
	3.18	870.29	113.12	0.56	1.08	1.08	3.18	1222.65	353.71	1.24	1.25	
Z180	0.61	16.37	14.87	0.92	0.92	1.00	0.59	22.92	20.83	0.91	1.00	
	0.90	36.02	29.96	1.02	1.02	1.07	0.90	52.39	44.81	1.05	1.10	
	1.23	67.13	37.05	0.88	0.95	0.99	1.22	96.60	63.18	1.04	1.06	
	1.63	117.88	40.97	0.73	0.97	0.95	1.64	173.55	91.53	1.11	1.12	
	2.11	198.11	46.46	0.64	1.01	0.97	2.12	289.80	128.91	1.22	1.23	
	2.63	307.81	52.86	0.60	1.05	1.03	2.64	450.25	171.13	1.32	1.33	
	3.28	478.08	58.08	0.54	1.06	1.07	3.28	697.48	216.22	1.37	1.38	
Z200a	0.65	39.62	36.15	0.94	0.94	1.01	0.64	54.34	49.53	0.93	1.01	
	0.94	83.77	68.80	1.04	1.04	1.09	0.94	116.60	98.97	1.08	1.12	
	1.28	155.09	82.62	0.88	0.98	1.01	1.28	216.23	139.62	1.07	1.09	
	1.71	276.23	92.76	0.74	1.02	0.99	1.71	383.78	186.22	1.06	1.08	
	2.19	452.83	108.85	0.68	1.09	1.06	2.19	628.30	247.91	1.12	1.13	
	2.73	706.42	124.11	0.63	1.14	1.12	2.73	981.51	317.45	1.17	1.18	
	3.38	1080.00	137.63	0.58	1.16	1.18	3.38	1501.14	397.74	1.21	1.22	
Z200b	0.70	29.72	26.91	0.96	0.96	1.02	0.70	42.45	38.52	0.96	1.02	
	1.00	60.85	46.53	1.02	1.02	1.05	1.00	86.32	70.17	1.08	1.12	
	1.35	110.38	53.71	0.84	0.98	0.99	1.34	157.08	96.30	1.06	1.08	
	1.78	193.87	59.80	0.71	1.00	0.97	1.79	277.36	138.67	1.15	1.16	
	2.26	312.74	69.11	0.65	1.06	1.03	2.26	444.34	182.58	1.21	1.22	
	2.83	489.62	77.84	0.60	1.10	1.08	2.83	697.64	232.32	1.25	1.26	
	3.48	738.68	84.44	0.54	1.09	1.11	3.48	1052.83	288.56	1.30	1.30	
Z200c	0.75	21.83	19.32	0.97	0.97	1.02	0.75	30.93	27.58	0.97	1.03	
	1.03	41.84	29.06	0.95	0.95	1.00	1.04	60.04	45.28	1.04	1.07	
	1.40	76.41	33.04	0.78	0.93	0.93	1.41	109.16	62.61	1.03	1.06	
	1.86	134.63	35.41	0.63	0.91	0.88	1.86	191.03	92.10	1.15	1.17	
	2.33	212.86	37.29	0.53	0.88	0.86	2.34	302.01	125.69	1.27	1.28	
	2.93	336.58	48.26	0.56	1.04	1.04	2.93	474.85	165.72	1.36	1.37	
	3.58	500.32	52.26	0.51	1.04	1.07	3.58	707.73	204.87	1.41	1.42	

Table B4-200: Numerical failure loads and their DSM estimates for the pinned and fixed rack-section columns at 200°C

Column	Pinned (P)						Fixed (F)					
	$\bar{\lambda}_{D.T}$	$P_{y,T}$ (kN)	$P_{u,T}$ (kN)	$\frac{P_{u,T}}{P_{n,D.T}^F}$	$\frac{P_{u,T}}{P_{n,D.T}^P}$	$\frac{P_{u,T}}{P_{n,D.T}^{P*}}$	$\bar{\lambda}_{D.T}$	$P_{y,T}$ (kN)	$P_{u,T}$ (kN)	$\frac{P_{u,T}}{P_{n,D.T}^F}$	$\frac{P_{u,T}}{P_{n,D.T}^{P*}}$	
R130	0.42	27.39	24.82	0.91	0.91	1.00	0.42	38.80	35.28	0.91	1.00	
	0.72	79.13	69.55	0.94	0.94	1.00	0.72	111.85	100.40	0.96	1.02	
	1.03	162.06	108.07	0.91	0.91	0.95	1.03	228.26	184.88	1.10	1.14	
	1.41	305.10	133.43	0.79	0.96	0.96	1.41	430.64	261.73	1.10	1.12	
	1.89	545.53	140.15	0.62	0.92	0.89	1.89	770.74	328.77	1.04	1.05	
	2.36	852.15	158.22	0.57	0.96	0.93	2.36	1203.67	405.59	1.04	1.05	
	3.01	1383.23	184.74	0.54	1.01	1.01	3.01	1953.11	514.23	1.06	1.07	
	0.47	19.55	17.70	0.91	0.91	1.00	0.47	28.24	25.58	0.91	1.00	
R150	0.77	53.23	46.97	0.98	0.98	1.04	0.77	76.04	67.82	0.99	1.05	
	1.09	106.46	64.94	0.87	0.87	0.93	1.09	152.09	117.99	1.11	1.14	
	1.49	197.71	75.13	0.72	0.91	0.90	1.49	282.44	158.65	1.07	1.09	
	1.96	344.37	101.01	0.74	1.12	1.08	1.96	494.28	218.24	1.12	1.13	
	2.46	540.99	112.62	0.67	1.14	1.11	2.46	775.64	274.36	1.14	1.15	
	3.11	863.63	124.45	0.60	1.15	1.15	3.11	1236.24	351.19	1.18	1.19	
	0.52	13.30	11.98	0.90	0.90	0.99	0.52	19.95	18.00	0.90	1.00	
	0.83	33.25	26.96	0.94	0.94	0.99	0.82	49.87	43.78	1.01	1.06	
R180	1.15	64.83	35.64	0.83	0.84	0.90	1.14	98.07	68.09	1.04	1.07	
	1.57	119.68	41.33	0.69	0.90	0.88	1.56	182.85	96.64	1.06	1.08	
	2.04	202.80	41.33	0.54	0.82	0.79	2.04	310.84	137.18	1.16	1.17	
	2.56	320.82	52.76	0.55	0.97	0.94	2.56	492.03	180.68	1.24	1.25	
	3.21	502.01	58.46	0.50	0.98	0.98	3.21	771.29	230.29	1.29	1.30	
	0.57	31.24	28.24	0.90	0.90	1.00	0.57	43.97	39.75	0.90	1.00	
	0.87	72.90	60.86	1.00	1.00	1.05	0.87	102.98	90.48	1.06	1.10	
	1.21	141.16	79.35	0.88	0.93	0.98	1.21	197.86	140.10	1.11	1.14	
R200a	1.64	259.19	87.47	0.71	0.95	0.92	1.64	363.32	183.05	1.06	1.07	
	2.11	431.59	103.64	0.66	1.03	0.99	2.11	606.31	240.27	1.08	1.10	
	2.66	684.99	119.83	0.61	1.09	1.07	2.66	960.38	311.87	1.14	1.15	
	3.31	1057.57	133.08	0.56	1.11	1.12	3.31	1484.53	390.69	1.18	1.18	
	0.62	24.48	22.06	0.91	0.91	0.99	0.62	36.00	32.46	0.91	1.00	
	0.92	54.72	42.50	0.97	0.97	1.01	0.92	77.77	67.02	1.08	1.12	
	1.27	103.69	53.14	0.84	0.93	0.96	1.27	148.33	98.03	1.08	1.11	
	1.71	187.21	57.97	0.68	0.93	0.91	1.71	270.74	136.87	1.11	1.13	
R200b	2.19	306.74	67.86	0.63	1.00	0.97	2.19	442.11	179.25	1.15	1.16	
	2.76	489.63	67.86	0.51	0.92	0.90	2.76	702.77	229.11	1.19	1.20	
	3.41	744.53	84.24	0.52	1.04	1.06	3.41	1071.43	288.04	1.24	1.25	
	0.66	18.44	16.47	0.92	0.92	0.99	0.68	29.51	26.47	0.94	1.00	
	0.96	38.73	27.73	0.93	0.93	0.96	0.97	60.86	49.53	1.06	1.10	
	1.33	73.77	33.83	0.78	0.90	0.91	1.32	112.51	67.75	1.03	1.05	
	1.78	132.79	37.43	0.64	0.91	0.88	1.79	204.72	100.62	1.13	1.14	
	2.26	213.94	38.95	0.53	0.87	0.84	2.26	328.29	136.38	1.22	1.23	
R200c	2.86	343.05	49.56	0.55	1.01	1.00	2.86	525.64	177.06	1.28	1.29	
	3.50	514.57	53.67	0.50	1.00	1.03	3.51	789.38	219.15	1.32	1.33	

Table B1-300: Numerical failure loads and their DSM estimates for the pinned and fixed lipped channel columns at 300°C

Column	Pinned (P)						Fixed (F)					
	$\bar{\lambda}_{D.T}$	$P_{y,T}$ (kN)	$P_{u,T}$ (kN)	$\frac{P_{u,T}}{P_{n,D.T}^F}$	$\frac{P_{u,T}}{P_{n,D.T}^P}$	$\frac{P_{u,T}}{P_{n,D.T}^{P*}}$	$\bar{\lambda}_{D.T}$	$P_{y,T}$ (kN)	$P_{u,T}$ (kN)	$\frac{P_{u,T}}{P_{n,D.T}^F}$	$\frac{P_{u,T}}{P_{n,D.T}^{P*}}$	
C130	0.45	27.73	22.74	0.82	0.82	1.04	0.44	38.05	31.38	0.82	1.05	
	0.74	76.10	60.57	0.87	0.87	1.02	0.74	106.41	84.23	0.86	1.02	
	1.05	152.20	100.45	0.91	0.91	1.01	1.05	212.17	156.30	1.02	1.11	
	1.43	282.47	120.42	0.78	0.95	0.97	1.43	394.68	210.39	0.98	1.03	
	1.90	501.74	139.18	0.68	1.00	0.98	1.90	700.37	281.29	0.98	1.02	
	2.37	779.69	165.17	0.65	1.10	1.07	2.37	1088.60	361.41	1.03	1.05	
	3.01	1259.50	193.18	0.62	1.16	1.17	3.01	1758.01	464.70	1.06	1.08	
C150	0.49	18.60	15.37	0.83	0.83	1.05	0.49	26.04	21.19	0.81	1.04	
	0.79	47.44	37.60	0.89	0.89	1.03	0.79	66.97	52.80	0.89	1.03	
	1.10	93.02	57.80	0.90	0.90	1.01	1.11	131.15	92.45	1.02	1.11	
	1.50	172.08	67.63	0.76	0.95	0.97	1.50	240.91	124.45	0.99	1.04	
	1.98	297.65	76.39	0.65	0.99	0.96	1.97	417.64	176.07	1.07	1.11	
	2.47	465.08	87.26	0.61	1.04	1.02	2.47	652.97	225.91	1.12	1.15	
	3.11	737.61	98.65	0.56	1.07	1.08	3.11	1036.19	291.71	1.17	1.20	
C180	0.54	11.48	9.08	0.79	0.79	1.01	0.55	17.22	13.64	0.79	1.01	
	0.83	27.26	20.86	0.89	0.89	1.02	0.84	40.18	30.99	0.90	1.03	
	1.16	53.09	29.59	0.84	0.86	0.96	1.16	77.49	48.86	0.95	1.03	
	1.57	97.57	33.62	0.69	0.91	0.91	1.57	142.06	72.53	1.03	1.08	
	2.05	165.01	38.25	0.61	0.95	0.92	2.05	241.07	105.46	1.16	1.19	
	2.57	259.72	44.30	0.58	1.01	0.99	2.57	378.82	141.37	1.26	1.29	
	3.21	404.65	49.60	0.53	1.03	1.04	3.21	592.62	182.94	1.33	1.36	
C200a	0.60	29.76	24.24	0.82	0.82	1.04	0.59	40.68	33.59	0.83	1.05	
	0.89	66.47	51.20	0.94	0.94	1.06	0.89	92.27	72.84	0.96	1.08	
	1.23	126.00	67.82	0.85	0.92	1.00	1.22	174.62	114.84	1.04	1.12	
	1.65	228.20	78.83	0.73	0.98	0.98	1.65	317.49	149.17	0.99	1.04	
	2.12	378.01	91.07	0.66	1.04	1.02	2.12	525.84	198.38	1.04	1.07	
	2.67	596.29	106.24	0.63	1.11	1.10	2.67	829.45	260.55	1.10	1.13	
	3.31	918.74	119.63	0.58	1.15	1.17	3.31	1276.91	330.74	1.16	1.18	
C200b	0.64	22.32	17.70	0.81	0.81	1.01	0.65	32.25	25.56	0.81	1.01	
	0.93	47.13	34.67	0.93	0.93	1.03	0.94	68.21	52.35	0.97	1.08	
	1.28	89.29	44.08	0.82	0.91	0.97	1.29	127.74	76.60	0.99	1.06	
	1.73	161.23	49.63	0.68	0.95	0.93	1.72	229.44	110.59	1.06	1.11	
	2.20	261.68	57.34	0.62	1.00	0.98	2.20	373.30	147.19	1.12	1.16	
	2.77	414.23	65.98	0.58	1.06	1.05	2.76	590.34	188.66	1.17	1.20	
	3.41	628.78	72.61	0.53	1.07	1.09	3.41	896.66	237.05	1.22	1.24	
C200c	0.68	15.94	12.54	0.82	0.82	1.00	0.70	23.92	18.83	0.83	1.00	
	0.98	33.48	23.06	0.91	0.91	1.00	0.99	47.83	36.03	0.99	1.10	
	1.34	62.18	28.01	0.78	0.90	0.94	1.35	89.29	49.66	0.96	1.02	
	1.79	111.61	31.44	0.65	0.92	0.91	1.79	157.85	73.11	1.07	1.11	
	2.27	178.58	35.96	0.59	0.97	0.95	2.27	253.52	101.49	1.18	1.22	
	2.86	283.82	41.23	0.55	1.02	1.01	2.86	401.81	134.95	1.28	1.30	
	3.50	425.73	45.18	0.51	1.02	1.05	3.50	602.71	169.82	1.34	1.36	

Table B2-300: Numerical failure loads and their DSM estimates for the pinned and fixed hat-section columns at 300°C

Column	Pinned (P)						Fixed (F)					
	$\bar{\lambda}_{D,T}$	$P_{y,T}$ (kN)	$P_{u,T}$ (kN)	$\frac{P_{u,T}}{P_{n,D,T}^F}$	$\frac{P_{u,T}}{P_{n,D,T}^P}$	$\frac{P_{u,T}}{P_{n,D,T}^{Ps}}$	$\bar{\lambda}_{D,T}$	$P_{y,T}$ (kN)	$P_{u,T}$ (kN)	$\frac{P_{u,T}}{P_{n,D,T}^F}$	$\frac{P_{u,T}}{P_{n,D,T}^{Fs}}$	
H130	0.39	21.93	17.76	0.81	0.81	1.03	0.40	30.96	25.68	0.83	1.06	
	0.69	67.07	54.89	0.86	0.86	1.04	0.69	94.16	77.02	0.86	1.04	
	1.00	139.94	98.61	0.94	0.94	1.03	1.00	195.41	146.33	1.00	1.10	
	1.38	266.99	121.93	0.81	0.95	0.99	1.38	373.40	207.29	0.98	1.04	
	1.85	481.74	139.71	0.69	1.00	0.98	1.85	673.92	284.88	1.01	1.04	
	2.32	757.12	149.97	0.60	0.99	0.97	2.32	1058.93	366.01	1.04	1.07	
	2.96	1234.35	174.28	0.56	1.04	1.04	2.96	1725.76	468.22	1.07	1.09	
H150	0.44	14.88	12.39	0.83	0.83	1.06	0.45	21.39	17.76	0.83	1.06	
	0.74	41.86	33.24	0.86	0.86	1.02	0.74	58.60	46.49	0.86	1.02	
	1.06	85.57	55.32	0.90	0.90	1.00	1.06	119.99	85.90	1.00	1.09	
	1.45	160.92	66.14	0.76	0.94	0.96	1.45	226.03	123.34	1.02	1.07	
	1.93	283.70	76.60	0.67	1.00	0.97	1.93	398.10	176.41	1.10	1.14	
	2.42	447.40	82.82	0.59	0.99	0.97	2.42	628.78	224.72	1.13	1.16	
	3.06	716.22	93.76	0.54	1.02	1.02	3.06	1006.42	288.90	1.18	1.20	
H180	0.51	10.04	8.04	0.80	0.80	1.02	0.48	12.91	10.35	0.80	1.02	
	0.79	24.39	19.02	0.88	0.88	1.02	0.79	34.44	26.97	0.88	1.02	
	1.11	48.79	29.32	0.88	0.88	0.99	1.11	68.88	45.97	0.97	1.05	
	1.53	91.83	34.02	0.72	0.92	0.93	1.53	130.58	68.35	1.03	1.08	
	2.00	157.84	37.89	0.62	0.94	0.92	2.00	223.85	99.45	1.15	1.19	
	2.52	249.67	43.67	0.58	1.00	0.98	2.52	354.42	133.79	1.25	1.28	
	3.16	393.17	48.99	0.53	1.02	1.03	3.16	556.75	171.76	1.31	1.33	
H200a	0.54	24.80	20.32	0.82	0.82	1.04	0.54	34.73	28.40	0.82	1.04	
	0.84	59.53	46.67	0.92	0.92	1.05	0.84	82.35	64.81	0.92	1.05	
	1.17	116.08	65.77	0.86	0.89	0.99	1.17	161.72	104.95	0.99	1.07	
	1.60	216.29	76.23	0.72	0.95	0.95	1.60	300.62	145.53	0.99	1.04	
	2.07	363.13	86.20	0.64	0.99	0.97	2.07	505.01	197.30	1.05	1.08	
	2.62	578.43	99.06	0.59	1.04	1.03	2.62	804.64	256.76	1.10	1.13	
	3.26	895.92	111.32	0.55	1.07	1.08	3.26	1247.15	329.36	1.16	1.18	
H200b	0.59	18.60	14.90	0.80	0.80	1.02	0.60	27.28	21.79	0.80	1.02	
	0.89	43.41	33.05	0.93	0.93	1.05	0.89	60.77	46.79	0.94	1.06	
	1.24	83.09	43.64	0.84	0.91	0.98	1.24	116.58	71.62	0.98	1.05	
	1.67	151.30	49.34	0.70	0.95	0.94	1.67	213.31	106.31	1.07	1.11	
	2.15	250.52	57.01	0.63	1.01	0.98	2.15	352.22	143.01	1.13	1.16	
	2.71	399.34	63.84	0.57	1.03	1.02	2.72	563.05	186.03	1.19	1.21	
	3.36	611.42	70.25	0.52	1.04	1.05	3.36	859.46	233.27	1.23	1.25	
H200c	0.64	14.35	11.31	0.81	0.81	1.00	0.65	20.73	16.37	0.81	1.00	
	0.93	30.30	21.94	0.92	0.92	1.02	0.94	43.05	32.21	0.95	1.05	
	1.29	57.40	27.58	0.80	0.89	0.95	1.30	82.91	48.53	0.98	1.04	
	1.75	106.83	31.13	0.66	0.92	0.91	1.75	149.88	71.81	1.07	1.12	
	2.22	170.61	35.64	0.60	0.97	0.95	2.22	242.36	100.79	1.20	1.23	
	2.81	274.25	40.52	0.55	1.01	1.00	2.81	389.05	133.60	1.28	1.31	
	3.46	414.57	44.45	0.50	1.01	1.03	3.46	586.77	167.57	1.34	1.36	

Table B3-300: Numerical failure loads and their DSM estimates for the pinned and fixed zed-section columns at 300°C

Column	Pinned (P)						Fixed (F)					
	$\bar{\lambda}_{D.T}$	$P_{y,T}$ (kN)	$P_{u,T}$ (kN)	$\frac{P_{u,T}}{P_{n,D.T}^F}$	$\frac{P_{u,T}}{P_{n,D.T}^P}$	$\frac{P_{u,T}}{P_{n,D.T}^{P*}}$	$\bar{\lambda}_{D.T}$	$P_{y,T}$ (kN)	$P_{u,T}$ (kN)	$\frac{P_{u,T}}{P_{n,D.T}^F}$	$\frac{P_{u,T}}{P_{n,D.T}^{P*}}$	
Z130	0.50	34.18	27.87	0.82	0.82	1.04	0.49	47.08	38.22	0.81	1.03	
	0.79	87.06	68.04	0.88	0.88	1.02	0.79	121.24	94.97	0.88	1.02	
	1.10	167.03	106.57	0.92	0.92	1.03	1.10	233.46	162.23	1.00	1.09	
	1.48	303.10	121.98	0.76	0.95	0.96	1.48	423.06	217.13	0.97	1.02	
	1.95	529.47	138.89	0.66	0.99	0.97	1.95	738.42	290.60	0.99	1.02	
	2.42	815.16	161.91	0.63	1.06	1.04	2.42	1136.97	374.14	1.04	1.07	
	3.06	1304.64	186.68	0.59	1.11	1.12	3.06	1819.92	482.21	1.09	1.11	
Z150	0.54	22.32	18.06	0.81	0.81	1.03	0.54	31.63	25.62	0.81	1.03	
	0.84	53.95	42.05	0.91	0.91	1.04	0.84	75.34	59.12	0.92	1.05	
	1.16	102.32	60.79	0.90	0.91	1.02	1.16	143.24	95.67	1.01	1.08	
	1.55	183.24	68.74	0.74	0.96	0.96	1.55	257.65	129.76	1.00	1.05	
	2.03	313.46	77.47	0.65	0.99	0.97	2.03	439.96	182.24	1.08	1.12	
	2.52	484.61	87.75	0.60	1.03	1.02	2.52	679.94	234.24	1.14	1.17	
	3.16	762.72	98.49	0.55	1.06	1.07	3.16	1071.53	299.24	1.19	1.21	
Z180	0.60	14.35	11.37	0.80	0.80	1.01	0.59	20.09	15.94	0.80	1.01	
	0.89	31.57	23.94	0.93	0.93	1.04	0.89	45.92	35.02	0.93	1.05	
	1.22	58.83	31.85	0.86	0.92	1.00	1.21	84.66	51.99	0.97	1.04	
	1.62	103.31	35.54	0.71	0.95	0.95	1.63	152.10	73.75	1.01	1.06	
	2.10	173.62	39.60	0.62	0.97	0.95	2.10	253.98	104.91	1.12	1.16	
	2.62	269.76	45.27	0.58	1.02	1.00	2.62	394.60	139.80	1.22	1.25	
	3.26	418.99	50.35	0.53	1.03	1.05	3.26	611.27	179.90	1.29	1.32	
Z200a	0.64	34.73	27.93	0.82	0.82	1.02	0.64	47.62	38.22	0.82	1.02	
	0.93	73.42	55.58	0.96	0.96	1.07	0.94	102.19	78.80	0.98	1.09	
	1.27	135.93	71.74	0.87	0.96	1.03	1.27	189.50	116.14	1.01	1.08	
	1.70	242.09	80.22	0.72	0.99	0.98	1.70	336.34	155.58	1.01	1.05	
	2.17	396.86	92.79	0.66	1.05	1.03	2.17	550.65	204.84	1.05	1.08	
	2.71	619.11	107.22	0.62	1.12	1.10	2.72	860.20	267.55	1.12	1.14	
	3.36	946.52	119.89	0.58	1.14	1.16	3.36	1315.60	338.40	1.17	1.19	
Z200b	0.69	26.04	20.66	0.84	0.84	1.01	0.69	37.21	29.55	0.84	1.01	
	0.99	53.33	38.48	0.96	0.96	1.05	0.99	75.65	56.01	0.98	1.08	
	1.34	96.74	46.76	0.83	0.96	1.00	1.33	137.66	79.66	0.99	1.06	
	1.77	169.91	51.66	0.69	0.97	0.96	1.77	243.08	113.15	1.06	1.10	
	2.25	274.08	58.89	0.63	1.02	1.00	2.25	389.42	151.37	1.13	1.17	
	2.81	429.11	67.05	0.58	1.06	1.06	2.81	611.42	193.95	1.18	1.21	
	3.46	647.38	73.47	0.53	1.07	1.09	3.46	922.71	243.27	1.24	1.26	
Z200c	0.74	19.13	14.83	0.84	0.84	0.99	0.74	27.11	21.12	0.85	1.00	
	1.03	36.67	24.32	0.90	0.90	1.00	1.03	52.62	36.64	0.95	1.04	
	1.39	66.97	28.64	0.76	0.91	0.94	1.40	95.67	50.57	0.95	1.00	
	1.84	117.99	30.75	0.62	0.89	0.88	1.85	167.42	73.86	1.05	1.09	
	2.32	186.55	32.61	0.53	0.87	0.85	2.32	264.68	101.82	1.16	1.19	
	2.91	294.98	41.49	0.55	1.01	1.01	2.91	416.16	136.32	1.27	1.29	
	3.55	438.48	45.32	0.50	1.02	1.05	3.55	620.25	170.23	1.33	1.35	

Table B4-300: Numerical failure loads and their DSM estimates for the pinned and fixed rack-section columns at 300°C

Table B1-400: Numerical failure loads and their DSM estimates for the pinned and fixed lipped channel columns at 400°C

Table B2-400: Numerical failure loads and their DSM estimates for the pinned and fixed hat-section columns at 400°C

Column	Pinned (P)						Fixed (F)					
	$\bar{\lambda}_{D.T}$	$P_{y.T}$ (kN)	$P_{u.T}$ (kN)	$\frac{P_{u.T}}{P_{n.D.T}^F}$	$\frac{P_{u.T}}{P_{n.D.T}^P}$	$\frac{P_{u.T}}{P_{n.D.T}^{Ps}}$	$\bar{\lambda}_{D.T}$	$P_{y.T}$ (kN)	$P_{u.T}$ (kN)	$\frac{P_{u.T}}{P_{n.D.T}^F}$	$\frac{P_{u.T}}{P_{n.D.T}^{F*}}$	
H130	0.39	18.27	12.43	0.68	0.68	1.05	0.39	25.80	16.77	0.65	1.01	
	0.67	55.89	37.45	0.70	0.70	1.04	0.68	78.46	53.36	0.71	1.05	
	0.97	116.62	75.68	0.85	0.85	1.05	0.97	162.84	108.63	0.87	1.08	
	1.34	222.49	103.69	0.81	0.93	1.03	1.34	311.17	166.43	0.93	1.05	
	1.81	401.45	113.85	0.66	0.94	0.95	1.81	561.60	227.76	0.94	1.02	
	2.26	630.93	124.52	0.58	0.95	0.94	2.26	882.44	297.81	0.99	1.05	
	2.89	1028.62	147.07	0.55	1.02	1.03	2.89	1438.14	387.35	1.04	1.08	
	0.43	12.40	8.56	0.69	0.69	1.07	0.44	17.83	11.77	0.66	1.02	
H150	0.72	34.88	23.29	0.72	0.72	1.03	0.72	48.83	33.03	0.73	1.05	
	1.03	71.31	43.49	0.83	0.83	1.02	1.03	99.99	63.49	0.87	1.05	
	1.42	134.10	54.78	0.74	0.90	0.96	1.42	188.36	95.05	0.92	1.03	
	1.88	236.41	61.80	0.63	0.93	0.93	1.88	331.75	138.10	1.01	1.08	
	2.36	372.84	67.11	0.55	0.93	0.92	2.36	523.98	178.21	1.05	1.11	
	2.99	596.85	78.52	0.52	0.99	1.00	2.99	838.69	232.53	1.11	1.15	
	0.49	8.37	5.65	0.67	0.67	1.04	0.47	10.76	7.15	0.66	1.03	
	0.77	20.33	13.23	0.72	0.72	1.01	0.77	28.70	18.71	0.72	1.01	
H180	1.09	40.66	23.42	0.82	0.82	1.00	1.08	57.40	34.43	0.85	1.02	
	1.49	76.53	28.48	0.71	0.89	0.94	1.49	108.81	51.94	0.91	1.01	
	1.95	131.53	31.76	0.61	0.91	0.91	1.95	186.54	74.59	1.01	1.08	
	2.46	208.06	35.67	0.55	0.94	0.94	2.46	295.35	101.56	1.11	1.17	
	3.08	327.64	40.77	0.51	0.98	1.00	3.08	463.95	134.05	1.19	1.24	
	0.53	20.67	13.85	0.67	0.67	1.04	0.53	28.94	19.39	0.67	1.04	
	0.82	49.61	32.96	0.77	0.77	1.03	0.82	68.62	45.77	0.77	1.03	
	1.14	96.74	54.11	0.84	0.84	1.02	1.15	134.77	82.54	0.91	1.07	
H200a	1.56	180.24	63.81	0.71	0.92	0.96	1.56	250.52	114.47	0.91	1.01	
	2.02	302.61	70.31	0.61	0.93	0.93	2.02	420.84	153.28	0.95	1.02	
	2.55	482.02	81.93	0.57	0.99	0.99	2.55	670.53	203.44	1.02	1.07	
	3.18	746.60	93.60	0.54	1.04	1.06	3.18	1039.29	265.94	1.09	1.14	
	0.57	15.50	10.50	0.68	0.68	1.05	0.58	22.74	15.45	0.68	1.05	
	0.87	36.17	23.48	0.78	0.78	1.01	0.87	50.64	32.95	0.78	1.01	
	1.21	69.24	35.72	0.81	0.86	1.00	1.21	97.15	55.29	0.89	1.03	
	1.63	126.09	41.66	0.69	0.92	0.95	1.63	177.76	80.45	0.95	1.04	
H200b	2.10	208.77	45.55	0.59	0.93	0.92	2.10	293.51	111.31	1.03	1.10	
	2.65	332.79	52.62	0.55	0.98	0.98	2.65	469.21	144.75	1.08	1.13	
	3.28	509.52	59.04	0.51	1.01	1.03	3.28	716.22	185.48	1.14	1.19	
	0.63	11.96	7.86	0.67	0.67	1.02	0.63	17.27	11.29	0.67	1.01	
	0.91	25.25	16.02	0.79	0.79	1.00	0.91	35.88	22.99	0.80	1.01	
	1.25	47.83	22.87	0.78	0.85	0.97	1.27	69.09	36.83	0.87	1.00	
	1.71	89.03	26.32	0.65	0.90	0.91	1.70	124.90	54.48	0.95	1.04	
	2.16	142.17	29.26	0.58	0.92	0.91	2.17	201.97	75.58	1.05	1.12	
H200c	2.74	228.54	33.36	0.53	0.96	0.96	2.75	324.21	102.75	1.15	1.20	
	3.37	345.47	37.20	0.49	0.98	1.00	3.37	488.98	130.53	1.22	1.26	

Table B3-400: Numerical failure loads and their DSM estimates for the pinned and fixed zed-section columns at 400°C

Column	Pinned (P)						Fixed (F)					
	$\bar{\lambda}_{D.T}$	$P_{y,T}$ (kN)	$P_{u,T}$ (kN)	$\frac{P_{u,T}}{P_{n,D.T}^F}$	$\frac{P_{u,T}}{P_{n,D.T}^P}$	$\frac{P_{u,T}}{P_{n,D.T}^{P*}}$	$\bar{\lambda}_{D.T}$	$P_{y,T}$ (kN)	$P_{u,T}$ (kN)	$\frac{P_{u,T}}{P_{n,D.T}^F}$	$\frac{P_{u,T}}{P_{n,D.T}^{P*}}$	
Z130	0.48	28.48	19.08	0.67	0.67	1.04	0.48	39.23	26.68	0.68	1.05	
	0.77	72.55	48.56	0.74	0.74	1.04	0.77	101.03	68.66	0.76	1.05	
	1.07	139.19	84.17	0.85	0.85	1.04	1.07	194.55	121.88	0.88	1.06	
	1.44	252.59	103.12	0.75	0.92	0.98	1.44	352.55	173.78	0.91	1.02	
	1.90	441.22	115.49	0.64	0.95	0.95	1.90	615.35	232.56	0.92	1.00	
	2.36	679.30	134.49	0.61	1.02	1.01	2.36	947.47	301.83	0.98	1.04	
	2.99	1087.20	157.68	0.58	1.09	1.10	2.99	1516.60	400.63	1.05	1.10	
Z150	0.53	18.60	12.98	0.70	0.70	1.08	0.53	26.35	17.66	0.67	1.04	
	0.82	44.96	29.59	0.76	0.76	1.02	0.82	62.79	41.55	0.76	1.02	
	1.13	85.26	48.96	0.85	0.85	1.04	1.13	119.37	72.84	0.90	1.06	
	1.51	152.70	58.10	0.74	0.93	0.98	1.51	214.71	101.07	0.91	1.01	
	1.98	261.22	63.69	0.62	0.94	0.94	1.98	366.63	142.79	0.99	1.06	
	2.46	403.84	72.30	0.58	0.98	0.98	2.46	566.62	185.33	1.05	1.11	
	3.08	635.60	82.79	0.54	1.03	1.04	3.08	892.94	241.88	1.12	1.16	
Z180	0.59	11.96	7.87	0.66	0.66	1.02	0.58	16.74	11.10	0.66	1.03	
	0.87	26.31	16.94	0.78	0.78	1.00	0.87	38.26	24.62	0.77	1.00	
	1.19	49.03	26.09	0.82	0.86	1.02	1.18	70.55	40.34	0.88	1.02	
	1.58	86.09	29.96	0.70	0.92	0.95	1.59	126.75	55.36	0.89	0.98	
	2.05	144.69	32.83	0.60	0.93	0.92	2.05	211.65	79.40	0.99	1.06	
	2.55	224.80	37.10	0.55	0.96	0.96	2.56	328.83	108.07	1.10	1.16	
	3.18	349.16	42.03	0.51	1.00	1.02	3.18	509.39	140.90	1.18	1.23	
Z200a	0.63	28.94	19.92	0.70	0.70	1.07	0.62	39.69	26.73	0.68	1.04	
	0.91	61.18	39.69	0.81	0.81	1.02	0.91	85.16	55.73	0.81	1.03	
	1.24	113.27	59.28	0.84	0.91	1.05	1.24	157.92	90.66	0.92	1.06	
	1.66	201.74	67.63	0.71	0.96	0.99	1.66	280.29	121.56	0.92	1.01	
	2.12	330.72	75.82	0.63	0.99	0.99	2.12	458.87	161.62	0.97	1.03	
	2.65	515.92	88.45	0.60	1.06	1.06	2.65	716.84	214.72	1.05	1.10	
	3.28	788.77	100.64	0.56	1.11	1.13	3.28	1096.34	275.44	1.11	1.15	
Z200b	0.68	21.70	14.31	0.69	0.69	1.02	0.68	31.01	20.56	0.69	1.03	
	0.97	44.44	28.38	0.83	0.83	1.03	0.97	63.04	40.45	0.83	1.03	
	1.30	80.61	38.98	0.81	0.92	1.03	1.30	114.72	63.38	0.93	1.06	
	1.73	141.59	43.32	0.68	0.94	0.96	1.73	202.57	86.31	0.95	1.03	
	2.19	228.40	48.21	0.60	0.96	0.96	2.19	324.52	117.26	1.03	1.09	
	2.75	357.59	55.39	0.56	1.02	1.02	2.75	509.52	152.18	1.08	1.13	
	3.37	539.49	61.84	0.52	1.04	1.07	3.37	768.92	193.91	1.15	1.19	
Z200c	0.72	15.94	10.24	0.69	0.69	0.99	0.72	22.59	14.53	0.69	1.00	
	1.00	30.56	18.50	0.81	0.81	0.99	1.01	43.85	27.13	0.83	1.01	
	1.35	55.81	23.93	0.75	0.87	0.95	1.36	79.72	38.66	0.85	0.96	
	1.80	98.33	26.52	0.62	0.89	0.90	1.80	139.52	54.99	0.91	0.99	
	2.26	155.46	27.74	0.52	0.86	0.85	2.26	220.57	76.50	1.02	1.08	
	2.84	245.82	29.20	0.45	0.82	0.83	2.84	346.80	104.78	1.14	1.19	
	3.47	365.40	37.91	0.49	0.98	1.01	3.47	516.88	133.09	1.21	1.25	

Table B4-400: Numerical failure loads and their DSM estimates for the pinned and fixed rack-section columns at 400°C

Column	Pinned (P)						Fixed (F)					
	$\bar{\lambda}_{D.T}$	$P_{y,T}$ (kN)	$P_{u,T}$ (kN)	$\frac{P_{u,T}}{P_{n,D.T}^F}$	$\frac{P_{u,T}}{P_{n,D.T}^P}$	$\frac{P_{u,T}}{P_{n,D.T}^{P*}}$	$\bar{\lambda}_{D.T}$	$P_{y,T}$ (kN)	$P_{u,T}$ (kN)	$\frac{P_{u,T}}{P_{n,D.T}^F}$	$\frac{P_{u,T}}{P_{n,D.T}^{P*}}$	
R130	0.41	20.00	13.85	0.69	0.69	1.07	0.41	28.34	18.42	0.65	1.01	
	0.70	57.79	38.65	0.71	0.71	1.04	0.70	81.68	53.10	0.69	1.01	
	1.00	118.36	68.81	0.77	0.77	0.95	1.00	166.70	106.51	0.85	1.04	
	1.37	222.83	94.14	0.74	0.87	0.95	1.37	314.51	170.19	0.95	1.07	
	1.83	398.42	103.59	0.61	0.88	0.89	1.83	562.90	223.62	0.93	1.01	
	2.29	622.36	109.28	0.52	0.86	0.85	2.29	879.08	279.05	0.94	1.00	
	2.92	1010.22	133.38	0.51	0.95	0.96	2.92	1426.43	363.54	0.99	1.03	
	0.45	14.28	9.48	0.66	0.66	1.03	0.46	20.63	13.70	0.66	1.03	
R150	0.75	38.88	25.14	0.71	0.71	1.00	0.75	55.54	35.80	0.70	1.00	
	1.06	77.75	47.72	0.86	0.86	1.04	1.06	111.07	69.22	0.87	1.04	
	1.44	144.40	59.20	0.76	0.93	0.99	1.44	206.28	104.37	0.93	1.04	
	1.90	251.50	74.51	0.72	1.07	1.07	1.90	360.99	141.28	0.96	1.03	
	2.38	395.10	80.63	0.63	1.07	1.06	2.39	566.48	182.03	1.00	1.06	
	3.01	630.74	92.94	0.59	1.12	1.13	3.01	902.87	237.85	1.06	1.10	
	0.51	9.71	6.27	0.65	0.65	1.00	0.50	14.57	9.41	0.65	1.00	
	0.80	24.28	15.38	0.72	0.72	0.98	0.79	36.42	23.30	0.72	0.99	
R180	1.12	47.35	24.00	0.74	0.74	0.91	1.11	71.63	42.55	0.86	1.02	
	1.52	87.41	29.69	0.66	0.84	0.88	1.51	133.54	59.23	0.86	0.95	
	1.97	148.11	29.69	0.51	0.77	0.77	1.97	227.02	84.03	0.94	1.01	
	2.48	234.31	43.59	0.61	1.04	1.03	2.48	359.35	114.96	1.04	1.10	
	3.11	366.63	42.02	0.48	0.91	0.93	3.11	563.30	150.56	1.11	1.16	
	0.55	22.82	15.07	0.66	0.66	1.02	0.55	32.11	21.19	0.66	1.02	
	0.84	53.24	34.19	0.75	0.75	1.00	0.84	75.21	48.45	0.76	1.00	
	1.17	103.10	54.14	0.80	0.82	0.98	1.17	144.51	86.89	0.92	1.07	
R200a	1.59	189.29	64.85	0.70	0.91	0.95	1.59	265.35	121.21	0.93	1.02	
	2.05	315.21	68.78	0.58	0.89	0.89	2.05	442.81	155.90	0.93	0.99	
	2.58	500.27	84.20	0.57	1.00	1.00	2.58	701.40	201.02	0.97	1.02	
	3.20	772.38	96.32	0.54	1.04	1.06	3.20	1084.21	269.40	1.07	1.11	
	0.60	17.88	11.59	0.65	0.65	1.00	0.60	26.29	16.97	0.65	1.00	
	0.89	39.97	25.27	0.77	0.77	0.99	0.89	56.79	36.32	0.78	1.00	
	1.23	75.73	36.30	0.76	0.82	0.95	1.23	108.33	62.34	0.92	1.06	
	1.65	136.73	43.02	0.67	0.90	0.92	1.66	197.73	85.65	0.92	1.01	
R200b	2.12	224.02	45.28	0.55	0.87	0.87	2.12	322.89	115.80	0.98	1.05	
	2.68	357.60	45.28	0.45	0.80	0.80	2.67	513.26	149.19	1.02	1.07	
	3.30	543.76	61.22	0.50	0.99	1.01	3.30	782.51	191.37	1.09	1.13	
	0.64	13.47	8.67	0.66	0.66	1.00	0.66	21.55	13.87	0.66	1.00	
	0.93	28.29	17.32	0.77	0.77	0.97	0.94	44.45	28.07	0.80	1.01	
	1.29	53.88	23.37	0.72	0.80	0.90	1.28	82.17	43.76	0.88	1.01	
	1.72	96.98	27.43	0.63	0.87	0.88	1.73	149.52	60.75	0.90	0.98	
	2.19	156.25	29.41	0.53	0.86	0.85	2.19	239.77	83.87	0.99	1.06	
R200c	2.77	250.54	30.51	0.45	0.81	0.81	2.77	383.89	113.15	1.08	1.13	
	3.39	375.81	38.82	0.48	0.95	0.97	3.40	576.51	142.51	1.14	1.18	

Table B1-500: Numerical failure loads and their DSM estimates for the pinned and fixed lipped channel columns at 500°C

Column	Pinned (P)						Fixed (F)					
	$\bar{\lambda}_{D,T}$	$P_{y,T}$ (kN)	$P_{u,T}$ (kN)	$\frac{P_{u,T}}{P_{n,D,T}^F}$	$\frac{P_{u,T}}{P_{n,D,T}^P}$	$\frac{P_{u,T}}{P_{n,D,T}^{ps}}$	$\bar{\lambda}_{D,T}$	$P_{y,T}$ (kN)	$P_{u,T}$ (kN)	$\frac{P_{u,T}}{P_{n,D,T}^F}$	$\frac{P_{u,T}}{P_{n,D,T}^{F*}}$	
C130	0.43	18.84	13.00	0.69	0.69	1.02	0.42	25.85	18.61	0.72	1.06	
	0.70	51.71	37.52	0.77	0.77	1.07	0.71	72.30	52.18	0.77	1.06	
	1.00	103.42	67.29	0.87	0.87	1.03	1.00	144.17	96.89	0.89	1.06	
	1.36	191.93	85.71	0.78	0.91	0.98	1.36	268.18	144.22	0.94	1.04	
	1.81	340.92	98.08	0.67	0.96	0.96	1.81	475.89	189.88	0.93	0.99	
	2.26	529.79	115.82	0.64	1.04	1.03	2.26	739.69	244.93	0.97	1.02	
	2.87	855.81	137.90	0.61	1.13	1.14	2.87	1194.54	322.76	1.03	1.07	
	0.47	12.64	8.85	0.70	0.70	1.03	0.47	17.70	12.92	0.73	1.07	
C150	0.75	32.23	22.76	0.77	0.77	1.04	0.75	45.51	31.64	0.76	1.02	
	1.05	63.20	39.76	0.87	0.87	1.04	1.05	89.12	58.96	0.92	1.08	
	1.43	116.92	48.22	0.76	0.92	0.97	1.43	163.69	84.14	0.94	1.04	
	1.88	202.25	54.66	0.65	0.96	0.96	1.88	283.78	116.85	0.99	1.06	
	2.35	316.01	61.23	0.59	0.99	0.98	2.35	443.68	152.17	1.05	1.10	
	2.96	501.20	70.77	0.56	1.04	1.05	2.96	704.08	199.61	1.12	1.16	
	0.51	7.80	5.39	0.69	0.69	1.02	0.52	11.70	8.05	0.69	1.01	
	0.79	18.53	12.54	0.76	0.76	1.00	0.80	27.30	18.54	0.77	1.00	
C180	1.11	36.08	20.58	0.83	0.83	0.99	1.10	52.65	31.94	0.88	1.02	
	1.50	66.30	24.24	0.70	0.88	0.92	1.50	96.53	46.32	0.92	1.01	
	1.95	112.13	27.60	0.62	0.93	0.92	1.95	163.80	67.39	1.03	1.10	
	2.45	176.48	30.91	0.56	0.95	0.95	2.44	257.40	92.02	1.14	1.19	
	3.05	274.95	35.33	0.52	1.00	1.01	3.06	402.68	121.68	1.24	1.28	
	0.57	20.22	14.36	0.71	0.71	1.05	0.56	27.64	19.90	0.72	1.06	
	0.85	45.17	31.40	0.82	0.82	1.03	0.85	62.70	44.19	0.83	1.05	
	1.17	85.62	48.75	0.86	0.89	1.04	1.16	118.65	76.65	0.98	1.12	
C200a	1.57	155.06	57.40	0.74	0.97	1.00	1.57	215.73	101.63	0.95	1.03	
	2.02	256.85	63.89	0.65	0.99	0.98	2.02	357.30	132.94	0.97	1.03	
	2.54	405.17	74.74	0.61	1.07	1.06	2.54	563.60	175.10	1.03	1.08	
	3.15	624.27	85.75	0.58	1.12	1.14	3.15	867.64	225.44	1.10	1.13	
	0.61	15.17	10.59	0.70	0.70	1.03	0.62	21.91	15.34	0.71	1.03	
	0.89	32.02	21.60	0.82	0.82	1.02	0.89	46.35	31.51	0.83	1.03	
	1.22	60.67	31.20	0.81	0.87	0.99	1.22	86.80	51.60	0.94	1.07	
	1.64	109.55	35.89	0.69	0.93	0.94	1.64	155.90	70.85	0.96	1.03	
C200b	2.09	177.81	39.24	0.60	0.93	0.92	2.09	253.65	96.61	1.03	1.09	
	2.63	281.46	46.54	0.57	1.01	1.01	2.63	401.13	125.94	1.09	1.13	
	3.24	427.25	52.15	0.53	1.04	1.06	3.24	609.27	159.86	1.15	1.18	
	0.65	10.83	7.43	0.70	0.70	1.01	0.66	16.25	11.17	0.71	1.01	
	0.93	22.75	14.88	0.83	0.83	1.00	0.94	32.50	22.31	0.87	1.06	
	1.27	42.25	20.00	0.78	0.86	0.96	1.28	60.67	34.14	0.93	1.04	
	1.71	75.84	22.61	0.65	0.90	0.91	1.71	107.26	46.62	0.95	1.02	
	2.16	121.34	25.19	0.58	0.92	0.91	2.16	172.27	65.73	1.07	1.13	
C200c	2.72	192.85	29.11	0.54	0.98	0.97	2.72	273.02	88.39	1.16	1.21	
	3.33	289.28	32.45	0.51	1.00	1.02	3.33	409.54	112.78	1.24	1.28	

Table B2-500: Numerical failure loads and their DSM estimates for the pinned and fixed hat-section columns at 500°C

Column	Pinned (P)						Fixed (F)					
	$\bar{\lambda}_{D.T}$	$P_{y,T}$ (kN)	$P_{u,T}$ (kN)	$\frac{P_{u,T}}{P_{n,D.T}^F}$	$\frac{P_{u,T}}{P_{n,D.T}^P}$	$\frac{P_{u,T}}{P_{n,D.T}^{P^*}}$	$\bar{\lambda}_{D.T}$	$P_{y,T}$ (kN)	$P_{u,T}$ (kN)	$\frac{P_{u,T}}{P_{n,D.T}^F}$	$\frac{P_{u,T}}{P_{n,D.T}^{P^*}}$	
H130	0.38	14.90	10.43	0.70	0.70	1.03	0.38	21.03	14.51	0.69	1.02	
	0.66	45.57	32.81	0.74	0.74	1.06	0.66	63.98	46.06	0.74	1.06	
	0.95	95.09	64.65	0.87	0.87	1.05	0.95	132.78	92.69	0.89	1.08	
	1.31	181.42	87.01	0.81	0.92	1.01	1.31	253.72	141.96	0.95	1.06	
	1.76	327.34	99.44	0.69	0.97	0.97	1.76	457.92	192.62	0.95	1.02	
	2.21	514.45	106.32	0.59	0.95	0.94	2.21	719.53	249.81	0.99	1.05	
	2.82	838.72	124.91	0.56	1.02	1.02	2.82	1172.63	326.58	1.04	1.08	
	0.42	10.11	7.18	0.71	0.71	1.05	0.42	14.54	10.18	0.70	1.03	
H150	0.70	28.44	20.02	0.75	0.75	1.04	0.70	39.82	28.12	0.75	1.04	
	1.01	58.15	37.38	0.86	0.86	1.02	1.01	81.53	54.44	0.89	1.06	
	1.38	109.34	47.50	0.77	0.91	0.98	1.38	153.58	80.84	0.93	1.03	
	1.83	192.77	53.82	0.66	0.95	0.95	1.83	270.51	116.45	1.01	1.08	
	2.30	304.00	58.40	0.58	0.95	0.94	2.30	427.25	152.48	1.07	1.12	
	2.91	486.66	67.24	0.54	1.00	1.00	2.91	683.85	197.78	1.12	1.16	
	0.48	6.83	4.81	0.71	0.71	1.04	0.46	8.78	6.12	0.70	1.03	
	0.75	16.58	11.32	0.75	0.75	1.01	0.75	23.40	15.97	0.75	1.00	
H180	1.06	33.15	20.09	0.85	0.85	1.01	1.06	46.80	29.80	0.89	1.04	
	1.45	62.40	24.54	0.73	0.90	0.95	1.46	88.73	43.59	0.92	1.01	
	1.91	107.25	27.03	0.62	0.91	0.91	1.91	152.10	63.13	1.02	1.08	
	2.40	169.65	30.61	0.56	0.95	0.94	2.40	240.83	87.28	1.13	1.19	
	3.01	267.15	34.90	0.52	0.99	1.00	3.01	378.30	113.92	1.21	1.25	
	0.52	16.85	12.13	0.72	0.72	1.06	0.52	23.60	16.75	0.71	1.05	
	0.80	40.45	28.24	0.79	0.79	1.03	0.80	55.96	38.99	0.79	1.03	
	1.12	78.88	46.08	0.85	0.85	1.02	1.12	109.89	69.78	0.93	1.07	
H200a	1.52	146.97	55.58	0.74	0.94	0.98	1.52	204.27	98.55	0.94	1.03	
	1.97	246.74	60.97	0.63	0.95	0.94	1.97	343.15	130.85	0.97	1.03	
	2.49	393.04	69.90	0.58	1.00	0.99	2.49	546.74	173.30	1.03	1.08	
	3.10	608.77	79.83	0.54	1.04	1.06	3.10	847.42	222.87	1.09	1.13	
	0.56	12.64	8.99	0.71	0.71	1.05	0.57	18.54	12.86	0.69	1.02	
	0.85	29.49	20.11	0.81	0.81	1.02	0.85	41.29	28.23	0.81	1.02	
	1.18	56.46	30.85	0.84	0.87	1.01	1.18	79.21	47.37	0.92	1.04	
	1.59	102.81	35.60	0.71	0.93	0.95	1.59	144.94	68.66	0.97	1.05	
H200b	2.05	170.23	39.39	0.61	0.94	0.93	2.05	239.33	94.56	1.04	1.10	
	2.58	271.35	45.13	0.56	0.99	0.98	2.59	382.59	124.68	1.11	1.16	
	3.20	415.45	50.50	0.52	1.01	1.03	3.19	583.99	156.39	1.15	1.19	
	0.61	9.75	6.71	0.70	0.70	1.01	0.62	14.08	9.67	0.69	1.01	
	0.89	20.59	13.72	0.81	0.81	1.00	0.89	29.25	19.69	0.82	1.02	
	1.22	39.00	19.57	0.80	0.85	0.97	1.24	56.34	31.70	0.90	1.02	
	1.67	72.59	22.53	0.66	0.90	0.91	1.66	101.84	45.74	0.96	1.03	
	2.11	115.93	24.89	0.59	0.92	0.91	2.11	164.68	64.13	1.06	1.12	
H200c	2.68	186.35	28.58	0.54	0.96	0.96	2.68	264.36	87.80	1.17	1.22	
	3.29	281.69	31.90	0.50	0.99	1.01	3.29	398.70	112.81	1.26	1.30	

Table B3-500: Numerical failure loads and their DSM estimates for the pinned and fixed zed-section columns at 500°C

Column	Pinned (P)						Fixed (F)					
	$\bar{\lambda}_{D.T}$	$P_{y,T}$ (kN)	$P_{u,T}$ (kN)	$\frac{P_{u,T}}{P_{n,D.T}^F}$	$\frac{P_{u,T}}{P_{n,D.T}^P}$	$\frac{P_{u,T}}{P_{n,D.T}^{P*}}$	$\bar{\lambda}_{D.T}$	$P_{y,T}$ (kN)	$P_{u,T}$ (kN)	$\frac{P_{u,T}}{P_{n,D.T}^F}$	$\frac{P_{u,T}}{P_{n,D.T}^{P*}}$	
Z130	0.47	23.22	16.26	0.70	0.70	1.03	0.47	31.99	22.71	0.71	1.05	
	0.75	59.16	41.26	0.76	0.76	1.03	0.75	82.38	57.99	0.77	1.04	
	1.04	113.49	71.96	0.87	0.87	1.04	1.04	158.63	104.14	0.91	1.06	
	1.40	205.96	88.07	0.77	0.92	0.98	1.40	287.46	148.37	0.93	1.03	
	1.86	359.77	98.43	0.65	0.95	0.95	1.86	501.74	196.70	0.93	1.00	
	2.30	553.89	114.17	0.62	1.02	1.01	2.30	772.55	254.93	0.99	1.04	
	2.91	886.49	133.97	0.59	1.09	1.09	2.91	1236.61	337.15	1.06	1.10	
Z150	0.51	15.17	11.05	0.73	0.73	1.07	0.52	21.49	15.13	0.70	1.04	
	0.80	36.66	25.41	0.79	0.79	1.02	0.80	51.19	35.49	0.79	1.02	
	1.10	69.52	42.12	0.87	0.87	1.04	1.10	97.33	62.24	0.92	1.07	
	1.47	124.51	50.09	0.76	0.94	0.99	1.48	175.07	87.06	0.94	1.03	
	1.93	212.99	55.13	0.64	0.96	0.95	1.93	298.95	121.28	1.01	1.07	
	2.40	329.29	61.84	0.59	0.99	0.98	2.40	462.01	156.84	1.06	1.11	
	3.01	518.26	70.62	0.55	1.03	1.04	3.01	728.09	204.04	1.13	1.17	
Z180	0.57	9.75	6.77	0.69	0.69	1.02	0.56	13.65	9.38	0.69	1.01	
	0.85	21.45	14.51	0.80	0.80	1.01	0.85	31.20	21.20	0.80	1.01	
	1.16	39.98	22.39	0.85	0.87	1.02	1.15	57.53	34.52	0.90	1.03	
	1.54	70.20	25.83	0.73	0.93	0.96	1.55	103.35	47.74	0.92	1.00	
	2.00	117.98	28.31	0.62	0.94	0.93	2.00	172.58	67.71	1.01	1.07	
	2.49	183.30	31.79	0.57	0.97	0.96	2.49	268.13	92.29	1.12	1.17	
	3.10	284.70	35.99	0.53	1.01	1.02	3.10	415.35	120.78	1.21	1.25	
Z200a	0.61	23.60	16.92	0.72	0.72	1.06	0.61	32.36	22.72	0.71	1.03	
	0.89	49.89	34.11	0.83	0.83	1.03	0.89	69.44	47.74	0.84	1.04	
	1.21	92.36	50.97	0.87	0.92	1.05	1.21	128.76	77.82	0.95	1.08	
	1.62	164.50	58.15	0.73	0.97	0.99	1.62	228.54	104.05	0.94	1.02	
	2.07	269.66	64.86	0.64	1.00	0.99	2.07	374.16	137.10	0.98	1.04	
	2.58	420.68	75.62	0.61	1.07	1.06	2.58	584.50	180.16	1.05	1.09	
	3.20	643.15	85.82	0.57	1.11	1.13	3.20	893.94	234.29	1.13	1.16	
Z200b	0.66	17.70	12.29	0.72	0.72	1.02	0.66	25.28	17.54	0.72	1.02	
	0.94	36.24	24.39	0.86	0.86	1.04	0.94	51.40	34.64	0.86	1.04	
	1.27	65.73	33.35	0.83	0.92	1.03	1.27	93.54	52.87	0.93	1.04	
	1.68	115.45	37.51	0.70	0.96	0.97	1.69	165.17	73.56	0.96	1.04	
	2.14	186.24	41.25	0.61	0.97	0.96	2.14	264.61	100.12	1.05	1.10	
	2.68	291.57	47.46	0.57	1.03	1.02	2.68	415.45	129.39	1.10	1.14	
	3.29	439.89	52.83	0.53	1.05	1.07	3.29	626.97	164.25	1.16	1.20	
Z200c	0.71	13.00	8.77	0.72	0.72	0.99	0.71	18.42	12.45	0.72	0.99	
	0.98	24.92	15.85	0.83	0.83	1.00	0.98	35.75	23.17	0.85	1.02	
	1.32	45.50	20.50	0.77	0.88	0.96	1.33	65.01	33.06	0.87	0.97	
	1.75	80.17	22.72	0.64	0.89	0.90	1.76	113.76	47.02	0.93	1.00	
	2.21	126.76	23.79	0.54	0.86	0.86	2.21	179.85	65.21	1.04	1.09	
	2.77	200.43	25.03	0.46	0.83	0.83	2.77	282.78	89.22	1.16	1.20	
	3.38	297.94	32.43	0.50	0.99	1.02	3.38	421.45	113.36	1.23	1.27	

Table B4-500: Numerical failure loads and their DSM estimates for the pinned and fixed rack-section columns at 500°C

Column	Pinned (P)						Fixed (F)					
	$\bar{\lambda}_{D.T}$	$P_{y,T}$ (kN)	$P_{u,T}$ (kN)	$\frac{P_{u,T}}{P_{n,D.T}^F}$	$\frac{P_{u,T}}{P_{n,D.T}^P}$	$\frac{P_{u,T}}{P_{n,D.T}^{P*}}$	$\bar{\lambda}_{D.T}$	$P_{y,T}$ (kN)	$P_{u,T}$ (kN)	$\frac{P_{u,T}}{P_{n,D.T}^F}$	$\frac{P_{u,T}}{P_{n,D.T}^{P*}}$	
R130	0.40	16.31	11.70	0.72	0.72	1.06	0.40	23.11	15.71	0.68	1.00	
	0.68	47.12	33.11	0.73	0.73	1.03	0.68	66.60	45.29	0.71	1.00	
	0.97	96.51	58.72	0.79	0.79	0.95	0.97	135.93	91.00	0.87	1.04	
	1.34	181.69	80.62	0.76	0.88	0.96	1.34	256.45	143.83	0.96	1.07	
	1.79	324.87	87.71	0.62	0.88	0.88	1.79	458.98	191.14	0.95	1.02	
	2.23	507.46	93.65	0.53	0.87	0.86	2.23	716.79	235.59	0.95	1.00	
	2.84	823.72	113.61	0.52	0.96	0.96	2.84	1163.09	306.13	0.99	1.03	
	0.44	11.64	8.07	0.69	0.69	1.02	0.44	16.82	11.65	0.69	1.02	
R150	0.73	31.70	21.51	0.73	0.73	1.00	0.73	45.28	30.75	0.73	1.00	
	1.03	63.40	40.85	0.88	0.88	1.05	1.03	90.57	59.26	0.89	1.05	
	1.41	117.74	47.10	0.72	0.87	0.92	1.40	168.20	89.22	0.96	1.06	
	1.85	205.07	63.82	0.74	1.08	1.08	1.86	294.35	120.17	0.97	1.04	
	2.33	322.16	68.89	0.65	1.07	1.06	2.33	461.90	154.64	1.01	1.06	
	2.94	514.30	79.20	0.60	1.12	1.13	2.94	736.19	200.97	1.07	1.11	
	0.49	7.92	5.37	0.68	0.68	1.00	0.49	11.88	8.06	0.68	1.00	
	0.78	19.80	13.17	0.74	0.74	0.98	0.77	29.70	19.99	0.75	0.99	
R180	1.09	38.61	20.55	0.76	0.76	0.91	1.08	58.40	36.45	0.89	1.03	
	1.48	71.27	25.42	0.68	0.84	0.88	1.48	108.89	50.66	0.88	0.97	
	1.93	120.77	25.42	0.52	0.78	0.77	1.93	185.11	71.69	0.96	1.02	
	2.42	191.05	31.43	0.52	0.88	0.87	2.42	293.01	98.07	1.06	1.11	
	3.03	298.95	35.97	0.49	0.92	0.93	3.03	459.31	128.51	1.13	1.17	
	0.54	18.60	12.86	0.69	0.69	1.02	0.54	26.18	17.98	0.69	1.01	
	0.82	43.41	29.28	0.78	0.78	1.00	0.82	61.33	41.46	0.78	1.00	
	1.14	84.06	46.19	0.82	0.82	0.98	1.14	117.83	74.32	0.94	1.08	
R200a	1.55	154.35	55.35	0.71	0.92	0.95	1.55	216.36	103.58	0.95	1.03	
	2.00	257.01	58.69	0.59	0.89	0.89	2.00	361.06	132.74	0.95	1.00	
	2.51	407.92	71.81	0.58	1.00	1.00	2.51	571.91	171.38	0.99	1.03	
	3.12	629.79	82.24	0.55	1.05	1.07	3.13	884.05	227.53	1.08	1.11	
	0.58	14.58	9.93	0.68	0.68	1.00	0.59	21.44	14.58	0.68	1.00	
	0.87	32.59	21.64	0.80	0.80	1.00	0.87	46.31	31.11	0.81	1.01	
	1.20	61.75	31.10	0.78	0.83	0.95	1.20	88.33	53.22	0.94	1.06	
	1.61	111.49	36.70	0.68	0.90	0.92	1.62	161.23	73.25	0.94	1.02	
R200b	2.07	182.67	38.95	0.57	0.88	0.87	2.07	263.28	98.97	1.00	1.06	
	2.61	291.58	38.95	0.46	0.81	0.80	2.61	418.50	126.98	1.04	1.08	
	3.22	443.37	52.37	0.51	1.00	1.01	3.22	638.05	162.11	1.10	1.14	
	0.63	10.98	7.43	0.69	0.69	1.00	0.64	17.57	11.88	0.69	1.00	
	0.91	23.06	14.82	0.80	0.80	0.98	0.92	36.24	24.06	0.83	1.01	
	1.25	43.93	20.02	0.74	0.81	0.91	1.25	67.00	37.53	0.91	1.02	
	1.68	79.08	23.73	0.65	0.88	0.89	1.69	121.91	52.09	0.92	1.00	
	2.13	127.41	25.10	0.54	0.86	0.85	2.14	195.50	71.79	1.02	1.07	
R200c	2.70	204.29	26.15	0.46	0.82	0.82	2.70	313.02	96.16	1.10	1.14	
	3.31	306.43	33.24	0.49	0.96	0.98	3.31	470.08	121.47	1.16	1.19	

Table B1-600: Numerical failure loads and their DSM estimates for the pinned and fixed lipped channel columns at 600°C

Column	Pinned (P)						Fixed (F)					
	$\bar{\lambda}_{D,T}$	$P_{y,T}$ (kN)	$P_{u,T}$ (kN)	$\frac{P_{u,T}}{P_{n,D,T}^F}$	$\frac{P_{u,T}}{P_{n,D,T}^P}$	$\frac{P_{u,T}}{P_{n,D,T}^{Ps}}$	$\bar{\lambda}_{D,T}$	$P_{y,T}$ (kN)	$P_{u,T}$ (kN)	$\frac{P_{u,T}}{P_{n,D,T}^F}$	$\frac{P_{u,T}}{P_{n,D,T}^P}$	
C130	0.45	10.67	6.61	0.62	0.62	1.03	0.44	14.63	9.51	0.65	1.08	
	0.74	29.27	18.73	0.69	0.69	1.07	0.74	40.93	26.60	0.71	1.08	
	1.04	58.54	34.58	0.82	0.82	1.04	1.04	81.61	49.33	0.83	1.05	
	1.42	108.64	45.39	0.76	0.92	1.01	1.42	151.80	74.32	0.89	1.03	
	1.89	192.98	51.46	0.65	0.96	0.97	1.89	269.37	99.23	0.90	0.98	
	2.36	299.88	60.68	0.62	1.04	1.04	2.36	418.69	128.97	0.95	1.01	
	3.00	484.42	72.24	0.60	1.13	1.14	3.00	676.16	171.36	1.02	1.07	
C150	0.49	7.16	4.51	0.63	0.63	1.05	0.49	10.02	6.33	0.63	1.05	
	0.79	18.25	11.72	0.72	0.72	1.07	0.79	25.76	16.30	0.71	1.05	
	1.10	35.78	20.55	0.83	0.83	1.05	1.10	50.44	30.08	0.86	1.07	
	1.50	66.18	26.24	0.76	0.96	1.03	1.49	92.66	43.27	0.89	1.02	
	1.97	114.48	29.40	0.65	0.98	0.99	1.97	160.63	60.74	0.96	1.04	
	2.46	178.88	32.26	0.58	0.99	0.99	2.46	251.14	79.17	1.01	1.08	
	3.10	283.70	36.91	0.54	1.03	1.05	3.10	398.53	104.34	1.09	1.14	
C180	0.54	4.42	2.75	0.62	0.62	1.04	0.55	6.62	4.06	0.61	1.02	
	0.83	10.49	6.31	0.70	0.70	1.00	0.83	15.45	9.33	0.70	1.01	
	1.16	20.42	10.60	0.78	0.80	0.99	1.16	29.80	15.66	0.79	0.96	
	1.57	37.53	12.63	0.68	0.88	0.93	1.57	54.64	23.53	0.86	0.97	
	2.04	63.47	14.03	0.58	0.90	0.90	2.04	92.72	34.70	0.98	1.07	
	2.56	99.89	14.76	0.50	0.87	0.87	2.56	145.70	47.48	1.09	1.16	
	3.19	155.63	18.29	0.50	0.98	1.00	3.20	227.93	62.93	1.19	1.24	
C200a	0.59	11.45	7.21	0.63	0.63	1.05	0.59	15.65	10.01	0.64	1.07	
	0.89	25.57	16.12	0.77	0.77	1.05	0.89	35.49	22.90	0.78	1.08	
	1.22	48.46	25.41	0.83	0.89	1.06	1.22	67.16	39.46	0.93	1.11	
	1.64	87.77	30.51	0.73	0.98	1.02	1.64	122.11	52.77	0.91	1.02	
	2.11	145.39	33.99	0.64	1.01	1.01	2.11	202.25	69.36	0.94	1.01	
	2.66	229.34	38.99	0.59	1.06	1.06	2.66	319.02	92.19	1.01	1.07	
	3.30	353.36	44.84	0.56	1.11	1.14	3.30	491.12	120.22	1.09	1.14	
C200b	0.64	8.59	5.42	0.65	0.65	1.05	0.64	12.40	7.65	0.63	1.03	
	0.93	18.13	10.96	0.76	0.76	1.02	0.94	26.24	15.93	0.77	1.02	
	1.28	34.34	16.29	0.78	0.87	1.01	1.28	49.13	26.39	0.89	1.05	
	1.72	62.01	18.82	0.67	0.93	0.95	1.72	88.25	36.29	0.91	1.01	
	2.19	100.65	20.89	0.59	0.95	0.95	2.19	143.58	49.70	0.98	1.06	
	2.76	159.32	24.10	0.55	1.00	1.01	2.75	227.05	65.16	1.05	1.10	
	3.39	241.84	27.07	0.51	1.03	1.06	3.39	344.87	83.98	1.12	1.17	
C200c	0.68	6.13	3.78	0.64	0.64	1.03	0.70	9.20	5.62	0.64	1.02	
	0.98	12.88	7.57	0.77	0.77	1.00	0.98	18.40	11.02	0.79	1.02	
	1.33	23.92	10.35	0.74	0.85	0.97	1.34	34.34	17.41	0.88	1.02	
	1.79	42.93	11.92	0.64	0.90	0.92	1.79	60.71	23.98	0.91	1.00	
	2.26	68.69	13.19	0.56	0.92	0.92	2.26	97.51	33.55	1.01	1.09	
	2.85	109.16	15.07	0.52	0.96	0.97	2.85	154.54	45.70	1.12	1.18	
	3.49	163.74	16.81	0.49	0.98	1.02	3.49	231.81	58.04	1.19	1.24	

Table B2-600: Numerical failure loads and their DSM estimates for the pinned and fixed hat-section columns at 600°C

Column	Pinned (P)						Fixed (F)					
	$\bar{\lambda}_{D.T}$	$P_{y,T}$ (kN)	$P_{u,T}$ (kN)	$\frac{P_{u,T}}{P_{n,D.T}^F}$	$\frac{P_{u,T}}{P_{n,D.T}^P}$	$\frac{P_{u,T}}{P_{n,D.T}^{P*}}$	$\bar{\lambda}_{D.T}$	$P_{y,T}$ (kN)	$P_{u,T}$ (kN)	$\frac{P_{u,T}}{P_{n,D.T}^F}$	$\frac{P_{u,T}}{P_{n,D.T}^{P*}}$	
H130	0.39	8.43	5.48	0.65	0.65	1.08	0.40	11.91	7.38	0.62	1.03	
	0.69	25.80	16.25	0.66	0.66	1.05	0.69	36.21	22.81	0.66	1.05	
	0.99	53.82	33.63	0.83	0.83	1.07	0.99	75.16	48.34	0.85	1.10	
	1.37	102.69	46.42	0.80	0.94	1.05	1.37	143.62	74.07	0.91	1.05	
	1.84	185.29	51.64	0.66	0.96	0.97	1.84	259.20	101.73	0.93	1.02	
	2.31	291.20	55.33	0.57	0.94	0.95	2.31	407.28	132.55	0.98	1.05	
	2.95	474.75	61.72	0.51	0.96	0.97	2.95	663.76	175.00	1.04	1.09	
	0.44	5.72	3.66	0.64	0.64	1.07	0.44	8.23	5.18	0.63	1.05	
H150	0.74	16.10	10.44	0.70	0.70	1.08	0.74	22.54	14.64	0.70	1.08	
	1.05	32.91	19.34	0.82	0.82	1.04	1.05	46.15	27.96	0.84	1.06	
	1.45	61.89	25.03	0.75	0.92	1.00	1.45	86.93	42.39	0.90	1.04	
	1.92	109.11	28.04	0.63	0.94	0.95	1.92	153.12	60.64	0.98	1.07	
	2.41	172.08	30.97	0.57	0.96	0.96	2.41	241.84	79.21	1.03	1.10	
	3.05	275.47	35.19	0.52	0.99	1.01	3.05	387.09	104.48	1.10	1.16	
	0.50	3.86	2.48	0.64	0.64	1.07	0.48	4.97	3.14	0.63	1.05	
	0.78	9.38	5.73	0.69	0.69	1.02	0.78	13.25	8.14	0.69	1.02	
H180	1.11	18.76	10.36	0.80	0.80	1.02	1.11	26.49	15.14	0.83	1.02	
	1.52	35.32	12.89	0.71	0.91	0.97	1.52	50.22	22.78	0.89	1.00	
	1.99	60.71	14.25	0.60	0.92	0.92	2.00	86.09	32.76	0.98	1.07	
	2.51	96.03	15.94	0.55	0.94	0.94	2.51	136.32	44.60	1.08	1.15	
	3.15	151.22	18.09	0.51	0.97	1.00	3.15	214.13	59.03	1.16	1.22	
	0.54	9.54	6.01	0.63	0.63	1.05	0.54	13.36	8.69	0.65	1.08	
	0.84	22.90	14.53	0.74	0.74	1.06	0.83	31.67	20.24	0.75	1.07	
	1.17	44.65	24.29	0.83	0.85	1.05	1.17	62.20	35.92	0.88	1.06	
H200a	1.59	83.19	29.07	0.71	0.94	0.99	1.59	115.62	51.08	0.90	1.01	
	2.07	139.67	31.93	0.61	0.95	0.95	2.07	194.23	67.89	0.93	1.01	
	2.61	222.47	35.60	0.55	0.97	0.97	2.61	309.48	90.68	1.00	1.07	
	3.25	344.58	41.81	0.53	1.04	1.06	3.25	479.67	117.70	1.07	1.12	
	0.58	7.16	4.65	0.65	0.65	1.08	0.60	10.49	6.53	0.63	1.04	
	0.89	16.70	10.20	0.75	0.75	1.02	0.89	23.37	14.31	0.75	1.02	
	1.23	31.96	15.89	0.79	0.86	1.02	1.23	44.84	24.89	0.89	1.06	
	1.66	58.19	18.96	0.69	0.94	0.98	1.67	82.04	35.56	0.93	1.03	
H200b	2.14	96.35	20.81	0.60	0.95	0.95	2.14	135.47	49.39	1.01	1.09	
	2.70	153.59	23.48	0.55	0.98	0.98	2.71	216.56	64.14	1.06	1.12	
	3.35	235.16	26.37	0.51	1.00	1.03	3.34	330.56	81.90	1.12	1.17	
	0.64	5.52	3.41	0.63	0.63	1.03	0.65	7.97	4.87	0.63	1.02	
	0.93	11.65	6.95	0.75	0.75	1.00	0.93	16.56	9.92	0.76	1.00	
	1.28	22.08	10.18	0.76	0.85	0.98	1.29	31.89	16.27	0.85	1.00	
	1.75	41.09	11.79	0.64	0.90	0.93	1.74	57.65	23.55	0.91	1.01	
	2.21	65.62	13.04	0.57	0.92	0.92	2.21	93.22	33.12	1.02	1.10	
H200c	2.80	105.48	14.85	0.52	0.95	0.96	2.80	149.64	45.15	1.12	1.18	
	3.44	159.45	16.57	0.49	0.97	1.01	3.44	225.68	57.59	1.19	1.24	

Table B3-600: Numerical failure loads and their DSM estimates for the pinned and fixed zed-section columns at 600°C

Column	Pinned (P)						Fixed (F)					
	$\bar{\lambda}_{D,T}$	$P_{y,T}$ (kN)	$P_{u,T}$ (kN)	$\frac{P_{u,T}}{P_{n,D,T}^F}$	$\frac{P_{u,T}}{P_{n,D,T}^P}$	$\frac{P_{u,T}}{P_{n,D,T}^{ps}}$	$\bar{\lambda}_{D,T}$	$P_{y,T}$ (kN)	$P_{u,T}$ (kN)	$\frac{P_{u,T}}{P_{n,D,T}^F}$	$\frac{P_{u,T}}{P_{n,D,T}^{F*}}$	
Z130	0.49	13.15	8.41	0.64	0.64	1.07	0.49	18.11	11.77	0.65	1.08	
	0.79	33.49	21.16	0.71	0.71	1.05	0.79	46.63	30.33	0.73	1.08	
	1.09	64.24	36.66	0.82	0.82	1.04	1.09	89.79	52.81	0.84	1.05	
	1.47	116.58	45.71	0.74	0.92	0.99	1.47	162.71	75.39	0.87	1.00	
	1.94	203.64	51.12	0.63	0.94	0.95	1.94	284.01	104.58	0.92	1.01	
	2.41	313.52	59.70	0.60	1.01	1.01	2.41	437.29	136.35	0.98	1.05	
	3.05	501.78	70.08	0.57	1.08	1.10	3.05	699.97	180.17	1.05	1.10	
Z150	0.54	8.59	5.41	0.63	0.63	1.05	0.54	12.16	7.88	0.65	1.08	
	0.84	20.75	13.01	0.73	0.73	1.05	0.83	28.98	18.24	0.73	1.05	
	1.15	39.35	21.75	0.83	0.84	1.05	1.15	55.09	32.05	0.87	1.06	
	1.54	70.48	26.17	0.73	0.94	1.00	1.54	99.10	45.54	0.91	1.03	
	2.02	120.56	29.12	0.63	0.96	0.97	2.02	169.22	63.84	0.98	1.07	
	2.51	186.39	32.28	0.57	0.98	0.99	2.51	261.52	82.45	1.04	1.10	
	3.15	293.36	36.83	0.53	1.02	1.04	3.15	412.13	107.52	1.10	1.15	
Z180	0.60	5.52	3.41	0.62	0.62	1.03	0.59	7.73	4.73	0.61	1.02	
	0.89	12.14	7.32	0.74	0.74	1.01	0.89	17.66	10.70	0.74	1.01	
	1.22	22.63	11.65	0.81	0.86	1.04	1.21	32.56	17.65	0.85	1.02	
	1.61	39.74	13.46	0.70	0.93	0.97	1.62	58.50	24.54	0.87	0.98	
	2.09	66.78	14.75	0.60	0.93	0.94	2.09	97.68	35.17	0.97	1.05	
	2.61	103.76	16.51	0.55	0.96	0.96	2.61	151.77	47.65	1.08	1.14	
	3.25	161.15	18.72	0.51	0.99	1.02	3.25	235.10	62.26	1.16	1.21	
Z200a	0.64	13.36	8.68	0.66	0.66	1.08	0.64	18.32	11.91	0.66	1.08	
	0.93	28.24	17.48	0.78	0.78	1.04	0.93	39.30	24.41	0.78	1.04	
	1.27	52.28	26.50	0.83	0.92	1.07	1.27	72.89	40.53	0.91	1.08	
	1.69	93.11	30.64	0.71	0.98	1.01	1.69	129.36	53.91	0.90	1.01	
	2.17	152.64	33.96	0.62	0.99	1.00	2.16	211.79	71.89	0.95	1.03	
	2.70	238.12	39.43	0.59	1.06	1.07	2.70	330.85	95.23	1.03	1.09	
	3.34	364.05	44.85	0.56	1.10	1.14	3.35	506.00	123.94	1.11	1.16	
Z200b	0.69	10.02	6.30	0.66	0.66	1.05	0.69	14.31	9.01	0.66	1.05	
	0.99	20.51	12.34	0.79	0.79	1.03	0.99	29.10	17.44	0.79	1.02	
	1.33	37.21	17.44	0.80	0.92	1.04	1.33	52.95	27.60	0.89	1.04	
	1.76	65.35	19.56	0.68	0.95	0.98	1.77	93.49	38.32	0.93	1.03	
	2.24	105.42	21.66	0.60	0.97	0.97	2.24	149.78	51.65	1.00	1.08	
	2.80	165.04	24.64	0.55	1.01	1.02	2.80	235.16	67.45	1.07	1.12	
	3.44	248.99	27.53	0.52	1.04	1.07	3.44	354.89	86.74	1.14	1.19	
Z200c	0.74	7.36	4.39	0.65	0.65	0.99	0.74	10.43	6.23	0.65	1.00	
	1.02	14.11	8.00	0.77	0.77	0.99	1.03	20.24	11.65	0.79	1.00	
	1.38	25.76	10.53	0.73	0.86	0.95	1.39	36.80	16.86	0.82	0.95	
	1.84	45.38	11.69	0.61	0.88	0.89	1.84	64.39	23.94	0.88	0.97	
	2.31	71.75	12.24	0.51	0.85	0.85	2.31	101.80	33.40	0.99	1.06	
	2.90	113.45	12.88	0.44	0.81	0.82	2.90	160.06	45.84	1.10	1.16	
	3.54	168.65	16.71	0.48	0.97	1.01	3.54	238.56	58.43	1.18	1.23	

Table B4-600: Numerical failure loads and their DSM estimates for the pinned and fixed rack-section columns at 600°C

Column	Pinned (P)						Fixed (F)					
	$\bar{\lambda}_{D.T}$	$P_{y.T}$ (kN)	$P_{u.T}$ (kN)	$\frac{P_{u.T}}{P_{n.D.T}^F}$	$\frac{P_{u.T}}{P_{n.D.T}^P}$	$\frac{P_{u.T}}{P_{n.D.T}^{Ps}}$	$\bar{\lambda}_{D.T}$	$P_{y.T}$ (kN)	$P_{u.T}$ (kN)	$\frac{P_{u.T}}{P_{n.D.T}^F}$	$\frac{P_{u.T}}{P_{n.D.T}^P}$	
R130	0.42	9.23	5.82	0.63	0.63	1.05	0.42	13.08	7.85	0.60	1.00	
	0.71	26.67	16.54	0.66	0.66	1.03	0.71	37.70	22.62	0.64	1.00	
	1.02	54.63	30.05	0.74	0.74	0.95	1.02	76.94	46.27	0.81	1.04	
	1.40	102.84	41.28	0.72	0.86	0.95	1.40	145.16	74.36	0.92	1.06	
	1.87	183.89	47.00	0.61	0.90	0.91	1.87	259.80	99.45	0.92	1.01	
	2.34	287.24	48.35	0.51	0.85	0.85	2.34	405.73	123.40	0.93	0.99	
	2.98	466.26	59.33	0.51	0.95	0.96	2.98	658.35	163.00	0.98	1.03	
R150	0.46	6.59	4.10	0.62	0.62	1.04	0.46	9.52	5.72	0.60	1.00	
	0.76	17.94	10.82	0.67	0.67	1.01	0.76	25.63	15.51	0.67	1.01	
	1.08	35.89	20.56	0.81	0.81	1.03	1.08	51.26	29.88	0.83	1.03	
	1.47	66.64	25.99	0.74	0.91	0.99	1.47	95.21	45.42	0.90	1.03	
	1.94	116.08	32.88	0.71	1.06	1.07	1.94	166.61	62.21	0.93	1.02	
	2.43	182.36	35.61	0.62	1.06	1.06	2.43	261.45	80.24	0.98	1.04	
	3.07	291.11	41.11	0.58	1.11	1.13	3.07	416.71	105.61	1.04	1.09	
R180	0.52	4.48	2.69	0.60	0.60	1.00	0.51	6.72	4.04	0.60	1.00	
	0.82	11.21	6.61	0.68	0.68	0.98	0.81	16.81	10.00	0.68	0.99	
	1.14	21.85	10.50	0.71	0.72	0.91	1.13	33.06	18.38	0.82	1.01	
	1.55	40.34	12.95	0.64	0.82	0.87	1.55	61.63	25.82	0.83	0.94	
	2.02	68.36	12.95	0.49	0.75	0.76	2.01	104.78	36.63	0.91	0.99	
	2.54	108.14	19.52	0.60	1.04	1.05	2.53	165.85	50.76	1.02	1.08	
	3.17	169.22	18.61	0.47	0.91	0.93	3.17	259.99	66.18	1.09	1.14	
R200a	0.56	10.53	6.53	0.62	0.62	1.03	0.56	14.82	9.21	0.62	1.04	
	0.86	24.57	14.70	0.71	0.71	1.00	0.86	34.71	20.86	0.72	1.00	
	1.19	47.58	23.67	0.77	0.81	0.98	1.19	66.69	37.54	0.87	1.05	
	1.62	87.37	28.33	0.67	0.89	0.94	1.62	122.47	53.15	0.90	1.01	
	2.09	145.48	30.32	0.56	0.88	0.88	2.09	204.37	68.50	0.91	0.98	
	2.63	230.90	37.02	0.56	0.98	0.99	2.63	323.72	88.20	0.94	1.00	
	3.27	356.48	42.49	0.53	1.03	1.06	3.27	500.40	120.29	1.06	1.11	
R200b	0.61	8.25	4.98	0.61	0.61	1.01	0.62	12.14	7.32	0.61	1.01	
	0.91	18.45	10.86	0.73	0.73	0.99	0.91	26.21	15.59	0.74	0.99	
	1.26	34.95	15.92	0.74	0.81	0.95	1.25	50.00	27.07	0.88	1.04	
	1.69	63.11	18.75	0.64	0.88	0.91	1.69	91.26	37.21	0.88	0.99	
	2.16	103.40	19.99	0.54	0.86	0.86	2.16	149.03	50.45	0.95	1.02	
	2.73	165.05	19.99	0.44	0.79	0.79	2.73	236.89	65.75	1.00	1.06	
	3.37	250.97	26.91	0.49	0.97	1.00	3.37	361.16	84.74	1.07	1.12	
R200c	0.66	6.22	3.72	0.62	0.62	1.00	0.67	9.95	5.95	0.62	1.00	
	0.95	13.06	7.48	0.73	0.73	0.97	0.96	20.52	12.06	0.76	1.00	
	1.31	24.87	10.27	0.70	0.79	0.90	1.31	37.92	18.81	0.84	0.98	
	1.76	44.76	12.18	0.61	0.86	0.89	1.77	69.01	26.08	0.86	0.95	
	2.23	72.12	12.98	0.52	0.85	0.85	2.24	110.66	36.36	0.95	1.03	
	2.83	115.63	15.25	0.50	0.91	0.92	2.83	177.18	49.76	1.05	1.11	
	3.47	173.45	17.09	0.46	0.93	0.97	3.47	266.08	62.37	1.10	1.15	

Table B1-700: Numerical failure loads and their DSM estimates for the pinned and fixed lipped channel columns at 700°C

Column	Pinned (P)						Fixed (F)				
	$\bar{\lambda}_{D.T}$	$P_{y,T}$ (kN)	$P_{u,T}$ (kN)	$\frac{P_{u,T}}{P_{n,D.T}^F}$	$\frac{P_{u,T}}{P_{n,D.T}^P}$	$\frac{P_{u,T}}{P_{n,D.T}^{P*}}$	$\bar{\lambda}_{D.T}$	$P_{y,T}$ (kN)	$P_{u,T}$ (kN)	$\frac{P_{u,T}}{P_{n,D.T}^F}$	$\frac{P_{u,T}}{P_{n,D.T}^{P*}}$
C130	0.45	4.62	2.77	0.60	0.60	1.04	0.45	6.34	3.87	0.61	1.06
	0.75	12.68	7.74	0.67	0.67	1.06	0.75	17.73	11.60	0.72	1.13
	1.06	25.37	14.79	0.82	0.82	1.06	1.06	35.36	20.71	0.82	1.05
	1.44	47.08	19.40	0.76	0.94	1.03	1.45	65.78	31.30	0.88	1.03
	1.93	83.62	22.11	0.65	0.97	0.99	1.92	116.73	42.21	0.90	0.99
	2.40	129.95	25.86	0.62	1.05	1.06	2.40	181.43	54.38	0.94	1.01
	3.05	209.92	30.63	0.60	1.13	1.15	3.05	293.00	72.67	1.01	1.07
C150	0.50	3.10	1.92	0.62	0.62	1.07	0.50	4.34	2.60	0.60	1.04
	0.80	7.91	4.83	0.69	0.69	1.06	0.80	11.16	6.96	0.71	1.08
	1.12	15.50	8.98	0.85	0.85	1.10	1.12	21.86	12.68	0.85	1.07
	1.52	28.68	11.47	0.78	0.99	1.07	1.52	40.15	18.35	0.89	1.02
	2.00	49.61	13.03	0.68	1.03	1.05	2.00	69.61	25.68	0.95	1.04
	2.50	77.51	14.14	0.60	1.03	1.04	2.50	108.83	33.45	1.01	1.08
	3.15	122.93	15.90	0.55	1.05	1.08	3.15	172.70	44.24	1.08	1.14
C180	0.55	1.91	1.17	0.61	0.61	1.06	0.55	2.87	1.70	0.59	1.03
	0.84	4.54	2.65	0.69	0.69	1.01	0.85	6.70	3.91	0.69	1.01
	1.18	8.85	4.49	0.78	0.80	1.00	1.18	12.91	7.19	0.85	1.05
	1.59	16.26	5.41	0.68	0.89	0.95	1.59	23.68	9.97	0.86	0.98
	2.07	27.50	6.03	0.59	0.91	0.92	2.07	40.18	14.65	0.98	1.07
	2.60	43.29	6.79	0.54	0.94	0.95	2.60	63.14	20.01	1.08	1.16
	3.25	67.44	7.74	0.50	0.98	1.01	3.25	98.77	26.43	1.17	1.23
C200a	0.60	4.96	3.03	0.61	0.61	1.06	0.60	6.78	4.46	0.66	1.14
	0.90	11.08	7.04	0.78	0.78	1.10	0.90	15.38	9.91	0.79	1.12
	1.24	21.00	11.33	0.87	0.94	1.13	1.24	29.10	16.95	0.93	1.13
	1.67	38.03	13.37	0.75	1.02	1.07	1.67	52.92	23.04	0.93	1.05
	2.15	63.00	15.11	0.67	1.06	1.07	2.15	87.64	29.71	0.94	1.03
	2.70	99.38	16.85	0.60	1.08	1.09	2.70	138.24	39.33	1.01	1.08
	3.35	153.12	19.23	0.57	1.13	1.16	3.35	212.82	50.90	1.08	1.14
C200b	0.65	3.72	2.34	0.64	0.64	1.09	0.65	5.37	3.43	0.66	1.10
	0.94	7.85	4.62	0.75	0.75	1.02	0.95	11.37	6.71	0.76	1.02
	1.30	14.88	7.05	0.79	0.89	1.04	1.30	21.29	11.25	0.89	1.06
	1.75	26.87	8.24	0.69	0.96	0.99	1.75	38.24	15.45	0.90	1.01
	2.23	43.61	9.07	0.60	0.97	0.98	2.23	62.22	20.98	0.97	1.06
	2.80	69.04	10.32	0.55	1.01	1.02	2.80	98.39	27.62	1.04	1.11
	3.45	104.80	11.55	0.52	1.04	1.07	3.45	149.44	35.58	1.12	1.17
C200c	0.69	2.66	1.60	0.63	0.63	1.04	0.71	3.99	2.37	0.63	1.03
	0.99	5.58	3.19	0.76	0.76	1.01	1.00	7.97	4.65	0.78	1.03
	1.36	10.36	4.52	0.76	0.89	1.01	1.37	14.88	7.44	0.88	1.04
	1.82	18.60	5.15	0.65	0.93	0.95	1.82	26.31	10.18	0.90	1.00
	2.30	29.76	5.74	0.58	0.95	0.95	2.30	42.25	14.22	1.01	1.09
	2.90	47.30	6.46	0.53	0.97	0.99	2.90	66.97	19.25	1.11	1.17
	3.55	70.95	7.15	0.49	0.99	1.03	3.55	100.45	24.53	1.18	1.23

Table B2-700: Numerical failure loads and their DSM estimates for the pinned and fixed hat-section columns at 700°C

Column	Pinned (P)						Fixed (F)				
	$\bar{\lambda}_{D,T}$	$P_{y,T}$ (kN)	$P_{u,T}$ (kN)	$\frac{P_{u,T}}{P_{n,D,T}^F}$	$\frac{P_{u,T}}{P_{n,D,T}^P}$	$\frac{P_{u,T}}{P_{n,D,T}^{P^*}}$	$\bar{\lambda}_{D,T}$	$P_{y,T}$ (kN)	$P_{u,T}$ (kN)	$\frac{P_{u,T}}{P_{n,D,T}^F}$	$\frac{P_{u,T}}{P_{n,D,T}^{P^*}}$
H130	0.40	3.65	2.19	0.60	0.60	1.04	0.40	5.16	3.10	0.60	1.04
	0.70	11.18	6.93	0.66	0.66	1.07	0.70	15.69	9.73	0.66	1.07
	1.01	23.32	13.99	0.81	0.81	1.06	1.01	32.57	20.19	0.83	1.10
	1.40	44.50	18.69	0.75	0.90	1.00	1.40	62.23	29.25	0.84	0.99
	1.87	80.29	22.94	0.69	1.01	1.03	1.87	112.32	43.32	0.93	1.03
	2.35	126.19	24.85	0.60	1.01	1.01	2.35	176.49	56.72	0.98	1.06
	3.00	205.72	26.74	0.52	0.98	1.00	3.00	287.63	74.23	1.03	1.09
	0.45	2.48	1.51	0.61	0.61	1.06	0.45	3.57	2.18	0.61	1.06
H150	0.75	6.98	4.46	0.70	0.70	1.11	0.75	9.77	6.06	0.68	1.07
	1.07	14.26	8.32	0.82	0.82	1.07	1.07	20.00	11.83	0.83	1.07
	1.47	26.82	10.95	0.77	0.95	1.04	1.47	37.67	18.09	0.90	1.05
	1.95	47.28	12.41	0.66	0.99	1.01	1.95	66.35	25.93	0.98	1.08
	2.45	74.57	13.37	0.57	0.98	0.99	2.45	104.80	33.62	1.03	1.10
	3.10	119.37	15.05	0.52	1.00	1.02	3.10	167.74	44.09	1.09	1.15
	0.51	1.67	0.99	0.59	0.59	1.03	0.49	2.15	1.28	0.59	1.03
	0.80	4.07	2.43	0.68	0.68	1.04	0.80	5.74	3.36	0.66	1.01
H180	1.13	8.13	4.45	0.81	0.81	1.04	1.13	11.48	6.42	0.82	1.03
	1.55	15.31	5.82	0.75	0.97	1.04	1.55	21.76	9.67	0.88	1.01
	2.03	26.31	6.20	0.62	0.95	0.96	2.03	37.31	13.83	0.97	1.06
	2.55	41.61	6.91	0.56	0.97	0.97	2.55	59.07	18.96	1.08	1.15
	3.20	65.53	7.76	0.51	0.99	1.02	3.20	92.79	25.06	1.16	1.22
	0.55	4.13	2.56	0.62	0.62	1.07	0.55	5.79	3.53	0.61	1.06
	0.85	9.92	6.19	0.74	0.74	1.08	0.85	13.72	8.71	0.75	1.10
	1.19	19.35	10.60	0.85	0.88	1.09	1.19	26.95	15.37	0.88	1.08
H200a	1.62	36.05	13.01	0.75	1.00	1.05	1.62	50.10	22.11	0.92	1.04
	2.10	60.52	14.18	0.64	1.00	1.01	2.10	84.17	28.81	0.93	1.01
	2.65	96.40	15.69	0.57	1.01	1.02	2.65	134.11	38.55	1.00	1.07
	3.30	149.32	17.89	0.53	1.05	1.08	3.30	207.86	50.15	1.07	1.13
	0.59	3.10	1.95	0.63	0.63	1.09	0.61	4.55	2.74	0.61	1.05
	0.91	7.23	4.33	0.74	0.74	1.04	0.90	10.13	6.06	0.74	1.04
	1.25	13.85	7.05	0.83	0.90	1.07	1.25	19.43	10.49	0.87	1.06
	1.69	25.22	8.29	0.71	0.98	1.02	1.69	35.55	15.18	0.93	1.04
H200b	2.18	41.75	9.11	0.62	0.98	0.99	2.18	58.70	21.01	1.01	1.10
	2.75	66.56	10.10	0.55	1.00	1.01	2.75	93.84	27.15	1.05	1.12
	3.40	101.90	11.26	0.51	1.02	1.05	3.40	143.24	34.79	1.12	1.17
	0.65	2.39	1.44	0.62	0.62	1.05	0.66	3.45	2.04	0.61	1.02
	0.95	5.05	2.92	0.74	0.74	1.01	0.95	7.18	4.19	0.75	1.01
	1.30	9.57	4.44	0.78	0.88	1.02	1.32	13.82	7.01	0.86	1.03
	1.78	17.81	5.21	0.67	0.94	0.97	1.77	24.98	10.01	0.91	1.02
	2.25	28.43	5.65	0.58	0.94	0.95	2.25	40.39	13.99	1.01	1.10
H200c	2.85	45.71	6.37	0.53	0.97	0.98	2.85	64.84	19.21	1.12	1.19
	3.50	69.09	7.09	0.49	0.99	1.02	3.50	97.80	24.44	1.19	1.24

Table B3-700: Numerical failure loads and their DSM estimates for the pinned and fixed zed-section columns at 700°C

Column	Pinned (P)						Fixed (F)					
	$\bar{\lambda}_{D.T}$	$P_{y,T}$ (kN)	$P_{u,T}$ (kN)	$\frac{P_{u,T}}{P_{n,D.T}^F}$	$\frac{P_{u,T}}{P_{n,D.T}^P}$	$\frac{P_{u,T}}{P_{n,D.T}^{P*}}$	$\bar{\lambda}_{D.T}$	$P_{y,T}$ (kN)	$P_{u,T}$ (kN)	$\frac{P_{u,T}}{P_{n,D.T}^F}$	$\frac{P_{u,T}}{P_{n,D.T}^{P*}}$	
Z130	0.50	5.70	3.53	0.62	0.62	1.07	0.50	7.85	4.86	0.62	1.07	
	0.80	14.51	8.90	0.70	0.70	1.06	0.80	20.21	12.73	0.72	1.09	
	1.11	27.84	15.34	0.80	0.80	1.04	1.11	38.91	22.19	0.83	1.05	
	1.49	50.52	19.12	0.72	0.91	0.99	1.49	70.51	32.31	0.88	1.01	
	1.97	88.24	21.47	0.62	0.94	0.95	1.97	123.07	44.01	0.91	1.00	
	2.45	135.86	25.15	0.59	1.01	1.02	2.45	189.49	57.54	0.97	1.04	
	3.10	217.44	29.53	0.56	1.08	1.10	3.10	303.32	76.35	1.05	1.10	
Z150	0.55	3.72	2.27	0.61	0.61	1.06	0.55	5.27	3.21	0.61	1.06	
	0.85	8.99	5.57	0.73	0.73	1.07	0.85	12.56	7.75	0.73	1.07	
	1.17	17.05	9.31	0.83	0.86	1.08	1.17	23.87	13.51	0.86	1.07	
	1.57	30.54	11.39	0.75	0.97	1.04	1.57	42.94	19.68	0.92	1.05	
	2.05	52.24	12.69	0.64	0.99	1.00	2.05	73.33	27.27	0.98	1.08	
	2.55	80.77	13.85	0.57	1.00	1.01	2.55	113.32	35.49	1.05	1.12	
	3.20	127.12	15.74	0.53	1.03	1.06	3.20	178.59	46.08	1.11	1.17	
Z180	0.61	2.39	1.44	0.61	0.61	1.04	0.60	3.35	1.99	0.60	1.03	
	0.91	5.26	3.08	0.72	0.72	1.02	0.90	7.65	4.50	0.73	1.02	
	1.24	9.81	4.94	0.81	0.87	1.05	1.23	14.11	7.48	0.84	1.03	
	1.64	17.22	5.87	0.72	0.96	1.01	1.65	25.35	10.54	0.88	0.99	
	2.13	28.94	6.47	0.61	0.97	0.98	2.13	42.33	15.12	0.98	1.07	
	2.65	44.96	7.10	0.55	0.98	0.99	2.65	65.77	20.25	1.08	1.15	
	3.30	69.83	8.00	0.51	1.01	1.04	3.30	101.88	26.49	1.16	1.22	
Z200a	0.65	5.79	3.59	0.64	0.64	1.07	0.65	7.94	4.87	0.63	1.06	
	0.95	12.24	7.42	0.78	0.78	1.06	0.95	17.03	10.42	0.78	1.06	
	1.29	22.65	11.48	0.84	0.94	1.10	1.29	31.58	17.32	0.91	1.09	
	1.72	40.35	13.30	0.73	1.01	1.04	1.72	56.06	23.21	0.91	1.03	
	2.20	66.14	14.78	0.64	1.03	1.03	2.20	91.77	30.51	0.95	1.03	
	2.75	103.18	16.77	0.59	1.07	1.08	2.75	143.37	40.71	1.03	1.10	
	3.40	157.75	19.06	0.56	1.11	1.15	3.40	219.27	52.80	1.11	1.16	
Z200b	0.70	4.34	2.70	0.66	0.66	1.08	0.70	6.20	3.83	0.65	1.07	
	1.00	8.89	5.18	0.78	0.78	1.03	1.00	12.61	7.41	0.78	1.04	
	1.35	16.12	7.51	0.81	0.94	1.07	1.35	22.94	11.84	0.90	1.06	
	1.79	28.32	8.57	0.70	0.99	1.02	1.80	40.51	16.36	0.93	1.04	
	2.28	45.68	9.43	0.61	1.00	1.01	2.27	64.90	21.97	1.00	1.08	
	2.85	71.52	10.56	0.56	1.03	1.04	2.85	101.90	28.79	1.07	1.13	
	3.50	107.90	11.72	0.52	1.04	1.08	3.50	153.78	36.76	1.14	1.19	
Z200c	0.75	3.19	1.83	0.63	0.63	1.00	0.75	4.52	2.60	0.63	1.00	
	1.04	6.11	3.34	0.75	0.75	0.98	1.05	8.77	4.88	0.77	1.00	
	1.41	11.16	4.39	0.71	0.85	0.95	1.41	15.94	7.07	0.80	0.94	
	1.87	19.67	4.90	0.60	0.87	0.89	1.87	27.90	9.93	0.85	0.95	
	2.35	31.09	5.13	0.50	0.84	0.84	2.35	44.11	13.99	0.97	1.05	
	2.95	49.16	6.29	0.50	0.94	0.96	2.95	69.36	19.10	1.08	1.14	
	3.60	73.08	7.01	0.47	0.96	1.00	3.60	103.38	24.52	1.17	1.22	

Table B4-700: Numerical failure loads and their DSM estimates for the pinned and fixed rack-section columns at 700°C

Column	Pinned (P)						Fixed (F)					
	$\bar{\lambda}_{D.T}$	$P_{y,T}$ (kN)	$P_{u,T}$ (kN)	$\frac{P_{u,T}}{P_{n,D.T}^F}$	$\frac{P_{u,T}}{P_{n,D.T}^P}$	$\frac{P_{u,T}}{P_{n,D.T}^{Ps}}$	$\bar{\lambda}_{D.T}$	$P_{y,T}$ (kN)	$P_{u,T}$ (kN)	$\frac{P_{u,T}}{P_{n,D.T}^F}$	$\frac{P_{u,T}}{P_{n,D.T}^P}$	$\frac{P_{u,T}}{P_{n,D.T}^{Ps}}$
R130	0.43	4.00	2.40	0.60	0.60	1.04	0.43	5.67	3.40	0.60	1.04	
	0.72	11.56	6.93	0.64	0.64	1.04	0.72	16.34	9.64	0.63	1.02	
	1.04	23.67	12.58	0.73	0.73	0.95	1.03	33.34	19.90	0.82	1.06	
	1.42	44.57	17.28	0.71	0.85	0.95	1.42	62.90	31.15	0.90	1.05	
	1.90	79.68	19.70	0.60	0.89	0.91	1.90	112.58	40.99	0.89	0.98	
	2.37	124.47	20.28	0.50	0.85	0.85	2.37	175.82	52.30	0.92	0.99	
	3.03	202.04	25.01	0.50	0.95	0.96	3.03	285.29	65.93	0.93	0.99	
R150	0.47	2.86	1.72	0.60	0.60	1.04	0.47	4.13	2.41	0.58	1.01	
	0.78	7.78	4.52	0.65	0.65	1.01	0.78	11.11	6.44	0.65	1.01	
	1.10	15.55	8.58	0.79	0.79	1.03	1.10	22.21	12.47	0.81	1.02	
	1.50	28.88	10.97	0.73	0.92	0.99	1.49	41.26	18.38	0.85	0.98	
	1.97	50.30	13.78	0.70	1.05	1.07	1.98	72.20	25.74	0.91	1.00	
	2.47	79.02	14.95	0.61	1.05	1.06	2.48	113.30	33.71	0.96	1.03	
	3.13	126.15	17.29	0.57	1.10	1.13	3.12	180.57	44.86	1.04	1.10	
R180	0.52	1.94	1.12	0.58	0.58	1.00	0.52	2.91	1.68	0.58	1.00	
	0.83	4.86	2.76	0.66	0.66	0.98	0.82	7.28	4.17	0.66	0.99	
	1.16	9.47	4.38	0.70	0.71	0.90	1.15	14.33	7.69	0.81	1.00	
	1.57	17.48	5.46	0.63	0.82	0.87	1.57	26.71	10.89	0.82	0.94	
	2.05	29.62	5.46	0.49	0.75	0.76	2.05	45.40	15.47	0.90	0.99	
	2.58	46.86	6.92	0.50	0.87	0.88	2.58	71.87	21.31	1.00	1.07	
	3.22	73.33	7.12	0.42	0.82	0.84	3.23	112.66	27.80	1.07	1.13	
R200a	0.57	4.56	2.73	0.60	0.60	1.04	0.57	6.42	3.73	0.58	1.01	
	0.87	10.65	6.13	0.69	0.69	1.00	0.88	15.04	8.72	0.70	1.00	
	1.21	20.62	9.90	0.76	0.80	0.98	1.21	28.90	15.72	0.86	1.05	
	1.65	37.86	11.91	0.66	0.89	0.94	1.64	53.07	21.80	0.87	0.98	
	2.12	63.04	13.12	0.57	0.90	0.91	2.13	88.56	28.69	0.89	0.97	
	2.68	100.05	15.42	0.54	0.97	0.98	2.67	140.28	38.30	0.96	1.03	
	3.32	154.48	17.77	0.52	1.02	1.05	3.33	216.84	51.01	1.06	1.11	
R200b	0.62	3.58	2.08	0.59	0.59	1.01	0.63	5.26	3.04	0.59	1.00	
	0.93	7.99	4.54	0.71	0.71	0.99	0.92	11.36	6.50	0.72	0.99	
	1.28	15.15	6.67	0.73	0.81	0.95	1.27	21.67	11.30	0.86	1.03	
	1.72	27.35	7.89	0.64	0.88	0.91	1.72	39.55	15.72	0.88	0.99	
	2.20	44.80	8.36	0.53	0.86	0.86	2.20	64.58	20.97	0.93	1.01	
	2.78	71.52	8.36	0.43	0.78	0.79	2.77	102.65	27.21	0.97	1.03	
	3.42	108.75	11.15	0.48	0.95	0.99	3.42	156.50	35.62	1.06	1.11	
R200c	0.67	2.69	1.55	0.60	0.60	1.00	0.68	4.31	2.48	0.60	1.00	
	0.97	5.66	3.12	0.72	0.72	0.97	0.98	8.89	5.03	0.74	0.99	
	1.33	10.78	4.30	0.69	0.79	0.90	1.33	16.43	7.85	0.82	0.97	
	1.79	19.40	5.02	0.59	0.84	0.87	1.80	29.90	11.01	0.85	0.95	
	2.27	31.25	5.37	0.51	0.83	0.83	2.27	47.95	15.19	0.94	1.01	
	2.88	50.11	6.32	0.48	0.89	0.90	2.88	76.78	20.53	1.02	1.08	
	3.52	75.16	7.11	0.45	0.92	0.95	3.53	115.30	26.07	1.09	1.13	

Table B1-800: Numerical failure loads and their DSM estimates for the pinned and fixed lipped channel columns at 800°C

Column	Pinned (P)						Fixed (F)					
	$\bar{\lambda}_{D.T}$	$P_{y,T}$ (kN)	$P_{u,T}$ (kN)	$\frac{P_{u,T}}{P_{n,D.T}^F}$	$\frac{P_{u,T}}{P_{n,D.T}^P}$	$\frac{P_{u,T}}{P_{n,D.T}^{P*}}$	$\bar{\lambda}_{D.T}$	$P_{y,T}$ (kN)	$P_{u,T}$ (kN)	$\frac{P_{u,T}}{P_{n,D.T}^F}$	$\frac{P_{u,T}}{P_{n,D.T}^{P*}}$	
C130	0.40	2.49	1.82	0.73	0.73	1.02	0.40	3.41	2.53	0.74	1.04	
	0.66	6.83	5.05	0.76	0.76	1.04	0.66	9.55	7.14	0.77	1.05	
	0.94	13.66	9.82	0.91	0.91	1.07	0.93	19.04	13.51	0.90	1.05	
	1.27	25.35	13.18	0.86	0.95	1.04	1.27	35.42	20.35	0.95	1.04	
	1.70	45.03	14.23	0.69	0.94	0.95	1.70	62.85	26.60	0.92	0.98	
	2.12	69.97	17.08	0.67	1.05	1.04	2.12	97.69	34.54	0.97	1.01	
	2.69	113.03	20.22	0.63	1.13	1.13	2.69	157.77	45.87	1.03	1.07	
	0.44	1.67	1.22	0.73	0.73	1.02	0.44	2.34	1.71	0.73	1.02	
C150	0.70	4.26	3.10	0.77	0.77	1.02	0.71	6.01	4.52	0.80	1.05	
	0.99	8.35	5.60	0.89	0.89	1.02	0.99	11.77	8.42	0.94	1.09	
	1.34	15.44	7.20	0.80	0.93	1.00	1.34	21.62	12.35	0.98	1.08	
	1.76	26.71	8.19	0.69	0.98	0.98	1.76	37.48	16.78	1.01	1.07	
	2.21	41.74	9.02	0.62	1.00	0.98	2.20	58.60	21.80	1.06	1.11	
	2.78	66.20	10.51	0.58	1.06	1.06	2.78	92.99	28.06	1.11	1.15	
	0.48	1.03	0.78	0.75	0.75	1.05	0.49	1.55	1.13	0.73	1.03	
	0.74	2.45	1.77	0.79	0.79	1.01	0.75	3.61	2.60	0.79	1.01	
C180	1.04	4.76	3.09	0.89	0.89	1.03	1.04	6.95	4.65	0.92	1.05	
	1.41	8.76	3.75	0.77	0.93	0.98	1.40	12.75	6.68	0.94	1.03	
	1.83	14.81	4.16	0.66	0.95	0.94	1.83	21.63	9.69	1.05	1.11	
	2.29	23.31	4.65	0.59	0.98	0.96	2.29	34.00	13.18	1.16	1.21	
	2.86	36.31	5.30	0.55	1.02	1.02	2.87	53.18	17.40	1.25	1.28	
	0.53	2.67	1.91	0.72	0.72	1.00	0.53	3.65	2.66	0.73	1.02	
	0.79	5.97	4.36	0.83	0.83	1.03	0.79	8.28	6.12	0.84	1.04	
	1.09	11.31	7.09	0.90	0.90	1.05	1.09	15.67	11.24	1.03	1.16	
C200a	1.47	20.48	8.50	0.78	0.97	1.01	1.47	28.49	15.54	1.03	1.11	
	1.90	33.92	9.50	0.68	1.01	1.00	1.90	47.19	19.31	1.00	1.05	
	2.38	53.51	10.94	0.63	1.07	1.05	2.38	74.44	26.32	1.10	1.14	
	2.96	82.45	12.58	0.60	1.12	1.13	2.95	114.59	33.80	1.16	1.20	
	0.57	2.00	1.47	0.73	0.73	1.02	0.58	2.89	2.18	0.75	1.06	
	0.83	4.23	3.07	0.85	0.85	1.03	0.84	6.12	4.39	0.84	1.02	
	1.15	8.01	4.55	0.85	0.86	1.00	1.15	11.46	7.62	1.00	1.12	
	1.54	14.47	5.75	0.78	1.01	1.03	1.54	20.59	10.22	0.98	1.05	
C200b	1.96	23.48	6.31	0.68	1.02	1.01	1.96	33.50	13.94	1.05	1.11	
	2.47	37.17	7.03	0.61	1.05	1.03	2.47	52.98	18.02	1.10	1.14	
	3.04	56.43	7.86	0.57	1.07	1.08	3.04	80.47	22.81	1.15	1.19	
	0.61	1.43	1.02	0.72	0.72	1.00	0.62	2.15	1.60	0.76	1.04	
	0.88	3.00	2.13	0.86	0.86	1.03	0.88	4.29	3.07	0.87	1.04	
	1.20	5.58	3.14	0.87	0.92	1.04	1.20	8.01	5.12	1.00	1.11	
	1.60	10.02	3.66	0.75	0.99	1.00	1.60	14.17	6.76	0.98	1.05	
	2.03	16.03	3.90	0.64	0.98	0.96	2.03	22.75	9.42	1.08	1.14	
C200c	2.55	25.47	4.45	0.59	1.02	1.01	2.56	36.06	12.76	1.19	1.23	
	3.13	38.21	4.93	0.54	1.04	1.05	3.13	54.09	16.19	1.26	1.29	

Table B2-800: Numerical failure loads and their DSM estimates for the pinned and fixed hat-section columns at 800°C

Column	Pinned (P)						Fixed (F)					
	$\bar{\lambda}_{D.T}$	$P_{y,T}$ (kN)	$P_{u,T}$ (kN)	$\frac{P_{u,T}}{P_{n,D.T}^F}$	$\frac{P_{u,T}}{P_{n,D.T}^P}$	$\frac{P_{u,T}}{P_{n,D.T}^{Ps}}$	$\bar{\lambda}_{D.T}$	$P_{y,T}$ (kN)	$P_{u,T}$ (kN)	$\frac{P_{u,T}}{P_{n,D.T}^F}$	$\frac{P_{u,T}}{P_{n,D.T}^{F*}}$	
H130	0.35	1.97	1.44	0.73	0.73	1.02	0.35	2.78	2.06	0.74	1.04	
	0.62	6.02	4.57	0.77	0.77	1.06	0.62	8.45	6.41	0.77	1.06	
	0.89	12.56	9.29	0.90	0.90	1.08	0.89	17.54	12.80	0.89	1.06	
	1.23	23.96	14.20	0.94	1.02	1.13	1.23	33.51	21.31	1.01	1.12	
	1.65	43.23	14.70	0.72	0.97	0.98	1.65	60.48	28.13	0.98	1.05	
	2.07	67.95	17.25	0.68	1.06	1.04	2.07	95.03	35.87	1.01	1.06	
	2.65	110.77	18.91	0.60	1.05	1.05	2.65	154.88	46.63	1.05	1.09	
	0.39	1.34	1.01	0.76	0.76	1.06	0.40	1.92	1.46	0.76	1.06	
H150	0.66	3.76	2.82	0.77	0.77	1.05	0.66	5.26	3.90	0.77	1.04	
	0.95	7.68	5.55	0.92	0.92	1.08	0.94	10.77	7.85	0.93	1.09	
	1.30	14.44	7.66	0.89	1.00	1.08	1.30	20.28	12.16	1.00	1.10	
	1.72	25.46	8.15	0.71	0.98	0.98	1.72	35.73	16.97	1.05	1.11	
	2.16	40.15	9.36	0.65	1.04	1.02	2.16	56.43	22.04	1.09	1.14	
	2.73	64.28	10.30	0.58	1.04	1.04	2.73	90.32	28.27	1.13	1.17	
	0.45	0.90	0.65	0.72	0.72	1.00	0.43	1.16	0.84	0.73	1.02	
	0.70	2.19	1.58	0.77	0.77	1.01	0.70	3.09	2.25	0.77	1.02	
H180	0.99	4.38	3.00	0.91	0.91	1.05	0.99	6.18	4.31	0.92	1.07	
	1.36	8.24	3.93	0.84	0.98	1.04	1.37	11.72	6.40	0.96	1.05	
	1.79	14.17	4.25	0.69	0.98	0.97	1.79	20.09	9.15	1.05	1.11	
	2.25	22.41	4.79	0.62	1.02	1.00	2.25	31.81	12.53	1.15	1.20	
	2.82	35.28	5.35	0.57	1.04	1.04	2.82	49.96	16.53	1.24	1.28	
	0.48	2.23	1.66	0.74	0.74	1.04	0.49	3.12	2.38	0.76	1.07	
	0.75	5.34	4.08	0.84	0.84	1.07	0.75	7.39	5.67	0.84	1.08	
	1.05	10.42	7.15	0.95	0.95	1.10	1.05	14.51	10.27	0.98	1.12	
H200a	1.43	19.41	8.78	0.83	1.01	1.05	1.43	26.98	14.64	0.99	1.08	
	1.85	32.59	9.78	0.71	1.04	1.03	1.85	45.32	19.07	1.00	1.06	
	2.34	51.91	10.83	0.64	1.06	1.04	2.34	72.21	24.70	1.04	1.08	
	2.91	80.40	12.07	0.58	1.08	1.08	2.91	111.92	31.79	1.10	1.13	
	0.52	1.67	1.21	0.73	0.73	1.02	0.53	2.45	1.79	0.73	1.03	
	0.80	3.90	2.87	0.84	0.84	1.04	0.80	5.45	3.96	0.82	1.02	
	1.11	7.46	4.79	0.93	0.93	1.09	1.10	10.46	7.06	0.98	1.10	
	1.49	13.58	5.70	0.80	1.01	1.04	1.49	19.14	10.05	1.01	1.08	
H200b	1.92	22.48	6.43	0.71	1.05	1.04	1.92	31.61	13.81	1.08	1.14	
	2.42	35.84	7.01	0.62	1.05	1.04	2.43	50.53	17.96	1.13	1.17	
	3.00	54.87	7.73	0.56	1.06	1.07	3.00	77.13	22.46	1.17	1.20	
	0.57	1.29	0.92	0.72	0.72	1.00	0.58	1.86	1.34	0.72	1.01	
	0.83	2.72	1.94	0.83	0.83	1.01	0.84	3.86	2.76	0.83	1.02	
	1.15	5.15	3.05	0.89	0.90	1.04	1.16	7.44	4.75	0.97	1.08	
	1.57	9.59	3.64	0.76	0.99	1.01	1.56	13.45	6.69	0.99	1.07	
	1.98	15.31	3.67	0.61	0.93	0.91	1.98	21.75	9.33	1.10	1.15	
H200c	2.51	24.61	4.43	0.59	1.02	1.01	2.51	34.92	12.71	1.20	1.24	
	3.09	37.20	4.88	0.54	1.03	1.04	3.09	52.66	16.17	1.27	1.31	

Table B3-800: Numerical failure loads and their DSM estimates for the pinned and fixed zed-section columns at 800°C

Column	Pinned (P)						Fixed (F)					
	$\bar{\lambda}_{D.T}$	$P_{y,T}$ (kN)	$P_{u,T}$ (kN)	$\frac{P_{u,T}}{P_{n,D.T}^F}$	$\frac{P_{u,T}}{P_{n,D.T}^P}$	$\frac{P_{u,T}}{P_{n,D.T}^{P*}}$	$\bar{\lambda}_{D.T}$	$P_{y,T}$ (kN)	$P_{u,T}$ (kN)	$\frac{P_{u,T}}{P_{n,D.T}^F}$	$\frac{P_{u,T}}{P_{n,D.T}^{P*}}$	
Z130	0.44	3.07	2.30	0.75	0.75	1.05	0.44	4.22	3.17	0.75	1.05	
	0.71	7.81	5.72	0.78	0.78	1.03	0.71	10.88	8.00	0.78	1.03	
	0.98	14.99	10.21	0.89	0.89	1.04	0.98	20.95	14.62	0.91	1.06	
	1.32	27.20	12.95	0.81	0.92	0.99	1.32	37.97	21.20	0.95	1.04	
	1.74	47.52	14.40	0.68	0.95	0.94	1.74	66.27	28.00	0.94	1.00	
	2.16	73.16	16.43	0.63	1.00	0.99	2.16	102.04	35.86	0.98	1.03	
	2.73	117.08	19.38	0.60	1.08	1.07	2.73	163.33	48.38	1.07	1.11	
	0.48	2.00	1.49	0.75	0.75	1.04	0.48	2.84	2.10	0.74	1.04	
Z150	0.75	4.84	3.66	0.83	0.83	1.06	0.75	6.76	5.08	0.82	1.05	
	1.03	9.18	6.29	0.94	0.94	1.08	1.03	12.86	9.08	0.97	1.11	
	1.38	16.44	7.73	0.84	0.99	1.05	1.38	23.12	12.95	1.00	1.08	
	1.81	28.13	8.85	0.73	1.05	1.04	1.81	39.48	17.78	1.05	1.11	
	2.25	43.49	9.61	0.65	1.05	1.03	2.25	61.02	22.86	1.09	1.14	
	2.82	68.45	10.66	0.58	1.07	1.07	2.82	96.16	30.00	1.17	1.21	
	0.54	1.29	0.93	0.72	0.72	1.01	0.53	1.80	1.30	0.72	1.01	
	0.80	2.83	2.03	0.81	0.81	1.01	0.80	4.12	2.97	0.82	1.02	
Z180	1.09	5.28	3.41	0.92	0.92	1.08	1.08	7.60	5.05	0.95	1.07	
	1.45	9.27	4.04	0.81	0.99	1.03	1.45	13.65	7.07	0.96	1.04	
	1.87	15.58	4.48	0.69	1.01	1.00	1.88	22.79	9.81	1.04	1.10	
	2.34	24.21	4.93	0.62	1.03	1.01	2.34	35.41	13.31	1.14	1.19	
	2.91	37.60	5.47	0.56	1.05	1.05	2.91	54.86	17.41	1.23	1.27	
	0.57	3.12	2.34	0.75	0.75	1.05	0.57	4.27	3.13	0.73	1.03	
	0.84	6.59	4.89	0.87	0.87	1.06	0.84	9.17	6.76	0.86	1.05	
	1.14	12.20	7.89	0.96	0.96	1.13	1.14	17.01	11.54	1.01	1.13	
Z200a	1.52	21.73	9.14	0.82	1.04	1.07	1.52	30.18	15.45	0.99	1.07	
	1.94	35.62	10.26	0.72	1.08	1.06	1.94	49.42	19.98	1.01	1.06	
	2.42	55.56	11.37	0.65	1.10	1.09	2.42	77.20	26.01	1.07	1.11	
	3.00	84.94	12.80	0.60	1.14	1.14	3.00	118.07	33.39	1.13	1.17	
	0.62	2.34	1.70	0.74	0.74	1.02	0.62	3.34	2.42	0.73	1.02	
	0.89	4.79	3.46	0.88	0.88	1.05	0.88	6.79	4.86	0.87	1.04	
	1.19	8.68	5.18	0.92	0.97	1.10	1.19	12.35	7.90	0.99	1.10	
	1.58	15.25	5.91	0.78	1.03	1.04	1.58	21.81	10.86	1.01	1.08	
Z200b	2.01	24.60	6.60	0.70	1.06	1.05	2.01	34.95	14.47	1.07	1.12	
	2.51	38.51	7.24	0.62	1.07	1.06	2.51	54.87	18.76	1.13	1.17	
	3.09	58.10	8.02	0.57	1.09	1.10	3.09	82.81	23.65	1.18	1.21	
	0.66	1.72	1.22	0.73	0.73	0.99	0.66	2.43	1.73	0.74	1.00	
	0.92	3.29	2.24	0.85	0.85	1.00	0.92	4.72	3.27	0.87	1.02	
	1.24	6.01	3.02	0.80	0.87	0.97	1.25	8.59	4.77	0.90	0.99	
	1.65	10.59	3.35	0.67	0.90	0.91	1.65	15.02	6.72	0.94	1.01	
	2.07	16.74	3.52	0.56	0.87	0.86	2.07	23.75	9.19	1.04	1.09	
Z200c	2.60	26.47	4.25	0.55	0.97	0.96	2.60	37.35	12.35	1.13	1.17	
	3.17	39.35	4.76	0.52	1.00	1.01	3.17	55.66	15.98	1.22	1.26	

Table B4-800: Numerical failure loads and their DSM estimates for the pinned and fixed rack-section columns at 800°C

Column	Pinned (P)						Fixed (F)					
	$\bar{\lambda}_{D.T}$	$P_{y,T}$ (kN)	$P_{u,T}$ (kN)	$\frac{P_{u,T}}{P_{n,D.T}^F}$	$\frac{P_{u,T}}{P_{n,D.T}^P}$	$\frac{P_{u,T}}{P_{n,D.T}^{Ps}}$	$\bar{\lambda}_{D.T}$	$P_{y,T}$ (kN)	$P_{u,T}$ (kN)	$\frac{P_{u,T}}{P_{n,D.T}^F}$	$\frac{P_{u,T}}{P_{n,D.T}^{F*}}$	
R130	0.38	2.15	1.61	0.75	0.75	1.04	0.38	3.05	2.23	0.73	1.02	
	0.64	6.22	4.54	0.75	0.75	1.02	0.64	8.80	6.33	0.74	1.01	
	0.91	12.75	8.33	0.81	0.81	0.96	0.91	17.95	12.57	0.87	1.03	
	1.25	24.00	11.72	0.79	0.86	0.96	1.25	33.87	20.43	0.98	1.08	
	1.68	42.91	13.43	0.67	0.91	0.92	1.68	60.62	27.39	0.97	1.03	
	2.09	67.02	14.02	0.57	0.89	0.87	2.09	94.67	33.56	0.96	1.01	
	2.67	108.79	16.45	0.53	0.95	0.94	2.67	153.62	43.08	0.99	1.02	
	0.41	1.54	1.12	0.73	0.73	1.02	0.42	2.22	1.61	0.72	1.01	
R150	0.68	4.19	2.99	0.75	0.75	1.00	0.68	5.98	4.27	0.75	1.00	
	0.97	8.37	5.73	0.89	0.89	1.03	0.97	11.96	8.32	0.90	1.05	
	1.32	15.55	7.00	0.76	0.87	0.94	1.32	22.21	12.37	0.95	1.04	
	1.74	27.08	7.85	0.65	0.90	0.90	1.74	38.88	16.99	0.98	1.04	
	2.18	42.55	10.13	0.67	1.08	1.06	2.18	61.01	22.13	1.03	1.07	
	2.76	67.93	11.52	0.62	1.12	1.12	2.76	97.23	28.13	1.05	1.09	
	0.46	1.05	0.75	0.71	0.71	1.00	0.46	1.57	1.12	0.71	1.00	
	0.73	2.61	1.84	0.76	0.76	0.98	0.72	3.92	2.78	0.76	0.99	
R180	1.02	5.10	2.97	0.79	0.79	0.91	1.01	7.71	5.16	0.90	1.04	
	1.39	9.41	3.69	0.70	0.83	0.88	1.39	14.38	7.26	0.90	0.98	
	1.81	15.95	3.69	0.54	0.77	0.76	1.81	24.45	10.12	0.96	1.02	
	2.27	25.23	4.75	0.56	0.91	0.90	2.27	38.70	14.12	1.08	1.12	
	2.84	39.48	5.40	0.52	0.95	0.95	2.85	60.66	18.36	1.14	1.18	
	0.50	2.46	1.78	0.72	0.72	1.01	0.50	3.46	2.53	0.73	1.02	
	0.77	5.73	4.08	0.79	0.79	1.00	0.77	8.10	5.76	0.79	1.00	
	1.07	11.10	6.73	0.85	0.85	0.99	1.07	15.56	10.52	0.95	1.08	
R200a	1.45	20.39	8.21	0.75	0.92	0.96	1.45	28.58	14.91	0.97	1.05	
	1.87	33.95	8.75	0.62	0.91	0.90	1.87	47.69	18.60	0.94	0.99	
	2.36	53.88	10.45	0.60	1.00	0.98	2.36	75.54	24.29	0.99	1.03	
	2.93	83.18	11.96	0.56	1.05	1.05	2.93	116.76	32.41	1.08	1.12	
	0.55	1.93	1.38	0.72	0.72	1.00	0.55	2.83	2.02	0.71	1.00	
	0.82	4.30	3.03	0.81	0.81	1.00	0.81	6.12	4.33	0.81	1.00	
	1.13	8.16	4.53	0.82	0.82	0.96	1.12	11.67	7.58	0.95	1.07	
	1.51	14.72	5.43	0.72	0.91	0.93	1.52	21.29	10.43	0.95	1.03	
R200b	1.94	24.13	5.75	0.59	0.89	0.88	1.94	34.77	13.76	0.99	1.04	
	2.45	38.51	5.75	0.48	0.81	0.80	2.45	55.27	17.65	1.02	1.06	
	3.02	58.56	7.69	0.53	1.00	1.01	3.02	84.27	22.82	1.09	1.12	
	0.59	1.45	1.03	0.71	0.71	1.00	0.60	2.32	1.65	0.72	1.00	
	0.85	3.05	2.09	0.81	0.81	0.99	0.86	4.79	3.35	0.84	1.01	
	1.18	5.80	2.94	0.77	0.80	0.92	1.17	8.85	5.40	0.93	1.04	
	1.58	10.44	3.50	0.68	0.88	0.90	1.58	16.10	7.36	0.93	0.99	
	2.00	16.83	3.74	0.57	0.87	0.86	2.01	25.82	10.17	1.02	1.07	
R200c	2.54	26.98	4.34	0.54	0.93	0.92	2.54	41.34	13.45	1.08	1.12	
	3.11	40.47	4.87	0.50	0.96	0.97	3.11	62.09	17.34	1.16	1.20	